Alpha-Actinin-4 Supports B Cell Survival by Limiting Lateral BCR Mobility

Dissertation

for the award of the degree

“Doctor rerum naturalium”

of the Georg-August-Universität Göttingen

within the doctoral program Molecular Medicine

of the Georg-August University School of Science (GAUSS)

submitted by Saed Alsouri

born in Khan Younis, Palestine

Göttingen 2023

This thesis was conducted from August 2019 until June 2023 in the Institute of Cellular and Molecular Immunology at Georg-August University of Göttingen under the supervision of Dr. Michael Engelke and Prof. Dr. Jürgen Wienands.

Thesis Committee

Prof. Dr. Jürgen Wienands, Institute for Cellular and Molecular Immunology, University Medical Center Göttingen (UMG)

Prof. Dr. Matthias Dobbelstein, Department of Molecular Oncology, University Medical Center Göttingen (UMG)

Prof. Dr. Markus Bohnsack, Department of Molecular Biology, University Medical Center Göttingen (UMG)

Members of the Examination Board

Referee: Prof. Dr. Jürgen Wienands, Institute for Cellular and Molecular Immunology, University Medical Center Göttingen (UMG)

2nd Referee: Prof. Dr. Matthias Dobbelstein, Department of Molecular Oncology, University Medical Center Göttingen (UMG)

Further members of the Examination Board

Prof. Dr. Markus Bohnsack, Department of Molecular Biology, University Medical Center Göttingen (UMG)

Prof. Dr. Holger Bastians, Department of Molecular Oncology, University Medical Center Göttingen (UMG)

Prof. Dr. Holger Reichardt, Institute for Cellular and Molecular Immunology, University Medical Center Göttingen (UMG)

Prof. Dr. Ralph Kehlenbach, Department of Molecular Biology, University Medical Center Göttingen (UMG)

Date of thesis defense: 13.09.2023

Affidavit

I hereby declare that the prepared thesis “Alpha-Actinin-4 Supports B Cell Survival by Limiting Lateral BCR Mobility” is my work. All sources and aids are acknowledged as references.

_____ Göttingen, 26.06.2023

Saed Alsouri

Acknowledgements

First and foremost, I would like to extend my deepest gratitude to Prof. Dr. Wienands for providing me the opportunity to conduct my Ph.D. thesis in his laboratory. I am sincerely appreciative of his guidance, support, and invaluable presence as a member of my thesis committee. Furthermore, I would like to express my profound thanks to Prof. Dr. Dobbelstein and Prof. Dr. Bohnsack for their unwavering commitment as committee members, providing valuable advice during our meetings, and their ongoing support.

I would like to take this opportunity to convey my heartfelt appreciation to Michael for his diligent supervision and unwavering support throughout the entirety of my Ph.D. project. I have acquired a wealth of knowledge and experience under his tutelage, and it has been an absolute pleasure to be part of his esteemed team. I am profoundly grateful for his support before, during, and after my TAC meetings and seminars. Moreover, I extend my gratitude for his meticulous proofreading of my dissertation. Words fail to adequately express the depth of my gratitude.

Additionally, I would like to express my gratitude to all current and former members of the department, both as colleagues and for the memorable experiences we shared during my thesis. Special thanks are due to Ines and Gabi for their invaluable technical assistance, as well as Anika for her help with organizational tasks. To Stela, Florian, Nadia, Cagil, Carolina, Richard, Matthias, Jens, Niklas, and Erdem, I am grateful for the enjoyable times we had together at the Mensa and during our barbecues.

I would also like to extend my sincere appreciation to Prof. Dr. Michael R. Gold and his lab members, Ashely, Kate, and Libin, for their expertise in single particle tracking analysis. Additionally, I want to express my thanks to Prof. Dr. Silvio Rizzoli, Dr. Felipe Opazo, and Nikos for their invaluable contributions to conducting STED microscopy. A special acknowledgement is also due to Prof. Dr. Thomas Oellerich and his esteemed research group in Frankfurt for their pivotal role in conducting the MS analysis. Additionally, I would like to express my gratitude to Dr. Jens Löber for his invaluable expertise in conducting the BH3 profiling. Their contributions have significantly enriched the outcome of my research. I also would like to thank my lab rotation and thesis students Cagil, Lea, and Nadia for their contribution to my PHD thesis.

I am deeply grateful to the Deutsche Forschungsgemeinschaft (DFG) for funding my project. I also wish to acknowledge the exceptional coordination provided by the graduate program "Molecular Medicine" within the GGNB.

Lastly, but certainly not least, I wish to convey my profound gratitude to my beloved family and friends for their unwavering support. Thanks are extended to my parents, siblings, and my life partner Miriam for their unconditional love and encouragement throughout this momentous journey.

Table of content

Affidavit ii
Acknowledgements iii
List of Figures vi
List of Tables vii
Abbreviations viii
1 Abstract 1
2 Introduction 2
2.1 Overview of the human immune system 2
2.2 B lymphocyte development 3
2.3 B cell antigen receptor signaling 5
2.4 Tonic BCR signaling 8
2.5 Dysregulated BCR signaling in B cell malignancies 9
2.6 B cell cytoskeleton dynamics in BCR-mediated signaling 10
2.7 F-Actin cross-linking by alpha-Actinin proteins 12
2.8 Aim of this study 13
3 Materials and Methods 15
3.1 Materials 15
3.1.1 Instruments 15
3.1.2 Software and databases 16
3.1.3 Consumables 16
3.1.4 Enzymes 17
3.1.5 Oligonucleotides 17
3.1.6 Chemicals and reagents 18
3.1.7 Buffers and solutions 19
3.1.8 Plasmids 21
3.1.9 Antibodies 21
3.1.10 Bacteria and bacterial culture 22
3.1.11 Eukaryotic cell lines 22
3.2 Methods 23
3.2.1 Molecular biology 23
3.2.2 Biochemistry 27
3.2.3 Cell Biology 28
4 Results 38
4.1 BCR signaling properties of the primary-like P493.6 B cell model 38
4.2 Generation of an ACTN4-deficient P493.6 cell line 39
4.3 Alpha-Actinin-4 positively regulates Ca^{2+} mobilization of resting P493.6 cells 41
4.4 Alpha-Actinin-4 supports the survival of resting P493.6 cells 43
4.5 Alpha-Actinin-1 is dispensable for the survival of resting P493.6 cells 45
4.6 Alpha-Actinin-4 supports the survival of primary human B cells 46

4.7 Alpha-Actinin-4 supports the survival of resting P493.6 cells *via* the BFL-1 survival axis 49
4.8 Alpha-Actinin-4-dependent stabilization of F-Actin correlates with P493.6 cell survival 51
4.8.1 Alpha-Actinin-4 alters the amount, but not the spatial organization of F-Actin 51
4.8.2 Generation of alpha-Actinin-4 variants with altered F-Actin binding properties 54
4.8.3 The localization of alpha-Actinin-4 at F-Actin requires its Actin-binding domain 55
4.8.4 Only F-Actin binding-competent alpha-Actinin-4 supports survival of resting P493.6 cells .. 57
4.9 Alpha-Actinin-4-dependent F-Actin remodeling regulates lateral BCR mobility and tonic BCR signaling 59
4.9.1 The Actin-binding domain of alpha-Actinin-4 is required for its co-localization with the BCR 59
4.9.2 F-Actin co-localizes with the BCR in tonic and activated BCR signaling 60
4.9.3 Alpha-Actinin-4 confines lateral BCR diffusion of resting P493.6 cells 62
4.10 Alpha-Actinin-4-dependent control of BCR diffusion correlates with efficient tonic BCR signaling 63
4.10.1 Alpha-Actinin-4 augments ITAM-tyrosine phosphorylation of CD79A 63
4.10.2 Alpha-Actinin-4 positively regulates the activities of the proximal BCR kinases SYK and LYN 65
4.10.3 Alpha-Actinin-4 mildly augments the phosphorylation of SLP65 67
4.10.4 Alpha-Actinin-4 supports the phosphorylation of AKT 68
4.10.5 Alpha-Actinin-4 moderately increases phosphorylation events of the MAPK ERK 69
4.11 Analysis of tonic BCR signaling cascades in *ACTN4*$^{-/-}$ P493.6 cells by mass spectrometry 70
5 Discussion 72
5.1 The primary-like B cell model P493.6 for the analysis of tonic BCR signals 72
5.2 Alpha-Actinin-4, but not alpha-Actinin-1, supports the survival of human B cells 73
5.3 The survival-supporting function of alpha-Actinin-4 depends on its F-Actin binding capacity 74
5.4 Alpha-Actinin-4 at F-Actin confines BCR diffusion and supports tonic BCR signals 76
5.5 Efficient tonic BCR signaling correlates with efficient survival 77
6 Conclusion and Outlook 80
7 References 81
8 Curriculum vitae 91

List of Figures

Figure 1: Schematic overview of B cell development. 4
Figure 2: Schematic overview of B cell antigen receptor signaling. 7
Figure 3: Schematic overview of ACTN4 and ACTN1 domain structures. 13
Figure 4: Intended workflow to address the aim of this study. 14
Figure 5: Schematic illustration of CRISPR/Cas9-mediated gene editing. 30
Figure 6: Schematic illustration of the PiggyBac Transposon System. 32
Figure 7: Resting P493.6 cells differ in the intensities of tonic and activated BCR signaling from their proliferative state and BL cell lines. 39
Figure 8: Generation and genetic characterization of ACTN4-deficient P493.6 clones #3 and #5. 40
Figure 9: Reconstitution and characterization of ACTN4-deficient clones #3 and #5. 41
Figure 10: ACTN4 positively regulates BCR-induced Ca^{2+} mobilization in resting P493.6 cells. 42
Figure 11: ACTN4 supports the survival of resting P493.6 cells. 44
Figure 12: Generation of cell lines with downregulation of ACTN1 expression. 45
Figure 13: Downregulation of ACTN1 expression in resting WT and ACTN4$^{-/-}$ cells does not affect their survival. 46
Figure 14: CRISPR/Cas9-based targeting of the ACTN4-encoding gene in human primary B cells. 47
Figure 15: ACTN4 supports resting primary B cell survival. 48
Figure 16: ACTN4 reduces the general sensitivity of resting P493.6 cells for apoptosis. 50
Figure 17: ACTN4-deficiency does not alter the spatial organization of filamentous Actin. 51
Figure 18: ACTN4 loss slightly reduces the overall amount of F-Actin. 52
Figure 19: ACTN4 reconstitution increases F-Actin overall amount in ACTN4-deficient cells. 53
Figure 20: ACTN4 loss reduces LifeAct-mCherry intensity in tonic and activated BCR signaling. 54
Figure 21: Generation of ACTN4 variants with modified F-Actin binding capacity. 55
Figure 22: The ABD of ACTN4 is necessary for its co-localization with F-Actin. 56
Figure 23: Only F-Actin binding-competent ACTN4 has the capacity to co-localize with F-Actin. 57
Figure 24: ACTN4 requires its ABD to support resting P493.6 cell survival. 58
Figure 25: The ABD of ACTN4 is indispensable for its co-localization with the IgM-BCR. 60
Figure 26: F-Actin/IgM-BCR co-localization analysis in tonic BCR signaling. 61
Figure 27: F-Actin/IgM-BCR co-localization analysis upon BCR stimulation. 62
Figure 28: ACTN4 loss increases BCR diffusion in resting P493.6 cells. 63
Figure 29: ACTN4 supports the phosphorylation intensity of ITAM-containing tyrosine residues of CD79A. 64
Figure 30: Analysis of the proximal BCR effectors SYK and LYN in resting P493.6 cells. 66
Figure 31: ACTN4 slightly augments SLP65 phosphorylation intensity in resting P493.6 cells. 67
Figure 32: ACTN4 mildly augments AKT phosphorylation intensity in resting P493.6 cells. 68
Figure 33: Analysis of tonic MAPKs singling in resting P493.6 cells. 69
Figure 34: Graphical illustration of tonic and activated BCR signaling in P493.6 cells. 73
Figure 35: Schematic illustration of the proposed mechanism by which ACTN4 supports tonic BCR survival signals. 79

List of Tables

Table 1: Instruments. 15
Table 2: Softwares. 16
Table 3: Data bases. 16
Table 4: Consumables. 16
Table 5: Reaction systems (kits). 17
Table 6: Enzymes. 17
Table 7: Sequencing primers. 17
Table 8: Synthetic oligonucleotides used for the generation of ACTN1 knock-down (ACTN1 KD). 17
Table 9: Synthetic oligonucleotides used for CRISPR/Cas9-based gene editing. 18
Table 10: Synthetic oligonucleotides used for cloning. 18
Table 11: Chemicals and reagents. 18
Table 12: Buffers and solutions. 19
Table 13: Expression and cloning plasmids. 21
Table 14: Primary antibodies. 21
Table 15: Secondary antibodies. 22
Table 16: Fluorochrome conjugated antibodies. 22
Table 17: PCR reaction mix for cloning purposes. 23
Table 18: PCR reaction mix for sequencing purposes. 24
Table 19: PCR reaction steps. 24
Table 20: Overlap extension PCR program. 25
Table 21: Composition of Resolving and Stacking gels. 27
Table 22: Electroporation parameters used for P493.6 cell line. 30
Table 23: Electroporation parameters used for primary B cells. 31
Table 24: P493.6 cell lines that express *ACTN1* shRNA. 32
Table 25: Antibodies used for intracellular staining. 33
Table 26: P493.6 cell lines that express LifeAct-mCherry. 35
Table 27: Overview of phospho-proteome analysis of resting P493.6 cells. 71

Abbreviations

α	Anti
aa	Amino acid
ABD	Actin-binding domain
ARP2/3	Actin-related protein 2/3 complex
BCR	B cell antigen receptor
BID	BH3 interacting domain death agonist
BIM	Bcl-2 interacting mediator of cell death
BFL-1	BCL-2-related protein A1
bp	Base pair
BSA	Bovine serum albumin
BTK	Bruton's tyrosine kinase
°C	Degree Celsius
Cas9	CRISPR-associated protein 9
Cbl	Casitas B-lineage lymphoma
CCL	Cleared cellular lysates
CD	Cluster of Differentiation
Cdc42	Cell division control protein 42
cDNA	Complementary DNA
CH	Calponin-homology
CIN85	Cbl-interacting protein of 85 kDa
CIP	Calf intestine phosphatase
CRISPR	Cluster Regulatory Interspaced Short Palindromic Repeats
CMV	Cytomegalovirus
CLSM	Confocal laser scanning microscopy
C-terminus	Carboxy-terminal
DAG	Diacylglycerol
d	Day
dATPs	Deoxyribose adenine triphosphate
DNA	Desoxyribonucleic acid
DAMPs	Damage-associated molecular patterns
DMSO	Dimethylsulfoxide
Dox	Doxycycline
DSMZ	Deutsche Sammlung für Mikroorganismen und Zellkulturen
EBV	Epstein-Barr virus
ECL	Enhanced chemiluminescence
E. coli	*Escherichia coli*
GFP	Green fluorescent protein
ER	Endoplasmic reticulum
ERK	Extracellular regulated kinase
F-Actin	Filamentous Actin
$F(ab')_2$	Bivalent antigen-binding fragment
FC region	Fragment crystallizable region
FCS	Fetal calf serum
FOXO	Forkhead-box-protein O
g	Gram
gag	Group specific antigen, gene encoding p55 (core protein)

GC	Germinal center
GDP	Guanosine diphosphate
GEF	Guanine-nucleotide exchange factor
GRB2	Growth factor receptor-bound protein 2
GTP	Guanosine triphosphate
h	Hours
HCK	Hematopoietic cell kinase
HEPES	N-2-Hydroxyethyl piperazine-N'-2-ethane sulphonic acid
HRK	Harakiri, Bcl-2 interacting protein
HRPO	Horseradish peroxidase
Ig	Immunoglobulin
Indo-1 AM	2-[4-(bis(carboxymethyl)amino)-3-[2-[(bis(carboxymethyl)amino)-5-methylphenoxy]ethoxy]phenyl]-1H-indo-6-carboxylic acide
IP_3	Inositol-1,4,5-trisphosphate
IP_3R	IP_3 receptor
IPTG	Isopropyl-β-D-thiogalacto-pyranoside
IRES	Internal ribosome entry site
ITAM	Immunoreceptor tyrosine-based activation motif
ITIM	Immunoreceptor tyrosine-based inhibition motif
JNK	C-Jun N-terminal kinase
l	Liter
LB	Lysogeny broth
LPC	Lymphoid progenitor cell
LYN	Lck/yes-related protein kinase
kDa	Kilo Dalton
KD	Knock-down
KO	Knock-out
M	Mole
mA	Milliampere
MAPK	Mitogen-activated protein kinases
MCS	Multiple cloning site
MFI	Mean fluorescence intensity
µg	Microgram
Mg	Milligram
MHC	Major histocompatibility complex
min	Minutes
µl	Microliter
ml	Milliliter
µM	Micromole
mM	Millimole
mRNA	Messenger RNA
MS	Mass spectrometry
neg	Negative
NFAT	Nuclear factor of activated T cell
NF-κB	Nuclear factor ‘kappa-light-chain-enhancer’ of activated B cells
nM	Nanomole

NP40	Nonidet P40
N-terminus	Amino-terminal
ORF	Open reading frame
Rac	Ras-related C3 botulinum toxin substrate
p38	Mitogen-activated protein kinase 14
PAGE	Polyacrylamide gel electrophoresis
Ras	Rat sarcoma
PBS	Phosphate buffered saline
PCR	Polymerase chain reaction
PH	Pleckstrin-homology
PI3K	Phosphoinositide 3'-kinase
PIP_3	Phosphatidyl-inositol-3,4,5-trisphosphate
PIP_2	Phosphatidyl-inositol-4,5-bisphosphate
PKB (AKT)	Protein kinase B
PKCβ	Protein kinase C beta
Perm/Wash Buffer	Permeabilization Wash Buffer
PRR	Pattern recognition receptors
PTKs	Protein tyrosine kinases
PUMA	p53-upregulated modulator of apoptosis
Rho	Ras homolog
RNA	Ribonucleic acid
ROS	Reactive oxygen species
pos	Positive
RPMI	Roswell Park Memorial Institute medium
RT	Room temperature
s	Seconds
SDS	Sodium dodecyl sulfate
sgRNA	Single guide RNA
SH2	Src-homology 2 domain
SH3	Src-homology 3 domain
shRNA	Short hairpin RNA
SLP65	SH2 domain-containing leukocyte adaptor protein of 65 kDa
SFKs	Src family kinases
SPT	Single particle tracking
STED	Stimulated emission depletion
SYK	Spleen tyrosine kinase
TAE buffer	Tris Acetate EDTA buffer
TBS	Tris buffered saline
TCR	T cell antigen receptor
TIRF	Total internal reflection microscopy
Tris	Tris-(hydroxymethyl)-amino methane
Triton-X-100	4-(1,1,3,3-Tetramethylbutyl) phenyl-polyethylene glycol ether
UV	Ultraviolet
V	Volt
v/v	Volume/volume
WAS	Wiskott-Aldrich syndrome

WB	Western blot
w/v	Weight/volume
WT	Wild type
X-Gal	5-Bromo-4-chloro-3-indolyl β-D-galactopyranoside

Desoxyribonucleotides

A	Deoxyadenosine monophosphate
C	Deoxycytidine monophosphate
G	Deoxyguanosine monophosphate
T	Deoxythymidine monophosphate

Single-letter amino acid code

A	Alanine
C	Cysteine
D	Aspartic Acid
E	Glutamic-Acid
F	Phenylalanine
G	Glycine
H	Histidine
I	Isoleucine
K	Lysine
L	Leucine
M	Methionine
N	Asparagine
P	Proline
Q	Glutamine
R	Arginine
S	Serine
T	Threonine
V	Valine
W	Tryptophan
Y	Tyrosine

1 Abstract

The B cell antigen receptor (BCR) is involved in many cellular processes that define B cell fate. Once engaged by a cognate antigen, the BCR initiates a series of signaling cascades that drive B cell activation, proliferation, and differentiation. However, even in the absence of antigen binding, the BCR emits a steady-state signal with a very low intensity referred to as antigen-independent BCR signaling or tonic BCR signaling, which is essential for mature B cell survival, since the genetic ablation of BCR expression leads to rapid cell death.

A substantial subset of Burkitt's lymphoma (BL), which is an aggressive form of non-Hodgkin B cell lymphoma, exploits tonic BCR signals for their survival. While large parts of the tonic BCR signal network in BL cells have been identified by mass spectrometry, the details of these signals in the physiological context remain unclear.

Among the identified tonic BCR effectors are many cytoskeleton regulators including the F-Actin cross-linking protein alpha-Actinin-4 (ACTN4), which has been shown to be crucial for BL cell survival. The aim of this thesis was, therefore, to functionally characterize the relevance of ACTN4 for tonic BCR survival signals in human primary B cells. For this purpose, a cellular model was established that enables the investigation of signal transduction in a primary-like B cell state. Based on generated cell lines with abrogated *ACTN4* expression as well as primary human B cells, I could show that ACTN4 contributes to resting mature B cell survival. This effect correlates with an ACTN4-dependent stabilization of the cortical F-Actin, thereby confining the lateral BCR mobility as revealed by single particle tracking microscopy. Analysis of critical BCR effector proteins revealed that less mobile BCRs more efficiently transduce tonic survival signals. This function is ACTN4-specific, since alpha-Actinin-1 (ACTN1), which is also expressed in B cells, is not involved in BCR survival signals.

Hence, this study characterizes ACTN4 as a tonic BCR effector protein in resting mature B cells and implies that the tight regulation of cortical F-Actin dynamics in B cells is critical to control tonic BCR survival signals.

2 Introduction

2.1 Overview of the human immune system

The human immune system, consisting of both the innate and adaptive branches, effectively combats and eliminates a wide variety of pathogens such as bacteria, viruses, and parasites that invade physical barriers of our body such as the skin and mucosal tissues. Additionally, the immune system recognizes and kills transformed or infected cells, preventing the growth of tumors and other diseases [1,2].

Immune cells differentiate from a hematopoietic stem cell (HSC) in the bone marrow into a common myeloid progenitor (CMP) and a common lymphoid progenitor (CLP). A CMP gives rise to various types and subtypes of effector cells that make up the innate immunity. On the other hand, a CLP differentiates into lymphocytes that form the basis of adaptive immunity, with the exception of natural killer (NK) cells, which are considered as innate immune cells [2].

Innate immune cells such as dendritic cells, macrophages and granulocytes constitute the first defense barrier against pathogenic invaders. These cells usually recognize highly conserved pathogen-derived structures known as pathogen-associated molecular patterns (PAMPs). In addition, they also recognize and respond to molecules released from damaged, necrotic, or virally infected cells known as damage-associated molecular patterns (DAMPs). Both PAMPs and DAMPs bind to pattern recognition receptors (PRRs) expressed by innate immune cells, which leads to their activation and cytokine production, thereby attracting other immune cells and triggering inflammation [3].

Adaptive immunity comprises B and T lymphocytes that elicit humoral and cell-mediated immune responses, respectively. In contrast to innate immune cells, which recognize a general antigenic pattern and elicit an immediate immune response, adaptive immune cells mediate a more delayed but highly specific immune response. Both B and T cells express an antigen receptor (BCR and TCR, respectively), which possesses a unique specificity against distinct peptide antigens that are otherwise not recognized by innate immune cells [4]. Furthermore, adaptive immune cells are characterized by the generation of memory after the clearance of invaders by differentiating into memory B and memory T cells that are rapidly reactivated upon a second encounter with the same antigen [2,4].

The precise interaction between innate and adaptive immune cells allows for a coordinated response against invading pathogens. For instance, pathogen-derived antigens are internalized, processed, and presented as peptides by antigen-presenting cells such as dendritic cells and macrophages on a major histocompatibility complex class II (MHC II) molecule for adaptive immune cells called $CD4^+$ helper T cells that elicit adaptive immune responses [5,6].

Since this study investigates the antigen-independent mode of BCR signaling, the next chapters will first introduce the development of B lymphocytes and subsequently discuss the importance of BCR signaling for normal and transformed B cell survival.

2.2 B lymphocyte development

The existence of cells with a pre-formed antibody receptor was first proposed in 1890 by Von Behring and Kitasato [7]. The explanation of the physical nature of antibodies as well as the concept of antigen-antibody interaction only emerged in the 1930s, while the identification of the cellular source of antibodies came later in 1948 with the observation that plasma cell development correlates with an antibody response after immunization [8,9]. However, the discovery and identification of B cells was reported in 1965 when Max Cooper and Robert Good suggested that cells in the chicken bursa of Fabricius are responsible for antibody production [10].

It is known that a multipotent HSCs can differentiate into CLPs, which are the precursors for B cells (Figure 1) [11,12]. A CLP further develops into a pro-B cell. At this developmental stage, B cells first rearrange variable (V_H), diversifying (D_H), and joining (J_H) gene segments of the immunoglobulin (Ig) heavy chain locus [13,14]. As a result, a pro-B cell further develops into a pre-B cell, which is endowed with a pre-B cell receptor (pre-BCR) [13]. The pre-BCR is composed of two Ig heavy chains paired with two surrogate light chains and the integral signal transduction moiety, made up of Igα and Igβ (CD79A and CD79B, respectively), which are bound together via disulfide bridges [13,15]. Thereafter, V_L- and J_L-gene segments of the Ig light chain locus are rearranged, and the pre-BCR is downregulated and replaced by a functional BCR composed of two Ig heavy and two Ig light chains [13–15].

After the successful generation of a fully functional BCR, B cells are still immature and migrate from the bone marrow to the secondary lymphoid tissue such as the spleen, lymph nodes, tonsils, or mucosa-associated lymphoid tissues, where they further develop into naïve mature B cells [13]. Upon encounter with their cognate antigen, naïve B cells become activated, leading to their proliferation and differentiation into short-lived plasma cells that secrete low-affinity antibodies, or they seed in lymphoid follicles to form a germinal center (GC) [13]. The GC is a specialized microenvironment within secondary lymphoid organs, where B cells undergo intense proliferation (clonal expansion), somatic hypermutation (SHM), and class switch recombination (CSR). Both SHM and CSR require the enzyme activation-induced deaminase (AID), the expression of which is initiated in the GC and in some extrafollicular B cells [16–19] (Figure 1).

SHM describes the process by which point mutations are introduced in the *IG* loci (*IGV*), which encode for the variable region of the Ig, resulting in an altered binding affinity of the Ig to its cognate antigen. Cells that express Igs with improved antigen-binding affinity are positively selected. In addition, AID induces DNA double-strand breaks (DSBs) in the *IG* heavy chain gene (*IGH*) that encodes the domains determining antibody class. Induced DSBs trigger CSR, by which an antibody's isotype is switched to another class, thereby fulfilling diverse biological properties. Therefore, both SHM and CSR are essential for adaptive humoral immune responses [17–19].

Finally, B cells that egress the germinal center can further differentiate into antibody-secreting cells, whereas some differentiate into long-lived memory B cells that are rapidly reactivated in case of reinfection with the same antigen [20].

The BCR is a crucial component of mature B cells. It consists of a transmembrane version of an Ig equipped with a CD79A and CD79B heterodimer [21]. This architecture enables the BCR to sense and react against extracellular stimuli, and to translate and convey signals into the cell-interior [21]. Igs, the building blocks of B cell receptors, are composed of two heavy chains and two light chains. These chains, bound together by disulfide bridges, exist in two variants: kappa (κ) and lambda (λ). Each variant contributes to the immunological diversity [22]. The different Ig classes IgM, IgD, IgG, IgA, and IgE have distinct immunological functions and are differentially distributed in our body [22]. For instance, IgG antibodies are the most abundant in humans and have crucial properties in humoral immune responses, including opsonization, neutralization, and activation of the complement system [23]. Recently, studies have also unveiled the profound importance of membrane-anchored IgM. Beyond its fundamental role in antigen capture, B cell activation, and differentiation, it mediates survival signals, indispensable for maintaining the pool of mature B cells [24].

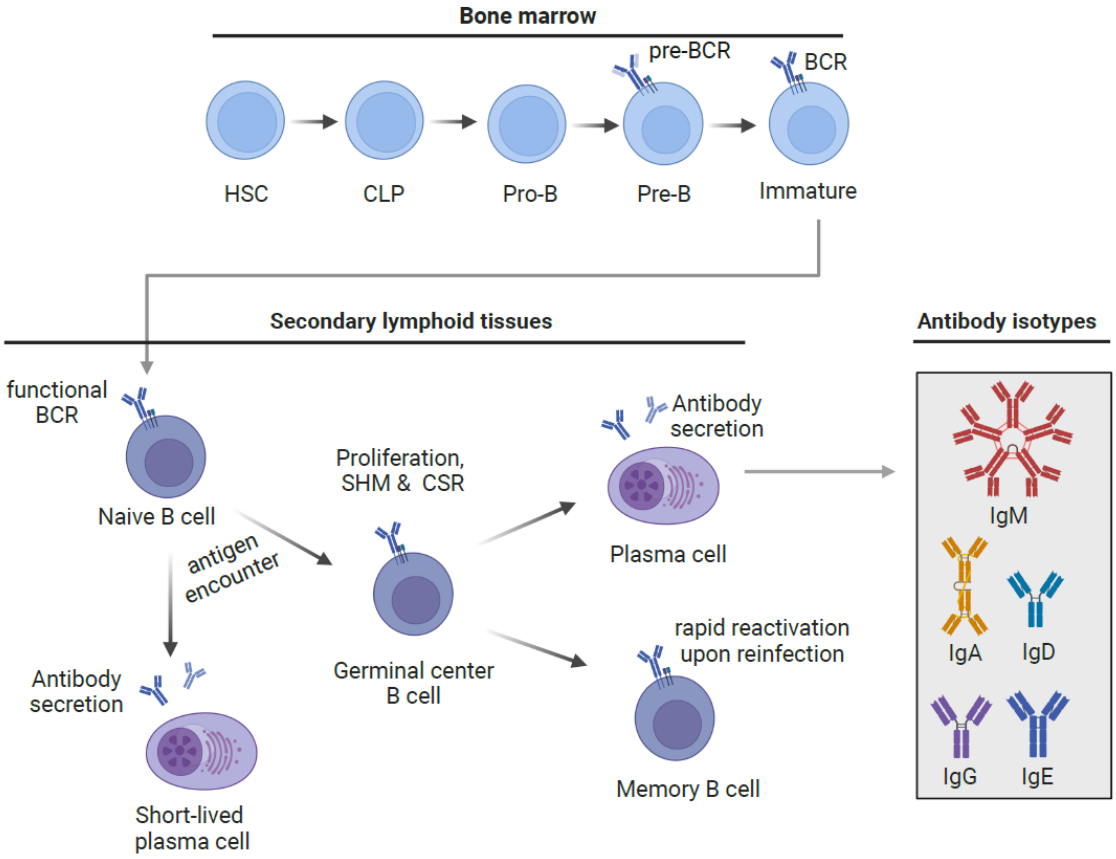

Figure 1: Schematic overview of B cell development.
Bone-marrow-resident hematopoietic stem cells (HSCs) differentiate into common lymphoid progenitors (CLPs) which further develop into pro-B cells. At the pro-B developmental stage, B cells rearrange their heavy chain gene segments which enable the expression of a pre-BCR composed of two identical heavy chains and two surrogate light chains. After the rearrangement of their light chain gene segments, pre-B cells develop into immature B cells that express a functional BCR and migrate to the circulation and periphery where they mature, encounter antigens, and form the germinal center (GC). In the GC, B cells improve not only the antigen binding affinity of their immunoglobulins (Igs) but also its biological function in processes referred to as somatic hypermutation (SHM) and class-switch recombination (CSM), respectively. As a result of GC reactions, B cells can further differentiate either into a plasma cell that secretes antibodies or into a memory B cell that is rapidly reactivated upon reinfection with the same antigen. Created with BioRender.com.

2.3 B cell antigen receptor signaling

Once the BCR is engaged by a cognate antigen, it initiates a series of signaling cascades, leading to B cell activation, proliferation, and differentiation. The process of signal transduction involves a set of phosphorylation and dephosphorylation events accomplished by kinases and phosphatases, respectively. Moreover, signal transduction also requires adaptor proteins, trafficking molecules, cytoskeleton regulators, and others that ultimately lead to the activation of transcription factors that drive gene transcription and *de novo* protein synthesis [25].

Since the BCR has been shown to determine B cell fate, researchers have aimed to understand how antigen binding induces BCR signaling. Currently, two different models of BCR activation are proposed. The first model is known as the association-dissociation model, which suggests that the BCRs are pre-clustered in protein islands on the surface of resting B cells. According to this model, antigen binding induces dissociation of the pre-clustered BCRs, which renders the cytoplasmic domain of CD79A and CD79B heterodimer accessible for phosphorylation and signaling initiation by kinases [26]. The second model is referred to as a conformation-induced oligomerization or cross-linking model. This model proposes that monomeric BCRs are dispersed on the surface of B cells and lack BCR-BCR interaction. However, once engaged by a polyvalent antigen, multiple BCRs are cross-linked, enabling the formation of BCR micro-clusters. BCR ligation, according to this model, results in a different conformation, facilitating the exposure of the CD79A and CD79B heterodimer for phosphorylation and signaling initiation [27]. In a recent study that utilized super-resolution stimulated emission depletion (STED) microscopy to assess these models, it was demonstrated that BCRs exist as a mixture of monomers and dimers on the surface of resting B cells, and no higher oligomeric BCR structures were observed. The results of this study substantiate the validity of the cross-linking model [28].

The transmembrane Ig itself is incapable of signal transduction and requires the non-covalently associated CD79A and CD79B heterodimer. Ligation of the BCR triggers the phosphorylation of intracellular immunoreceptor tyrosine-based activation motifs (ITAMs) located in this signaling heterodimer by protein tyrosine kinases (PTKs) such as Src family kinases (SFKs) [21]. SFKs are non-receptor PTKs that comprise LYN, SRC, YES, YRK, FYN, BLK, and HCK [29]. SFKs are kept in an inactive conformation by a phosphorylated inhibitory tyrosine residue at its C-terminus, the dephosphorylation of which allows SFKs to adopt an open conformation, leading to further auto-phosphorylation events that render the kinase fully active [30]. The Lck/Yes-related novel protein tyrosine kinase (LYN) also plays a prominent role in the negative regulation of BCR-mediated signaling since it also phosphorylates immunoreceptor tyrosine-based inhibition motifs (ITIMs) located in the cytoplasmic tail of inhibitory receptors such as CD22, CD5, and FCγRIIB. Consequently, phosphorylated ITIMs recruit phosphatases such as the protein tyrosine phosphatase non-receptor type 6 (PTPN6, also known as SHP-1) and the inositol polyphosphate phosphatase like 1 (INPPL1, also known as SHIP2) that attenuate BCR signaling [31–33].

ITAM phosphorylation in CD79A and CD79B provides binding sites for the PTK spleen tyrosine kinase (SYK), which is essential for BCR signal initiation. This protein consists of tandem SH2 domains, allowing for binding to doubly phosphorylated ITAMs [34]. Due to SYK recruitment, its kinase domain is

relieved, and this allows for further auto- and trans-phosphorylation on activatory tyrosine residues, such as Y525/Y526, rendering the kinase fully active [35]. Once SYK is activated, it phosphorylates the SH2-domain-containing leukocyte adaptor protein of 65 kDa (SLP65). SLP65, also known as BLNK, is recruited to the phosphorylated non-ITAM tyrosine residue 204 located only in CD79A. This brings SLP65 in close proximity to SYK and enables further phosphorylation events that create docking sites for SH2 domain-containing proteins [36–38]. In addition, various proline-rich regions are present in SLP65 and serve as interaction motifs for SH3 domain-containing proteins. These properties allow SLP65 to have multiple interactions with signaling molecules, facilitating their recruitment and signalosome formation [39,40]. Hence, SLP65 is considered the central scaffold platform in BCR signaling, which is also evident from the fact that in humans, mutations in *SLP65* result in the arrest of B cell development at the pro-B to pre-B cell transition, leading to agammaglobulinemia [41,42].

SLP65 is a permanent interaction partner of a molecule known as the Cbl-interacting protein of 85 kDa (CIN85). A stable interaction between both proteins is required to ensure proper Ca^{2+} mobilization and the activation of the nuclear factor of kappa-light-chain-enhancer of activated B cells (NF-κB) [38,43]. In antigen-dependent BCR signaling, the SLP65 and CIN85 complex together with Burton's tyrosine kinase (BTK) and Phospholipase c gamma 2 (PLCγ2) form the so-called Ca^{2+}-initiation complex [44]. BTK, PLCγ2, and the guanine nucleotide exchange factors of the Vav family (VAV) mainly occupy phosphorylated tyrosine residues of SLP65 *via* their SH2 domains [38,45]. Subsequently, BTK further activates PLCγ2, which hydrolyzes phosphatidyl-insoitol-4,5-bisphosphate (PIP_2) into inositol-1,4,5-trisphosphate (IP_3) and diacylglycerol (DAG) [46]. While DAG remains anchored in the inner leaflet of the plasma membrane, IP_3 molecules are free to bind their receptors (IP_3R), which are ligand-gated Ca^{2+} channels located at the outer membrane of the endoplasmic reticulum (ER). As a result, Ca^{2+} channels are opened and Ca^{2+} is released from the ER into the cytosol [44]. Released Ca^{2+} is then sensed by Ca^{2+}-dependent serine/threonine Phosphatases called Calcineurins, which in turn dephosphorylate the cytosolic transcription factor, the nuclear factor of activated T cells (NFAT), resulting in its nuclear translocation and thereby driving NFAT-dependent gene expression [44]. Furthermore, DAG recruits and activates protein kinase C beta (PKCβ), which ultimately leads to the activation of the transcription factor NF-κB by facilitating its relief from its inhibitor IKBα [47]. As a result, NF-κB enters the nucleus, allowing for NF-κB-dependent gene expression (Figure 2).

In addition, antigen-induced BCR signaling leads to the recruitment of the adaptor protein growth factor receptor-bound protein 2 (GRB2) to the BCR and thereby contributes to the activation of the mitogen-activated protein kinase 3 and 1 (MAPK3/1 or ERK1/2) [48]. Similarly, BCR ligation also activates the MAPK8, also known as C-Jun N-terminal kinase (JNK), and the MAPK14 (p38) [49]. Furthermore, the co-receptor CD19 lowers the threshold for BCR activation by recruiting the phosphoinositide-3 kinase (PI3K), which converts PIP_2 into phosphatidylinositol (3,4,5)-trisphosphate PIP_3 [50,51]. The generated PIP_3 serves as an anchor for PH domain-containing proteins such as BTK, PLCγ2, and the serine/threonine protein kinase B (PKB, also known as AKT) [52,53]. The latter is involved in different aspects of B cell fate, particularly B cell survival, by regulating the activity of many downstream target proteins [54,55]. Among AKT-downstream effector proteins is the transcription factor forkhead-box-protein O (FOXO). The phosphorylation of FOXO by AKT inhibits its transcriptional activities that otherwise contribute to

apoptosis induction [56,57]. Another study revealed that Nck-mediated recruitment of phosphoinositide-3-kinase adaptor protein (PIK3AP1, also known as BCAP) to the BCR also regulates the PI3K-AKT pathway in B cells [58].

Collectively, BCR signaling controls B cell fate in many aspects including proliferation, differentiation, and survival. This takes place through the activation of effector proteins such as AKT and the MAP-kinases ERK, JNK, and p38, as well as transcription factors such as NF-κB and NFAT (Figure 2).

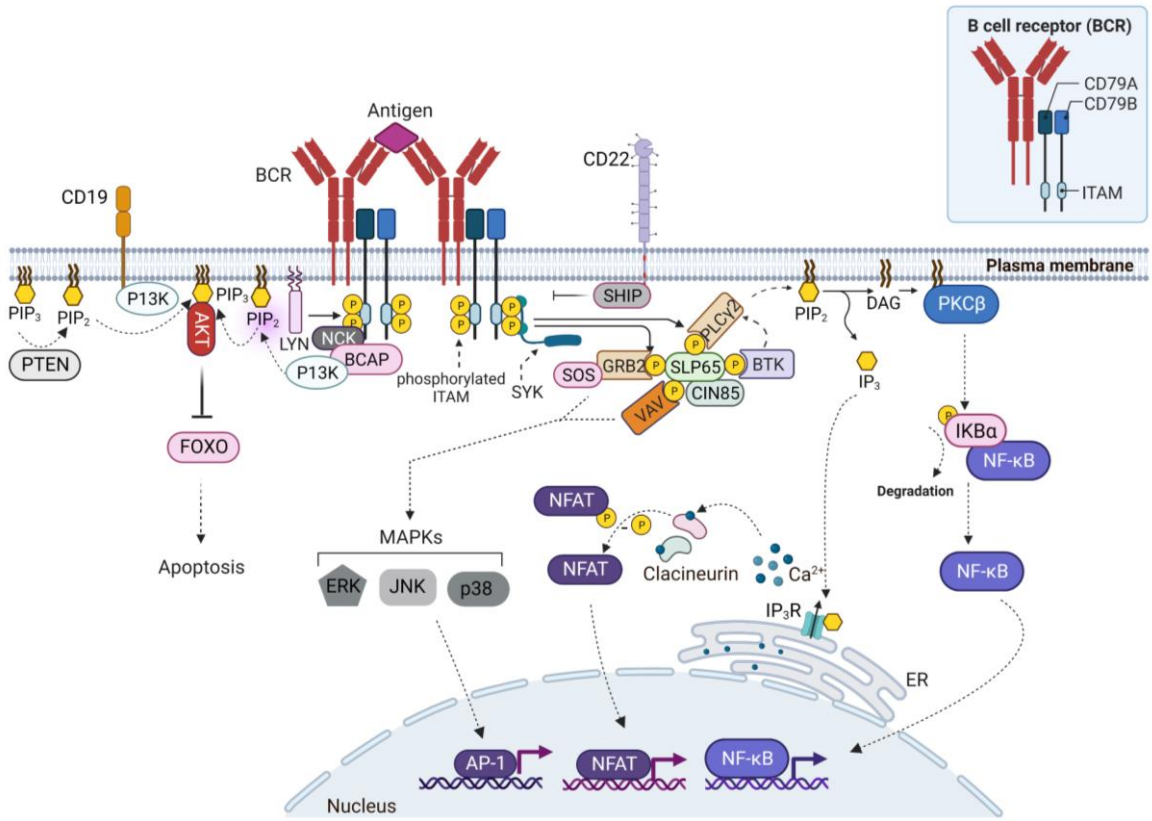

Figure 2: Schematic overview of B cell antigen receptor signaling.
Engagement of the BCR with its cognate antigen results in the phosphorylation of ITAMs located within the CD79A and CD79B heterodimer, which is accomplished by PTKs, such as SYK and LYN. In turn, SYK is recruited to phosphorylated ITAMs, allowing for its activation. Activated SYK phosphorylates the adaptor molecule SLP65, resulting in the recruitment of several signaling molecules such as BTK, GRB2, and PLCγ2. BTK further promotes PLCγ2 activity, which hydrolyzes PIP_2 into DAG and IP_3. DAG remains anchored in the plasma membrane and activates PKCβ, resulting in the relief of NF-κB from its inhibitor IκBα and allowing for its activation. IP_3 binds IP_3R expressed on the surface of the ER, resulting in Ca^{2+} release into the cytosol. Consequently, Ca^{2+} binds to and activates the phosphatase Calcineurin, leading to the dephosphorylation of NFAT, resulting in its activation. Similarly, the MAPKs ERK, JNK, and p38 are also activated, resulting in the phosphorylation of downstream targets. In addition, BCR signaling is further promoted by CD19, which lowers the threshold for BCR activation by recruiting PI3K to the BCR. NCK-mediated recruitment of BCAP to the BCR also regulates PI3K activity. Subsequently, PI3K phosphorylates PIP2 to PIP3, which serves as an anchor point for AKT and allows for its activation. As a result, AKT promotes cell survival by inhibiting FOXO, which is involved in apoptosis induction. Moreover, phosphorylated ITIMs located within the cytoplasmic tail of negative co-receptors such as CD22 create docking sites for phosphatases such as SHIP, which attenuates BCR signaling. Created with BioRender.com.

2.4 Tonic BCR signaling

While antigen binding to the BCR triggers signal transduction, numerous studies conducted in the last two decades provided evidence that the BCR emits a steady-state, low-intensity signal that is essential for healthy mature B cell survival [24,59]. The first indications for the ability of BCR complexes to signal independently of ligand binding were provided based on phosphatase-inhibitor studies that showed a BCR-dependent *de novo* tyrosine phosphorylation of BCR-associated signaling proteins [60]. This study was also the first to implicate reactive oxygen species (ROS) in the regulation of basal signaling activity of ligand-independent signaling by inactivating protein tyrosine phosphatases (PTPs) [60].

Later studies showed that a permanent expression of the BCR is essential to maintain the peripheral B cell pools. This is evident since its diminished expression on the surface of mature B cells using an inducible gene targeting system led to rapid cell death [59]. However, the first study to directly evaluate the functional role for tonic signaling through the BCR of resting mature B cells was conducted by Kraus *et al.* using an inducible system to abrogate *CD79A* and *CD79B* expression *in vivo*. This study highlights the notion that signals *via* the BCR, rather than the BCR complex *per se*, are essential for tonic BCR survival signals [24].

Effector proteins of tonic BCR signaling were deduced after conditionally ablating the BCR expression combined with conditional activation of candidate signaling cascades. Srinivasan *et al.* reported that the activation of the PI3K/AKT signaling pathway or the inhibition of its opponent the phosphatase PTEN ensured BCR-negative (BCR^{neg}) resting mature B cell survival [57]. In addition, the regulation of tonic BCR signaling requires the spatial organization of signaling complexes within specialized compartments known as lipid rafts. These compartments are usually formed in response to antigen binding and are believed to stabilize signaling complexes in resting B cells [61–63].

Moreover, previous studies proposed that tonic BCR signaling is coordinated by positive and negative co-receptors [61]. The phosphatase CD45 is believed to contribute to tonic BCR signaling as a positive regulator by dephosphorylation of inhibitory tyrosine residues of the signal-initiating SFKs [61,64]. A recent report showed that CD45-deficient mice B cells have an altered B cell development and reduced tonic BCR signaling intensity, while BCR-engaged signaling was not affected [65]. On the other hand, BCR co-receptors such as CD22 negatively regulate antigen-induced BCR signaling by recruiting the BCR phosphatase SHP-1. Hence, it is proposed that it also attenuates BCR signaling in the absence of antigens [66].

Considering that tonic BCR signaling is vital for B cells, a model for the integration of tonic and activated BCR signaling was developed to predict primary B cell survival. This study reported that primary B cells with high BCR expression levels survive more efficiently than those with low BCR expression levels in an antigen-independent manner [67]. Moreover, they could also show that the efficiency of primary B cell survival can be influenced in response to the strength and duration of BCR-engagement, as BCR cross-linking with low doses of anti-IgM decreases cell survival, its ligation with higher anti-IgM doses enhances cell survival [67].

Besides healthy mature B cells, a substantial portion of Burkitt's lymphoma (BL) cells exploit a dysregulated form of tonic BCR signaling for their survival [68]. In the next chapter, the different pathogenic forms of BCR signaling, with emphasis on tonic BCR signaling in BL cells, will be briefly illustrated.

2.5 Dysregulated BCR signaling in B cell malignancies

Many B cell neoplasms depend on BCR expression and BCR-mediated signaling for their survival, and this seems to be an important feature in their pathogenesis [69]. Different stimuli can trigger aberrant BCR-mediated signaling in B cell lymphomas and leukemias, such as tonic BCR signaling, chronic exposure of the BCR to self-antigen, self-binding properties of the BCR, continuous BCR stimulation by microbial antigens, and activating mutations within the BCR complex or downstream signaling component [70,71]. For example, in activated B cell diffuse large B cell lymphoma (ABC-DLBCL), the BCR is chronically active and thereby activating signaling pathways such as PI3K/AKT, MAPKs, NFAT, and NF-κB. BL cells, however, exploit tonic signaling similarly to healthy mature B cells, and signal transduction primarily occurs through the PI3K/AKT/mTOR pathway. Notably, both signaling modes (chronic and tonic) require SFKs and SYK to drive downstream effectors [72].

Since BCR signaling has been shown to be implicated in several types of B cell lymphoma, targeting of the BCR signaling pathway and BCR effectors has become a matter of particular interest. Currently, BCR-associated signaling molecules such as BTK, PI3K, SYK, and PKCβ are suggested as main targets for the treatment of B cell malignancies [72]. Particularly, the BTK inhibitor ibrutinib has been shown to be quite efficient for the treatment of B cell malignancies with chronic BCR singling and an active NF-κB pathway [72,73]. By contrast, treating BL cells with ibrutinib is less efficient in most cases because the NF-κB pathway seems to be dispensable for a significant portion of BL cells [73,74]. Therefore, since the elucidation of mechanisms that underlie the dysregulated tonic BCR signaling network in BL cells could reveal novel BCR effectors as targets for therapy, researchers aim to decipher the pathological form of tonic BCR signaling in BL cells.

Recently, mass spectrometry (MS)-based phospho-proteome analysis was conducted to elucidate both tonic and activated BCR signaling in BL cell lines. This study revealed a number of tonic BCR effectors that have not been described yet in terms of BCR signaling [68]. Most of these effectors were identified by reduced phosphorylation upon CD79A downregulation and/or SYK inhibition. Although the majority of uncovered BCR effectors seems to participate in both modes of signaling (tonic and activated), others appear to be restricted in their contribution to either of the BCR signaling modes [68]. In accordance with previously published data [58,75], their study identified the PI3K-activating complex consisting of LYN, NCK, and BCAP to be phosphorylated in tonic BCR signaling. Many cytoskeleton proteins also seem to be involved in tonic BCR signaling, such as Tubulin alpha 1b (TUBA1B), Actin gamma 1 (ACTG1), Abelson protein tyrosine kinase 2 (ABL2) and Leupaxin (LPXN) [68]. Notably, LPXN has been described as a negative regulator of BCR signaling [76]. Moreover, their results revealed the membrane trafficking molecule Brefeldin A-Inhibited Guanine Nucleotide-Exchange Factor 2 (ARFGEF2) and the cytoskeleton cross-linking protein Alpha-Actinin-4 (ACTN4) to be involved in tonic BCR signaling and

required for BL cell survival [68]. The next chapter will describe the role of B cell cytoskeleton components in BCR signaling.

2.6 B cell cytoskeleton dynamics in BCR-mediated signaling

As recently reported, a mature B cell possesses up to 200,000 BCRs on its surface [77]. The cortical area underneath the plasma membrane comprises a meshwork of Actin filaments that constitute the cortical Actin cytoskeleton in B cells. Actin polymerization is regulated by monomeric Actin-binding proteins such as Profilin and Thymosin as well as Actin filament nucleators such as the Actin-related protein 2/3 complex (ARP2/3) and Formin [78]. The structure and dynamics of this network are further coordinated by Actin-severing proteins such as Cofilin and cross-linkers such as alpha-Actinins (ACTNs). This facilitates Actin polymerization and depolymerization and serves the dynamic nature of the cortical Actin meshwork in response to extracellular stimuli [78]. The existence of the cortical Actin cytoskeleton creates barriers and forms compartments that constrain BCR diffusion (known as the fence and picket model) [79,80].

The fence and picket model emphasizes the fluidity and mosaic nature of the plasma membrane, highlighting the interactions and mobility of its components. This concept is supported by studies that have addressed the impact of cortical B cell cytoskeleton disruption on BCR conformation as well as on BCR-associated signals [81]. For instance, treatment of resting B cells with the Actin depolymerization agent Latrunculin A or Cytochalasin D is sufficient to trigger BCR signaling without BCR cross-linking [81]. The extent of calcium release resulting from cytoskeleton disruption is akin to that induced by BCR engagement. By contrast, treatment of resting B cells with the Actin stabilization agent Jasplakinolide prevents Actin depolymerization and the formation of BCR clusters upon stimulation [81] .

The cortical Actin cytoskeleton of B cells is attached to membrane proteins through the cytoskeleton protein “Ezrin” [82]. Cross-linking of the BCR induces its dephosphorylation, which is one of the earliest events upon BCR stimulation. Once dephosphorylated, Ezrin is detached from the plasma membrane [83]. Consequently, the cortical Actin network depolymerizes, thereby facilitating BCR diffusion (lateral BCR mobility) and the formation of BCR micro-clusters [83,84]. Subsequently, the cortical Actin reassembly enables signaling maintenance. Ultimately, the coalescence of BCR micro-clusters into a super-cluster allows for signaling termination and BCR internalization. Thus, the cortical Actin cytoskeleton plays a pivotal role in signaling initiation, maintenance, and termination [82–84].

Although the role of the cortical Actin cytoskeleton in B cells is poorly described with respect to BCR-mediated signaling, immunodeficiencies affecting cytoskeletal proteins such as Wiskott-Aldrich syndrome (WAS) have been well described in the literature [85,86]. This immunodeficiency occurs due to mutations affecting *WAS* or *WIPF1* genes, encoding WAS protein (WASP) and WASP-interacting protein (WIP), respectively, resulting in defects in Actin polymerization and branched F-Actin nucleation [86]. Thus, WASP is considered a key regulator of Actin homeostasis in hematopoietic cells [85]. The fact that partial loss of cytoskeleton integrity causes broad and severe defects in immune cell functions, such as B cell activation, proliferation, and migration, emphasizes the crucial role of F-Actin remodeling in B cell biology [86]. Previously, it was reported that B cells originating from patients with WASP deficiency show aberrant BCR signaling [87].

Moreover, it was demonstrated that the WASP-like Actin nucleation-promoting factor (N-WASP), which is co-expressed with WASP in all immune cells, negatively regulates BCR signaling [88]. WASP is an upstream negative regulator of N-WASP in mouse and human primary B cells [88]. While BTK-induced WASP activation suppresses N-WASP activation, the activation of SH2 domain-containing inositol 5-phosphatase (SHIP-1) inhibits WASP activation, thereby relieving N-WASP inhibition [88]. Hence, Actin polymerization and depolymerization are fine-tuned by kinases and phosphatases during BCR signaling.

Since the impact of cortical Actin on BCR signaling is evident, and as BCRs assembled in different conformations such as micro-clusters or large central clusters exhibit different levels of signaling activity, several studies aimed to elucidate the correlation between Actin dynamics, BCR conformation, and BCR signaling [84]. The first major pathway that connects BCR signaling with Actin polymerization involves the activation of ARP2/3 by WAS proteins to promote the formation of branched Actin filaments [89,90]. A recent study demonstrated that inhibition of ARP2/3 in murine primary B cells results in reduced BCR diffusion, less micro-cluster formation, and increased signaling in response to BCR ligation [91]. In an antigen-independent manner, ARP2/3 inhibition results in increased BCR diffusion and augmented BCR signaling indicated by enhanced basal phosphorylation levels of ERK and AKT [91].

Moreover, a study conducted in primary murine B cells revealed eight different diffusive states with distinct signaling properties for tracked BCR populations upon BCR engagement [92]. Their study reported that although the inhibition of ARP2/3 or Formin (Actin polymerization protein) decreases BCR diffusion in response to BCR stimulation, specific BCR diffusive states are affected. Their data suggest a complex correlation between BCR diffusivity and BCR signaling, which requires several cytoskeleton proteins that control cortical filamentous Actin (F-Actin) remodeling [92]. According to their results, BCR ligation leads to an increased number of BCR populations with a low diffusive state accompanied by an equivalent reduced number of BCR populations with higher diffusive states, suggesting a transition between the different diffusion states. While single BCRs are more likely to exist in a higher diffusive state than BCRs in clusters, a transition from higher to lower diffusive states increases the probability that single BCRs are coalesced into a cluster, reducing the overall BCR diffusion and increasing BCR signaling [92]. This confirms previous observations that during B cell activation BCR monomers have high mobility and low signaling. However, once incorporated into clusters, they become less mobile and exhibit increased signaling [78,83]. Thus, cytoskeleton dynamics maintain the heterogeneity of BCR diffusion and nanoscale organization, thereby controlling BCR signaling [27,83].

Since Corso *et al.* revealed ACTN4 to be an effector protein in tonic BCR signal transduction and to be vital for BL cells, the next chapter will illustrate the diverse functions of ACTN4 and its highly homologous protein ACTN1, especially as F-Actin cross-linking proteins in the context of cell signaling and survival processes.

2.7 F-Actin cross-linking by alpha-Actinin proteins

ACTNs are ubiquitous Actin cross-linking family proteins with four members (ACTN1-4) expressed by distinct genes. While *ACTN4* and *ACTN1* are mainly expressed in non-muscle cells, *ACTN2 and ACTN3* are expressed in muscle cells [93]. ACTNs form an anti-parallel rod-shaped dimer *via* spectrin domains with one Actin-binding domain (ABD) at each end of the dimer serving Actin binding (Figure 3). In addition, ACTNs were reported to have interactions with cytoskeletal and signaling molecules and to be recruited to the cytoplasmic tail of transmembrane receptors and ion channels. In terms of tumorigenesis, accumulating evidence is highlighting that the non-muscle ACTNs, particularly ACTN4, contribute to the malignant phenotype of cancer cells [93_95].

ACTN4 is implicated in several cellular processes and functions including adhesion, proliferation, and migration [96]. In addition, it has been identified as a transcriptional regulator of NF-κB in the nucleus regardless of its Actin binding capacity [97,98]. In numerous types of malignant tumors such as ovarian, colorectal, and breast cancer, *ACTN4* expression is dysregulated and its overexpression is involved in the tumorigenesis by providing tumor cells with a metastatic potential [96,99]. The non-muscle ACTN1 has also been shown to contribute to the malignant phenotype of some cancer cells, but to a lesser degree than ACTN4. For instance, its overexpression in gastric cancer cells promotes epithelial-mesenchymal transition and inhibits apoptosis by impacting the AKT/GSK3β/β-catenin pathway [100].

Although ACTN4 and ACTN1 share 80% nucleotide and 86.7% amino acid (aa) similarity, rendering the general domain structures highly homologous, they are differentially regulated and have distinct interaction partners [99,101_105] (Figure 3). Tyrosine phosphorylation of ACTN4 and ACTN1 is critical for cytoskeletal processes such as stress fiber establishment, maintenance, and focal adhesion maturation, though each has distinct modes of regulation. While tyrosine phosphorylation at Y12 is critical for the cytoskeletal function of ACTN1, phosphorylation at Y265 is crucial for ACTN4 [103,106]. Furthermore, it was reported that ACTN4, but not ACTN1, is more abundant in the Actin cytoskeleton of astrocytoma cells. The downregulation of ACTN4 expression, but not ACTN1, results in reduced cortical Actin and RhoA signaling, suggesting different biochemical properties and regulatory mechanisms [95]. In T cells, ACTN1 was identified as a novel phospho-tyrosine-containing protein following TCR ligation, raising the possibility of a role in TCR signaling [107].

According to the literature, only *ACTN4* and *ACTN1* are expressed in B cells, and they are poorly described in the context of hematopoietic cells, particularly in B cells, although a recent study suggested ACTN4 and ACTN1 as a component of the cortical cytoskeleton in B cells [78]. In response to BCR ligation, ACTN4 has been shown to be phosphorylated at Y265 [68].The phosphorylation of ACTN4 at Y265 was also affected by CD79A downregulation and SYK inhibition in tonic BCR signaling [68]. In other cell lines, phosphorylated ACTN4 at Y265 has shown to increase the binding affinity of ACTN4 to F-Actin [108].

In general, ACTN4 binding affinity to F-Actin is tightly regulated by several factors such as phosphorylation events, Ca^{2+} binding, and various interaction partners. For instance, tyrosine phosphorylation events within the N-terminus of ACTN4 attenuate its F-Actin binding affinity, while phosphorylation events occurring in its ABD increase its affinity to F-Actin [108]. Its C-terminus, however, regulates its susceptibility to m-calpain-mediated degradation [109]. ACTN4 also possesses

a calmodulin-like domain composed of two EF-hands, which are reported to be Ca^{2+}-sensitive in non-muscle cells. Ca^{2+} binding to EF-hands decreases ACTN4 binding affinity to F-Actin [110,111]. *In vivo*, ACTN4 forms a homodimer to cross-link F-Actin, which facilitates F-Actin dynamics and organization. The binding of ACTN4 to F-Actin is enabled by its ABD, which compromises three Actin-binding sites (ABSs) [110,112].

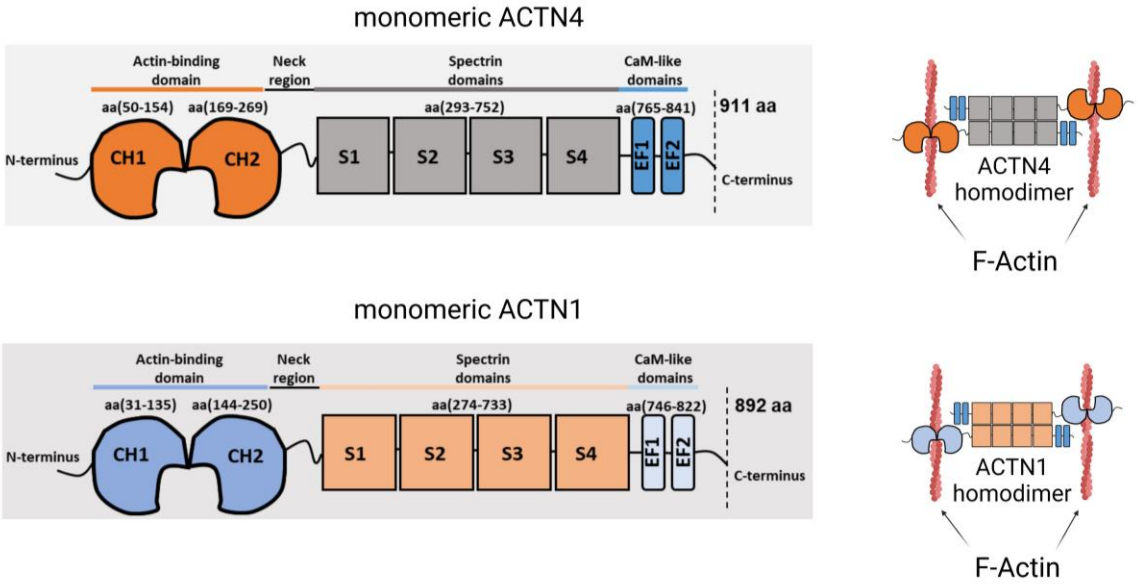

Figure 3: Schematic overview of ACTN4 and ACTN1 domain structures.
Monomeric ACTNs are composed of two calponin homology domains (CH1 & CH2) that form the Actin-binding domain (ABD; enabling F-Actin binding), neck region, four spectrin domains (S1-S4) that serve ACTNs homodimerization, and calmodulin-like domain (CaM-LD) comprising two Ca^{2+}-sensitive EF-hands that regulate the binding affinity of ACTNs to F-Actin. To cross-link F-Actin, monomeric ACTNs form an anti-parallel homodimer facilitated by spectrin domains.

2.8 Aim of this study

ACTN4 has been revealed by elucidation of tonic BCR signaling in BL cells and has been shown to be crucial for their survival. However, its role in tonic BCR signal transduction of human primary B cells remains to be explained. Hence, this study aims to analyze the function of ACTN4 in tonic BCR survival signaling of human primary B cells (Figure 4).

For this purpose, I sought to establish a cellular model that is suitable for the investigation of BCR signaling processes that resemble primary human B cells. This is important since functional analyses in primary human B cells harbor several obstacles, such as a limited lifespan and limited options for gene targeting. To this end, I will utilize the B cell model P493.6, which allows for a tetracycline inducible abrogation of *MYC* expression leading to cell cycle arrest. Thus, the treatment of P493.6 cells with tetracycline switches the cell phenotype from a proliferative (BL-like) into a resting state that resembles the situation of human primary B cells. By comparing the signaling properties of these cells with commonly used BL-derived B cell lines I will elaborate on the suitability of this B cell model for my study.

On the genetic background of the P493.6 cell model, *ACTN4* expression will be targeted by CRISPR/Cas9-based gene editing. Moreover, the role of ACTN1, the close relative of ACTN4, will be

assessed by reducing its expression *via* shRNA-mediated downregulation. The generated cell lines will be characterized with a specific focus on their survival behavior.

Based on the described ACTN4 role in F-Actin crosslinking, the impact of ACTN4 on the cortical F-Actin in B cells will be investigated. This will include the analysis of the ACTN4 localization by imaging methods, such as STED microscopy and imaging flow cytometry. Moreover, the cortical F-Actin will be characterized in the presence and absence of ACTN4 by imaging methods. These approaches will be complemented by the reconstitution of ACTN4-deficient B cells with ACTN4 variants that have altered F-actin binding properties. The functional analysis of these cells will reveal whether the ACTN4 function in tonic BCR signaling depends on its F-Actin binding capacity.

Since the cortical F-Actin plays a pivotal role in controlling the mobility and subsequent signaling capabilities of BCRs, the impact of ACTN4 on the lateral BCR mobility will be assessed by single particle tracking (SPT). This approach will be complemented by analyzing the activities of BCR-proximal effector proteins and how they correlate with downstream signaling pathways. To have a more comprehensive characterization of the ACTN4 impact on the tonic BCR signal network, MS-based analysis of protein phosphorylation efficiencies will be performed.

By employing these experimental approaches, I intend to elucidate how F-Actin-regulating proteins control the efficiency of tonic BCR survival signals.

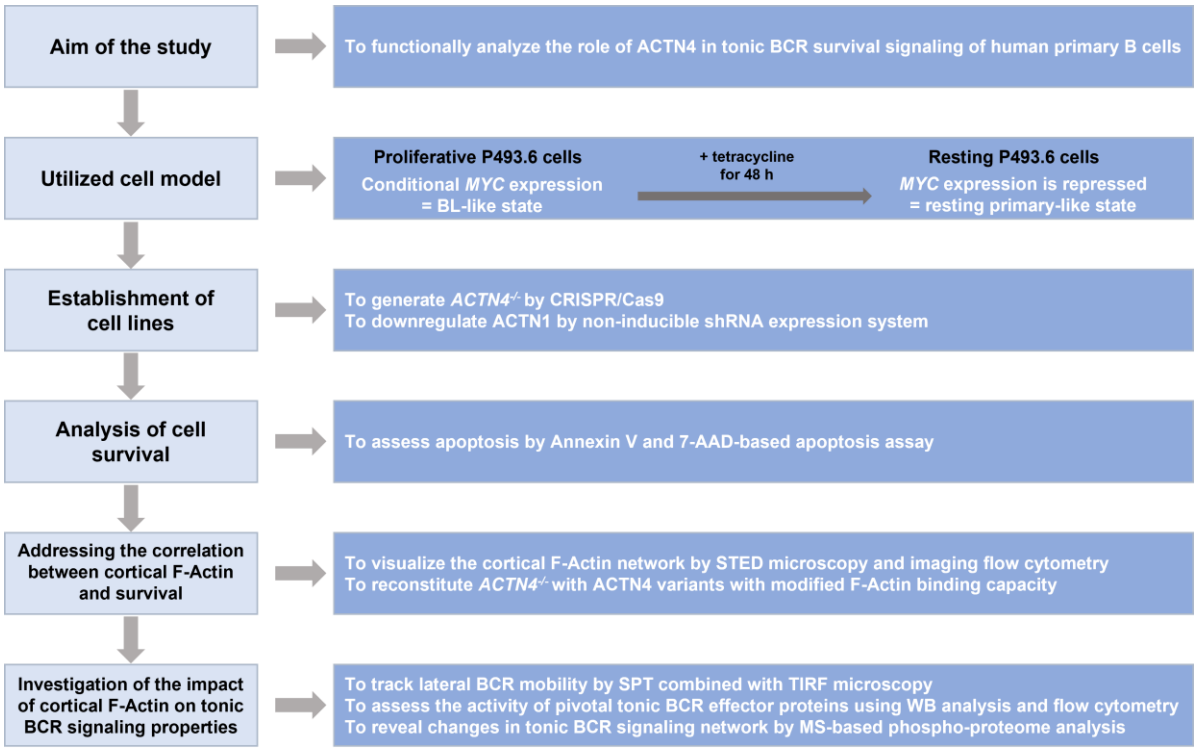

Figure 4: Intended workflow to address the aim of this study.
Light blue boxes illustrate the conceptual framework utilized to investigate the role of ACTN4 in tonic BCR signal transduction in the primary-like B cell model P493.6. The blue boxes indicate the corresponding methodology used to assess this conceptual framework.

3 Materials and Methods

3.1 Materials

3.1.1 Instruments

Table 1: Instruments.

Instrument	Manufacturer
Agarose Gel Electrophoresis System	Peqlab
Amnis ImageStream®X MarkII Imaging Flow Cytometer	Merck
Cell Culture Incubator Hera Cell 150 CO2	Heraeus
Cell Drop BF Cell Counter	DeNovix
Centrifuge Sorvall RC3B Plus	Sorvall
Chemi Lux Gel Imager	Intas Science Imaging
Countess Cell Counter	Invitrogen
Electrophoresis Power Supply EPS 301	Amersham Biosciences
Electrophoresis System Hoefer SE600	Amersham Biosciences
Flow Cytometer LSR II	Becton Dickinson
Freezer HeraFreeze	Heraeus
Ice Machine	Ziegra
Incubation Shaker Unitron	Infors
Incubator Kelvitron T	Heraeus
Laminar Flow Cabinet HeraSafe	Heraeus
Light Microscope Teraval 31	Zeiss
LSM 510 Meta	Zeiss
Magnetic stirrer M21/1	Framo Gerätetechnik
Mastercycler Epgradient	Eppendorf
Microcentrifuge 5417R	Eppendorf
Microcentrifuge MiniSpin™	Eppendorf
Mini Protean Tetra Cell	Bio-Rad Laboratories
Multifuge 3SR	Heraeus
NanoDrop 2000	Thermo Scientific
Neubauer improved counting chamber	Laboroptik
Neon Transfection System	Invitrogen
pH-Meter inoLab®	WTW
Pipettes	Eppendorf
Rocking Shaker	Neolab
Rocking Shaker Duomax 1030	Heidolph
Rotor SW41 Ti	Beckman
Semiphor Transphor Unit TE77	Amersham Biosciences
Sprout Minizentrifuge	Biozym
Thermomixer Comfort	Eppendorf
ThermoMixer® C	Eppendorf
UV-Illuminator	Intas Systems
Vortex Genie 2	Scientific Industries
Water Bath	Schütt Labortechnik
Water Purification System Milli-Q	Millipore, Sartorius

3.1.2 Software and databases

Table 2: Softwares.

Application	Software	Manufacturer
Agarose Gel Imaging	Gel Documentation	Intas
Citation Software	Citavi 6.14	Swiss Academic Software
Flow cytometry data acquisition	FACSDiva	BD Bioscience
Flow cytometry data analysis	FlowJo 7.6.5	Treestar
Graphing and statistical analysis	Prism 5.03	GraphPad
Scientific illustration software	BioRender	S. Aoki & R. Marien
Image processing	ImageJ	W. Rasband, NIH
Sequence Data Analysis	SnapGene® Viewer 4.2.11	Dotmatics
Text processing, spreadsheets, illustrations	Microsoft Office	Microsoft
Western Blot Data Analysis	Chemostar Professional	Intas
Imaging flow cytometry data analysis	IDEAS	Amnis

Table 3: Data bases.

Data base	Application
https://www.primer3plus.com	Primer design
https://blast.ncbi.nlm.nih.gov/Blast.cgi	Sequence alignment
chopchop.cbu.uib.no	CRISPR/Cas9 guide RNA design
crispor.tefor.net	CRISPR/Cas9 guide RNA design
https://eu.idtdna.com	CRISPR/Cas9 guide RNA design
https://www.uniprot.org/	General protein data
https://www.genecards.org/	General gene/protein data
https://www.phosphosite.org/	Phosphorylation sites
https://string-db.org/	Protein-Protein Interactions
https://www.ensembl.org/index.html	Genomic and mRNA data
https://www.ncbi.nlm.nih.gov	Genomic and mRNA data
https://www.phosphosite.org/	Protein post-translational modifications

3.1.3 Consumables

Table 4: Consumables.

Consumable	Manufacturer
Cell culture dishes 60 mm, 100 mm, 25 mm	Greiner bio-one
Cell culture dish 35 mm	Mattek
Cell culture serological pipettes 2 ml, 5 ml, 10 ml, 25 ml	Greiner bio-one
6-, 12-, 24-, 96-well plates	Greiner bio-one
384-well plate	Sarstedt
CELLSTAR tubes 15 ml, 50 ml	Greiner bio-one
Cryo tubes	Greiner bio-one
FACS tubes	Sarstedt
Filter tips	Greiner bio-one
Finnpipette & Tips	ThermoFisher Scientific
Nitrocellulose membrane	Amersham Bioscience
PCR tubes 0.2 ml	Sarstedt
Pipette tips	Greiner bio-one
Reaction tubes 1.5 ml, 2 ml	Greiner bio-one
Sterile filter Filtropur S 0.2, S 0.45	Sarstedt
Whatman Blotting Paper	GE Healthcare

Table 5: Reaction systems (kits).

Kit	Application	Company
APC Annexin V Detection Kit with 7-AAD	Apoptosis assay	Biolegends
Nucleobond® XTRA Midi EF Plasmid Kit	Preparation of plasmid DNA (Midi Prep)	Macherey-Nagel
Nucleobond® Plasmid EasyPure	Preparation of plasmid DNA (Mini Prep)	Macherey-Nagel
Nucleobond® Gel and PCR Clean-Up Kit	Purification of DNA fragments, Agarose gel extraction	Macherey-Nagel
MACSxpress LRSC Pan B Cell Isolation Kit, human	Isolation of primary B cells	Miltenyi
Neon Transfection System 10 µl Kit	Electroporation of crRNA/tracrRNA duplex with Cas9 protein	Thermo Fisher
Neon Transfection System 100 µl Kit	Electroporation of transposon/transposase vectors	Thermo Fisher
TA™ cloning Kit with pCR™2.1	TA cloning	Invitrogen
Taq PCR Master Mix Kit	Amplification of small DNA sequences	QIAGEN

3.1.4 Enzymes

Table 6: Enzymes.

Enzyme	Supplier
Alt-R S.p. Cas9 Nuclease V3	IDT
Calf intestine phosphatase	NEB
Phusion High-Fidelity DNA polymerase	NEB
Restriction Endonucleases	NEB
T4 DNA Ligase	NEB
Taq PCR Master-Mix	NEB
Proteinase K	Macherey-Nagel

3.1.5 Oligonucleotides

Table 7: Sequencing primers.

Primer	Sequence	Vector
M13-for	TGTAAAACGACGGCCAG	pCR™2.1
M13-rev	CAGGAAACAGCTATGAC	pCR™2.1
CMV-for	CGCAAATGGGCGGTAGGCGTG	CMV-MCS/GFP (PiggyBac Vector)
EGFP-N-rev	GCTTGCCGTAGGTGGCATC	CMV-MCS/GFP (PiggyBac Vector)
FGNF-for	TGCATGTCGCTATGTGTTCTGGGA	CMV-GreenPuro-H1-MCS (PiggyBac Vector)

Table 8: Synthetic oligonucleotides used for the generation of ACTN1 knock-down (ACTN1 KD).

Purpose	Oligonucleotides	Sequence
Generation of ACTN1 KD	shRNA template	TGCTGTTGACAGTGAGCGACCGCGAAGTG ACAGTTTACAATAGTGAAGCCACAGATGTA TTGTAAACTGTCACTTCGCGGGTGCCTACT GCCTCGGA
Cloning of shRNA template into PB-CMV-GreenPuro-H1-MCS (PiggyBac Vector)	Forward primer with *Bam*HI	TGAAGGATCCAAGGTATATTGCTGTTGACA GTGAGCG
	Reverse primer with *Eco*RI	TCTCGAATTCTAGCCCCTTGAAGTCCGAGG CAGTAGGC

Table 9: Synthetic oligonucleotides used for CRISPR/Cas9-based gene editing.

Purpose	Oligonucleotides	Sequence
Generation of *ACTN4*$^{-/-}$ in P493.6 and ACTN4 KD in primary B cells	crRNA exon 2	GCAUGAGCUUGAGCCCGUCUGUUUU AGAGCUAUGCU
CD79B KD in primary B cells	crRNA exon 3	AACACCUCGGAGGUCUACCAGUUUU AGAGCUAUGCU
Sequencing of exon 2 in *ACTN4*$^{-/-}$ clones	Forward primer	CAAAATTGACAGACCTGGGTTCAAATC
	Reverse primer	ATTGTTGATTTTGTGCACTCTCATCTT

Table 10: Synthetic oligonucleotides used for cloning.

Purpose	Oligonucleotides	Sequence
Cloning of WT ACTN4 cDNA into PiggyBac in-frame with GFP-tag	ACTN4-cl-for-*Eco*RI	TAATGAATTCATGGTGGAC TACCACGCG
	ACTN4-cl-rev-*Kpn*I	TAATGGTACCAGGTCGCT CTCGCCATAC
Cloning of ACTN4∆aa(100-252) cDNA into PiggyBac in-frame with GFP-tag	ACTN4 aa (1-100)-cl-for-*EcoR*I	TAATGAATTCATGGTGGAC TACCACGCG
	ACTN4 aa (1-100)-cl-rev	AGGTCATTATGGCCTTCTC GTCCGGCTTAGGTAACCG CTCC
	ACTN4 aa (252-910)-cl-for	GGAGCGGTTACCTAAGCC GGACGAGAAGGCCATAAT GACCT
	ACTN4 aa (252-910)-cl-rev-*Kpn*I	TAATGGTACCAGGTCGCT CTCGCCATAC
Cloning of K255E ACTN4 cDNA into PiggyBac in-frame with GFP-tag	ACTN4 aa (1-258)-cl-for-*EcoR*I	AATGAATTCATGGTGGACT ACCACGCG
	ACTN4 aa (1-258)-cl-rev	TCATTATGGCCTCCTCGTC GG
	ACTN4 aa (252-910)-cl-for	CCGACGAGGAGGCCATAA TGA
	ACTN4 aa (252-910)-cl-rev-*Kpn*I	TAATGGTACCAGGTCGCT CTCGCCATAC

∆aa: deleted amino acids, K255E: substitution of the aa lysine at position 255 by glumatic acid

3.1.6 Chemicals and reagents

Table 11: Chemicals and reagents.

Reagent	Supplier
Annexin V binding buffer	Biolegend
Annexin V-APC (8 µg/ml)	Biolegend
7-AAD (50 µg/ml)	Biolegend
Acrylamide/bis-acrylamide	Roth
Agarose	Seqlab
Alamethicin	Enzo Life Sciences
Ammonium persulfate (APS)	Roth
Ampicillin	Roth
β-glycerophosphate	Sigma-Aldrich
Bovine serum albumin (BSA)	Serva
Trypan blue solution (0.4 %)	Thermo Scientific
Calcium chloride ($CaCl_2$)	Merck
CytoFix Fixation Buffer	BD Biosciences
Dimethyl sulfoxide (DMSO)	Roth
DNA Ladder GeneRuler 1kb	Fermentas
Deoxynucleoside triphosphate (dNTP) mix	NEB
Dithiotreitol (DTT)	Roth
Digitonin	Sigma Aldrich
Ethylenediaminetetraacetic acid (EDTA)	Roth

Ethanol	Roth
Ethidium bromide	Roth
Fetal Calf Serum (FCS), dialyzed	PAN Biotech
Fetal Calf Serum (FCS)	Biochrom
Gel Loading dye (6x), purple	NEB
Glycerol	Roth
Glycine	Roth
Hydrogen peroxide (H_2O_2)	Roth
Hydrochloric acid (HCl)	Roth
Hoechst 33342	Sigma Aldrich
4-(2-hydroxyethyl)-1piperazineethanesulfonic acid (HEPES)	Roth
Igepal CA-630 (NP40)	Sigma-Aldrich
INDO-1 AM	Life Technologies
InstantBlue Coomassie Protein Stain	Expedeon
L-Arginine:HCL	Cambridge Isotype Laboratories
L-Lysine:2HCL	Cambridge Isotype Laboratories
L-Glutamine (200 mM)	Gibco
Isopropyl-β-D-thiogalactopyranosid (IPTG)	Sigma
Isopropanol	Roth
Luminol	Sigma-Aldrich
Magnesium chloride ($MgCl_2$)	Roth
Methanol	Roth
NEB buffer 1.1, 2.1, 3.1 and CutSmart	NEB
Perm/Wash Buffer	BD Biosciences
Penicillin/Streptomycin (100x)	Gibco
Pluronic F-127	Life Technologies
Potassium chloride (KCl)	Roth
Potassium dihydrogen phosphate (KH_2PO_4)	Merck
Poly-L-Lysine	Sigma-Aldrich
L-Proline	Sigma-Aldrich
Protease Inhibitor Cocktail P2714	Sigma-Aldrich
Prestained Protein Marker, Broad Range	NEB
Puromycin	Invitrogen
Roswell Park Memorial Institute (RPMI) 1640	Gibco
Sodium Pyruvate (100 mM)	Gibco
T4 Ligase Buffer	NEB

3.1.7 Buffers and solutions

Table 12: Buffers and solutions.

Buffer/Solution	Components
Antibody dilution solution	1% (w/v) BSA 0.01% (w/v) NaN_3 in TBS-T
Agar plates	2% (w/v) agar in LB-medium
Blocking buffer	5% (w/v) BSA 0.01% (w/v) NaN_3 in TBS-T
Blotting buffer	48 mM Tris 39 mM Glycine 0.0375% (w/v) SDS 0.01% (w/v) NaN_3 20% (v/v) Methanol in ddH_2O
ECL solution	6 ml ECL solution A 600 µl solution B 1.8 µl 30% (v/v) H_2O_2

ECL solution A	100 mM Tris/HCl, pH 8.6 0.28 mM luminol in ddH_2O
ECL solution B	6.7 mM p-coumaric acid in DMSO
Freezing media	10% (v/v) DMSO in FCS
Krebs-Ringer buffer	140 mM NaCl 10 mM D-glucose 10 mM HEPES (pH 7.4) 4 mM KCl 1 mM $MgCl_2$ 1 mM $CaCl_2$ in ddH_2O
Laemmli buffer (4x)	120 mM Tris/HCl, pH 6.8 400 mM DTT 40% (v/v) glycerol 12% (w/v) SDS 0.04% (w/v) bromphenol blue in ddH_2O
Lysogeny broth (LB) medium	10 g/l Tryptone 5 g/l Yeast Extract 5 g/l NaCl (pH 7.0) in ddH_2O
Lysis buffer for global pYome MS-based analysis	20 mM HEPES, pH 8.0 9 M Urea 1 mM sodium orthovanadate 2.5 mM sodium pyrophosphate 1 mM b-glycerophosphate in ddH_2O
MEB2 buffer for BH3 profiling	150 mM mannitol 150 mM KCl 10 mM HEPES-KOH 5 mM succinate 1 mM EGTA 1 mM EDTA 0.1% BSA pH 7.5
N2 buffer for BH3 profiling	1.7 M Tris base 1.25 M glycin pH 9.1
RIPA Lysis buffer supplemented with NP-40	50 mM Tris/HCl, pH 7.5 150 mM NaCl 1 mM EDTA 5 mM NaF 5 mM β-glycerophosphate 1 mM Na_3VO_4 1:50 protease inhibitor cocktail 0.1% sodium deoxycholate 1% (v/v) NP-40 in ddH_2O
Phosphate buffered saline (PBS)	137 mM NaCl, pH 7.4 4.3 mM Na_2HPO_4 2.4 mM KCl 1.4 mM KH_2PO_4 in ddH_2O
Resolving gel solution	375 mM Tris/HCl, pH 8.8 10% (v/v) acrylamide/bis-acrylamide 0.1% (w/v) APS 0.1% (w/v) TEMED in ddH_2O

RPMI media with 10% FCS	10% (v/v) heat inactivated FCS 1x Pen/Strep 1 mM sodium pyruvate 1 mM L-glutamine 50 µM β-mercaptoethanol in RPMI-1640 medium
SDS-PAGE buffer	25 mM Tris 192 mM Glycine 0.1% (w/v) SDS in ddH_2O
Stacking gel solution	125 mM Tris-HCl, pH 6.8 3.5 mM SDS 10% (v/v) acrylamide/bis-acrylamide in ddH_2O
TAE-buffer	40 mM Tris 20 mM glacial acetic acid 1 mM EDTA in ddH_2O
TAG-lysis buffer	10 mM Tris-HCl, pH 8.0 50 mM KCl 0.45% (v/v) NP-40 0.45% (v/v) Tween 20 in ddH_2O
Tris buffered saline/Tween 20 (TBS-T)	137 mM NaCl 20 mM Tris-HCl, pH 7.6 0.1% (v/v) Tween 20 in ddH_2O

3.1.8 Plasmids

Table 13: Expression and cloning plasmids.

Vector	Insert	Purchased from
pMD18-T Simple Vector	ACTN4 cDNA	Sino Biological (SB)
pMSCV-bleo-RFP	LifeAct-mCherry cDNA	Dr. Michael Engelke
CMV-MCS-GFP-EF1-Puro (PiggyBac/Transposon)	ACTN4 cDNA ACTN4Δaa(100-252) cDNA K255E ACTN4 cDNA LifeAct-mCherry cDNA	This study
CMV-Transposase vector (PiggyBac/Transpoasase)	Transposase cDNA	This study
CMV-GreenPuro-H1-MCS (PiggyBac/non-inducible shRNA expression system)	ACTN1 shRNA-expression template	System Biosciences

3.1.9 Antibodies

Table 14: Primary antibodies.

Antibody	Isotype	Supplier
α-ACTN4	Mouse IgG1	Santa Cruz
α-ACTN1	Mouse IgG1	Santa Cruz
α-β-Actin	Mouse IgG2b	CST
α-CD79B	Rabbit	CST
α-JNK	Rabbit	CST
α-pan ERK (Clone 16)	Mouse IgG2a	Becton Dickinson
α-pERK (T202/Y204)	Rabbit	CST
α-pan JNK	Mouse IgG1	CST
α-pJNK (T183/Y185)	Mouse IgG1	CST

α-pan p38	Rabbit	CST
α-pp38 (T180/Y182)	Mouse IgG1	Becton Dickinson
α-pSYK (Y525/Y526)	Rabbit	CST

Table 15: Secondary antibodies.

Antibody	Species	Supplier
α-mouse IgG-HRPO	Goat	Southern Biotech
α-mouse IgG2a-HRPO	Goat	Southern Biotech
α-mouse IgG2b-HRPO	Goat	Southern Biotech
α-rabbit IgG-HRPO	Goat	Southern Biotech

Table 16: Fluorochrome conjugated antibodies.

Antibody	Fluorochrome	Species/Isotype	Supplier
α-human IgM	APC	Mouse IgG1	Southern Biotech
α-human IgM specific nanobody	AZDye568	Alpaca	NanoTag
α-human IgM Fab fragment	Cy-3	Goat	Jackson Immunoresearch
α-pCD79A (Y188/Y182)	Alexa Fluor® 647	Rabbit mAb	Cell Signaling
α-pSYK (Y525/Y526)	Alexa Fluor® 647	Rabbit mAb	Cell Signaling
α-pSLP65 (Y84)	Alexa Fluor® 647	Mouse mAb	BD Biosciences
α-pAKT (S473)	Alexa Fluor® 647	Rabbit	CST
α-Cytochrome c	Alexa Fluor® 647	Mouse IgG1	Biolegend

3.1.10 Bacteria and bacterial culture

The amplification of plasmids used in this study was carried out by transforming One Shot TOP10F´ chemically competent *E. coli* (Invitrogen). *E. coli* were then grown in lysogeny broth (LB) medium supplemented with 100 µg/ml ampicillin or 50 µg/ml kanamycin. Of note, LB medium was autoclaved for 30 min at 121 °C and 1.25 bar prior to its storage at 4 °C.

3.1.11 Eukaryotic cell lines

DG75 (ACC 83)

DG75 is a human BL cell line. Cells were originally isolated from the pleural effusion of a 10-year-old male with refractory, terminal BL in 1975 [113]. DG75 cells were identified as Epstein-Barr virus-negative (EBV^{neg}) and express surface IgM with kappa light chain [114]. DG75 cells have a chromosomal translocation t(8;14)(q24;q32) leading to an enhanced cell proliferation with a doubling time of approximately 20-24 h [115].

Ramos (ACC 603)

Ramos is a human BL cell line that was derived from the ascitic fluid of a 3-year-old male in 1972 [116]. Ramos cells are characterized as EBV^{neg} and are known to express both surface and secreted Igs (IgM, lambda light chain) [117]. Ramos cells carry a t(8;14) translocation, exhibit *TP53* mutation, and possess an approximate doubling time of 48 h [118].

Daudi (ACC 78)

Daudi is a human BL cell line that was derived from a left orbital biopsy of a 16-year-old male in 1967. Daudi cells are characterized as EBV^{pos} and known to express surface IgM with kappa light chain [119]. In addition, Daudi cells carry a t(8;14)(q24;q32) translocation and possess an inactivating *ID3* mutation [120]. *ID3* gene has been shown to co-operate with MYC in the pathogenesis of BL [121].

P493.6 (ACC 915)

The P493.6 B cell model is a human cell line transfected with a vector carrying a doxycycline regulatable promotor that allows for a conditional abrogation of *MYC* expression. P493.6 cell line was derived from a clone of EREB2-5 EBV^{pos} lymphoblastoid cells [122]. The ectopic expression of *MYC* in EBV-transformed cells allows for the establishment of an EBNA2-independent BL-like cell line [123]. Thus, the clone P493-6 proliferates independently of EBNA2 activity and has been analyzed in detail [122]. P493.6 cells constitutively express *MYC* when cultured without tetracycline. The addition of tetracycline diminishes *MYC* expression and arrests cells in G0/G1 phase, resembling resting primary B cells. P493.6 cells have the same morphology and surface antigen expression as BL cells, including CD10 and CD38 [122].

3.2 Methods

3.2.1 Molecular biology

3.2.1.1 Isolation of genomic DNA

Genomic DNA was isolated from P493.6 cells by lysing 1 x 10^6 cells in 200 µl TAG lysis buffer containing 1 µl proteinase K (20 mg/ml, Macherey-Nagel) at 56 °C for 3 h followed by heat inactivation at 95 °C for 15 min. The isolated DNA was used as a template for polymerase chain reaction (PCR) or stored at -20 °C for further use.

3.2.1.2 Polymerase chain reaction (PCR)

PCR was used to amplify DNA fragments for sequencing or cloning purposes (tables 17 & 19). DNA amplification was performed by using specific forward and reverse primers harboring the desired restriction site. Taq polymerase was utilized to amplify short DNA fragments intended for sequencing. However, for long DNA fragments, phusion® DNA polymerase (NEB) was used, as Taq polymerase does not possess 3´ to 5´ exonuclease or “proofreading” activity [124].

Table 17: PCR reaction mix for cloning purposes.

Reagent	Volume (µl)	Final concentration
5x Phusion HF buffer	10	1x
dNTPs (10 mM, NEB)	1	200 µM
Forward primer (10 µM)	2.5	0.5 µM
Reverse primer (10 µM)	2.5	0.5 µM
Template	1	50-200 ng/µl
Phusion polymerase (2000 U/ml, NEB)	0.5	1 U/reaction
ddH_2O	32.5	
Final volume	50	

To determine genomic changes induced by CRISPR/Cas9-based genome targeting, genomic DNA was used as a template. Specific primers were then utilized to amplify targeted exon using a master mix that contains the Tag polymerase, adequate buffer, and dNTPs. PCR was conducted at an annealing temperature that is typically 3-5 °C lower than the melting temperature (T_m) of used primers (tables 18 & 19). Finally, PCR product was cloned into pCR.2.1 vector using TA cloning according to the manufacturer's recommendations. The resulting vector was then sent to Microsynth Seqlab in Göttingen for sequencing, using M13 forward and reverse sequencing primers.

Table 18: PCR reaction mix for sequencing purposes.

Reagent	Volume (µl)	Final concentration
2x Taq PCR master mix	5	1x
Forward primer (100 µM)	1	1 µM
Reverse primer (100 µM)	1	1 µM
Template	1	50-200 ng/µl
ddH_2O	2	
Final volume	10	

Table 19: PCR reaction steps.

	Step	PCR with Phusion® polymerase	PCR with Tag polymerase
	Initial denaturation	98 °C, 30 s	94 °C, 2 min
35x	Denaturation	98 °C, 10 s	94 °C, 2 s
35x	Annealing	x °C*, 30 s	x °C*, 30 s
35x	Extension	68 °C, 30 s/kb	72 °C, 60 s/kb
	Final Extension	68 °C, 2-fold extension time	72 °C, 2-fold extension time
	Stop	10 °C, ∞	10 °C, ∞
		* Annealing temperature = T_m (primer) – (3-5) °C	

3.2.1.3 Site-directed mutagenesis

Site-directed mutagenesis was performed by an overlap extension PCR, which allowed for the substitution of a single nucleotide or the partial/complete removal of specific protein domains. For the first variant, K255E ACTN4-GFP, forward and reverse primers harboring the desired mutation were obtained from Eurofins Scientific. ACTN4 cDNA served as a template for the 1st and 2nd PCR reactions (table 10). The resulting amplicons were used for the overlap extension PCR, where no additional primers were needed because the amplicons prime each other (table 20). The PCR product was then used as a template to generate the desired DNA fragment that encodes the protein variant. In the second variant, ACTN4Δaa(100-252)-GFP, the primers used for the 1st and 2nd PCR were designed to exclude the DNA sequence encoding amino acids 100-252 (table 10). Ultimately, PCR products that encode ACTN4 variants were cloned into pCR.2.1 vector for sequencing purposes, or directly into a PiggyBac vector in-frame with GFP-tag.

Table 20: Overlap extension PCR program.

	Step	PCR with Phusion® polymerase
	Initial denaturation	95 °C, 2 min
25x	Denaturation	95 °C, 30 s
25x	Annealing	x °C*, 30 s
25x	Extension	72 °C, 60 s/kb
	Final Extension	72 °C, 2-fold extension time
	Stop	10 °C, ∞

x °C*: Annealing temperature depends on used primer.

3.2.1.4 Restriction enzyme digestion of DNA

Restriction enzymes cleave plasmid DNA or PCR products at specific recognition sequences. The enzymatic digest was conducted by incubating DNA with the desired restriction enzyme(s) (NEB or Thermo Scientific), according to the manufacturer's recommendations, for 1-2 h. As a result, DNA fragments with desired sticky or blunt ends are produced. Digested DNA was then subjected to agarose gel electrophoresis to separate these fragments. Gel-extracted, desired DNA fragments were then directly used for cloning or sequencing purposes. Furthermore, the enzymatic digest was also used to confirm the presence or absence of a certain restriction site upon gene editing triggered by CRISPR/Cas9 or to check the direction of DNA inserts following blunt ligation or TA cloning.

3.2.1.5 Agarose gel electrophoresis

DNA electrophoresis is a standard laboratory technique used to identify, quantify, and separate desired DNA fragments. Agarose gel was prepared by melting 1-2% (w/v) of agarose in Tris-acetate-EDTA (TAE) buffer. Boiled agarose was cooled down to 65 °C, before the addition of ethidium bromide (Roth) at a final concentration of 0.5 µg/ml. DNA samples were then mixed with 6x DNA loading buffer (NEB) and loaded into the wells of an agarose gel. The gel was subjected to an electric field at 220 mA and 100 V for 30-45 min. Finally, DNA was visualized using UV light.

3.2.1.6 DNA extraction from agarose gels

Agarose gel containing the desired DNA fragment was placed on a UV light-emitting plate, and the agarose around the fragment was carefully cut and melted at 50 °C for 10 min. The DNA was then purified using a NucleoSpin® Gel and PCR Clean-up system (Macherey-Nagel). Column-trapped DNA was then eluted in 10-30 µl of 5 mM Tris-HCl (pH 8.5). The concentration of eluted DNA was determined by nanodrop and stored at -20 °C until use.

3.2.1.7 Cloning of DNA fragments into plasmids

DNA fragments with sticky or blunt ends (inserts) were cloned into linearized vector backbones that have the appropriate ends. Linearized backbones with only one restriction enzyme or two different enzymes that create compatible ends, were further treated with calf intestinal phosphatase (CIP) for 30 min at 37 °C. CIP treatment prevents vector self-ligation by dephosphorylating 5´ and 3´ ends of the linearized backbone. The Ligation of DNA inserts and backbone was conducted at a molar ratio of (3:1) either for 1 h at RT for short inserts (up to 1000 bp) or overnight at 16 °C for long inserts (up to 5000 bp). Finally, 5 µl of the ligation reaction was directly used for bacterial transformation (see 3.2.1.9).

3.2.1.8 Cloning of LifeAct-mCherry into CMV-MCS-GFP PiggyBac Vector

mCherry-tagged LifeAct-encoding DNA sequence was cut from a pMSCV vector and ligated into a CMV-MCS-GFP PiggyBac Vector *via Bgl*II and *Not*I restriction sites.

LifeAct DNA sequence
ATGGGTGTCGCAGATTTGATCAAGAAATTCGAAAGCATCTCAAAGGAAGAA

3.2.1.9 Bacterial transformation

Transformation is the process by which foreign genetic material is taken up by bacteria, enabling its rapid amplification. In this study, chemically competent bacterial strains, such as *E. coli* TOP10F´, were utilized. To perform the transformation, frozen bacteria (50 µl tube at -80 °C) were thawed on ice for 5 min. The bacteria were then incubated with 5 µl of the ligation reaction or 1 µl of pre-existing plasmid for 20-30 min on ice. Subsequently, a heat shock was performed at 42 °C for 45 min, followed by incubation on ice for 5 min. For recovery, 200 µl of prewarmed antibiotic-free LB medium was added and samples were incubated under constant agitation, at 37 °C for 30-60 min. The transformed bacteria were plated on agar plates containing the appropriate antibiotic and incubated overnight at 37 °C. Bacteria transformed with pCR2.1 plasmid, were plated on agar plates pre-treated with 50 µl X-gal (5-bromo-4-chloro-3-indolyl-beta-D-galacto-pyranoside, 50 mg/ml in DMF) and 50 µl IPTG (isopropyl-β-D-thiogalacto-pyranoside, 0.1M) to allow for blue-white screening. Blue-white screening enables the discrimination between empty plasmids (blue colonies) and plasmids with inserts (white colonies).

3.2.1.10 Isolation of plasmid DNA from bacterial culture

Mini/Midi Preparation

A culture tube containing 4 ml of LB medium supplemented with the appropriate antibiotic (100 µg/ml ampicillin or 50 µg/ml kanamycin) was inoculated with a single bacterial colony and placed in an incubation shaker at 37 °C for 16 h. After incubation, the bacteria were lysed, and plasmid DNA was extracted using the NucleoSpin® Plasmid Easy according to the manufacturer's recommendations Pure kit. The extracted plasmid DNA was either sequenced or enzymatically digested at specific sites to validate successful ligation. In cases where higher concentrations of plasmid DNA were required, 200 ml of LB medium was inoculated with the preculture (4 ml). Midi bacterial cultures were placed in an incubation shaker for 16 h at 37 °C, and plasmid DNA was then extracted using NucleoBond®Xtra Midi EF Plasmid kit according to the manufacturer's recommendations.

3.2.1.11 Sequencing of extracted plasmid DNA

For sequencing, 1.2 µg DNA was diluted in ddH_2O to a final volume of 15 µl. DNA was then sequenced by Microsynth Seqlab in Göttingen. Primers used for sequencing were either selected from the standard primer list provided by the company or premixed at a final concentration of 100 pmol/µl.

3.2.2 Biochemistry

3.2.2.1 Stimulation of B cells

1.2 x 10^6 cells were resuspended in Krebs-Ringer buffer and stimulated with 2-5 µg/ml $F(ab')_2$ goat anti-human IgM for 5 min to assess calcium release (see 3.2.3.12). To assess the phosphorylation events of BCR effectors upon stimulation, an equal cell number was resuspended in 100 µl RPMI medium devoid of FCS. Cells were then stimulated for 3 min with 5 µg/ml $F(ab')_2$ goat anti-human IgM. Stimulation was stopped by adding an equal volume of 4% formaldehyde (Cytofix). The phosphorylation of analyzed proteins was then assessed by intracellular staining or by subjecting cleared cellular lysates to analysis.

3.2.2.2 Preparation of cleared cellular lysates

Cleared cellular lysates (CCLs) were prepared by lysing 1 x 10^6 cells in 20 µl of RIPA buffer containing 0.5 % NP40 detergent at 4 °C for 1 h under mild rotation. After cell lysis, samples were spun down at 20800 rcf, 4 °C for 15 min. The supernatant was then transferred to a new reaction tube and mixed with 0.25 volumes of 5x Laemmeli buffer followed by boiling at 95 °C for 5 min. Samples were either directly used for WB analysis or stored at -20 °C for later use.

3.2.2.3 Sodium dodecyl sulfate polyacrylamide gel electrophoresis

Sodium dodecyl sulfate polyacrylamide gel electrophoresis (SDS-PAGE) is an analytical biochemical approach to separate proteins from CCLs according to their sizes. SDS-PAGE was originally described by Weber and Osborn in 1969 [125]. Their results showed that this method can be used with great confidence to determine the molecular weight of polypeptide chains for a wide variety of proteins. In this study, gel electrophoresis was carried out in Mini-PPOTEIN system (Bio Rad). CCLs were boiled for 5 min at 95 °C, and 15-25 µl of boiled samples was then loaded onto a 5% polyacrylamide stacking gel followed by a 10% polyacrylamide gel (table 21). Gels were initially run at 10 mA/gel to collect and condense proteins in the stacking gel, and the current was increased to 20 mA/gel once the bands entered the resolving gel where the separation of protein bands took place. Gel electrophoresis was followed by immunoblotting.

Table 21: Composition of Resolving and Stacking gels.

Reagent	Resolving Gel	Stacking Gel
Resolving gel Buffer	375 mM Tris/HCL (pH 8.8)	-
Stacking gel Buffer	-	125 mM Tris/HCL (pH 6.8)
Acrylamide/Bis-acrylamide	10%	5%
SDS	0.1%	0.1%
TEMED	0.1%	0.1%
10% APS	10%	10%
ddH_2O	add to a final volume	add to a final volume

3.2.2.4 Western blot transfer

The electrophoretic transfer of proteins from polyacrylamide gels to nitrocellulose membrane was introduced by Towbin *et al.* in 1979 [126]. Currently, this fundamental technique is widely used for protein analysis. In this study, gel-embedded proteins were transferred to a nitrocellulose membrane using semi-dry WB transfer. To conduct this, the gel, two Whatman papers, and nitrocellulose membrane were equilibrated in 1x blotting buffer. Subsequently, the gel on the top of the nitrocellulose membrane was placed between two Whatman papers, and the electrophoretic transfer took place at 220 mA, 16 V for 1 h. It is important to note that the efficient transfer of proteins requires the careful removal of air bubbles between the gel and the nitrocellulose membrane.

3.2.2.5 Immunostaining

After protein transfer, the nitrocellulose membrane was incubated in 1x TBS blocking solution containing 5% BSA and 0.1% NaN_3, for 45 min at RT under constant agitation. Blocking solutions are usually used to block unspecific binding of used antibodies thereby preventing undesired staining and high background. For staining, primary antibodies were prepared according to the manufacturer's recommendations in TBST containing 1% BSA and 0.01% NaN_3. The membrane was incubated with primary antibody solution at 4 °C overnight at constant agitation. In turn, the membrane was washed 3-4 times with TBS-T for 15 min each, followed by incubation with secondary HRPO-conjugated antibodies at a dilution of 1:10.000 for 1 h at RT. After that, the nitrocellulose membrane was washed again 3-4 times with TBS-T for 15 min, and proteins of interest were visualized by an enhanced chemiluminescence (ECL) solution using Chemi Lux Imager (Intas). In cases of a renewed incubation with another primary antibody, the membrane was stripped with 1% NaN_3 in TBS-T for 1 h to inactivate HPRO from previous secondary antibodies.

3.2.3 Cell Biology

3.2.3.1 Cell culture and maintenance

Cells were cultured in RPMI cell media containing 10% FCS at 37 °C and 5% CO_2 in a humidified incubator. For maintenance, P493.6 cells were passaged every other day at a volume ratio of 1:4-1:5 in RPMI medium under sterile conditions using a laminar-flow clean bench. To determine cell density, cells were counted either manually using a Neubauer improved counting chamber (Laboroptik) or automatically using Cell Drop BF Cell Counter (DeNovix). Dead cells were excluded by staining with 0.4% trypan blue.

3.2.3.2 Storage and revitalization of cells

5-10 x 10^6 cells were washed one time with 1x PBS, resuspended in 1 ml of freezing medium (10% DMSO in FCS), and transferred to cryotubes. The cryotubes were then stored at -80 °C in a polystyrene box for short-term storage and at -150 °C for long-term storage. To revitalize the cells, frozen cell batches were placed on ice for 5 min before being thawed in a water bath at 37 °C. Thawed cells were washed 2-3 times with 1x PBS to remove residual DMSO. Thereafter, the cell pellet was transferred into a 10 cm cell culture dish containing pre-warmed RPMI medium.

3.2.3.3 SILAC labeling of human B cell lines

To reveal potential changes in the phospho-proteome of ACTN4-deficient cell line compared to the parental or ACTN4-GFP reconstituted cell line, MS-based analysis was conducted. For this purpose, cells were cultured in “intermediate” (M) SILAC RPMI 1640 medium supplemented with either 0.115 mM L-arginine ($^{13}_{6}C$, $^{14}_{4}N$)-L-arginine and 0.27 mM 4,4,5,5-d4-L-lysine (R+6/K+4) or non-labeled “light” (L) amino acids (Sigma). The SILAC medium was also supplemented with 10 to 20% dialyzed FCS, penicillin/streptomycin, 1 mM L-glutamine and 0.2 g/l L-proline. To ensure a high incorporation rate of modified amino acids, cells were expanded for 10 days. For global phospho-proteome analysis (GPome) as well as phospho-tyrosine enriched analysis (pYome), a total number of 1 x 10^8 cells per condition were lysed in 1 ml of urea buffer at RT. The lysates were then mixed at a 1:1 ratio and sent for MS analysis at the DKTK Proteomics Core Facility, University Hospital Frankfurt. There, the samples were separated by size using SDS-PAGE and subjected to quantitative MS analysis as described by Corso *et al.* [68].

3.2.3.4 CRISPR/Cas9-based gene editing

Clustered regularly interspaced palindromic repeats (CRISPR)/Cas9 is an innovative genome editing technology. CRISPR gene-cassettes comprise several variable spacers originated from the invader, regularly separated by palindromic repeats, and associated with Cas genes. Consequently, spacer-immunized prokaryotic organisms such as bacteria and archaea can generate a sgRNA that encompasses a transcript of the spacer itself and an invariable tracrRNA. If the same virus invades an immunized prokaryotic organism, the sgRNA complementary binds the same spacer [127]. Therefore, CRISPR/Cas9 gene-cassettes system helps bacteria and archaea to eliminate viruses or mobile genetic elements by generating a memory resembling the adaptive immunity in this aspect [128].

CRISPR/Cas9-based gene editing is widely used in gene research and to study the role of gene-causing diseases in cell lines and animal models. Furthermore, it holds promise as a tool for future gene therapy [129]. In CRISPR/Cas9-based gene targeting, cells are transfected with a single guide RNA (sgRNA) composed of a pre-formed duplex of crRNA and tracrRNA together with Cas9 protein. In cells that receive both the sgRNA and Cas9 protein, the sgRNA forms a complex with Cas9 nuclease which in turn recognizes a proto-spacer adjacent motif (PAM) sequence located at 3´ ends of targeted sequence. As a result, Cas9 protein (derived from streptococcus pyogenes) induces a double-strand breaks (DSBs). In turn, the repair of DS-broken DNA is performed by non-homologous end joining (NHEJ) and/or homologous direct repair (HDR) resulting in a deletion/insertion of few nucleotides (indel mutations) [130] (Figure 5).

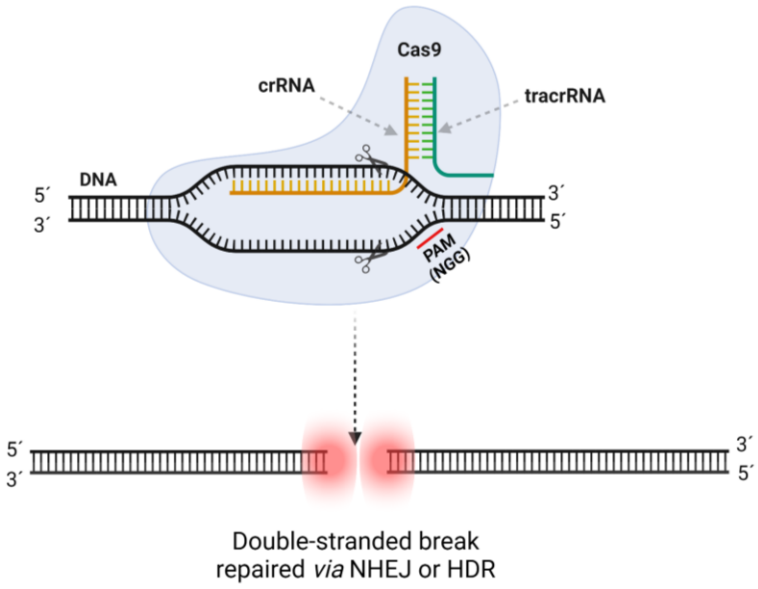

Figure 5: Schematic illustration of CRISPR/Cas9-mediated gene editing.
The graphical illustration represents the modified CRISPR/Cas9-based gene editing in eukaryotic cells following transfection with a pre-formed duplex of crRNA/tracrRNA along with Cas9 endonuclease. After binding the targeted exon, Cas9 protein recognizes a PAM sequence and induces a double-strand break (DSB), which is recognized and repaired by non-homologous end joining (NHEJ) repair, resulting in indel mutations and premature stop codons. Created with BioRender.com.

3.2.3.5 Generation of an ACTN4-deficient (*ACTN4*$^{-/-}$) cell line

To generate an *ACTN4*$^{-/-}$ cell line, 0.5 x 10^6 cells were electroporated with a duplex of crRNA/tracrRNA (sgRNA) together with Cas9 endonuclease using a Neon electroporation system. For electroporation, the following parameters were used (table 22). Used RNAs and Cas9 protein were ordered from INTEGRATED DNA TECHNOLOGIES (IDT) (see 3.1.5). The electroporation experimental setup, including used buffers, and cuvettes were used according to manufacturer recommendations.

Table 22: Electroporation parameters used for P493.6 cell line.

Electroporation program	
Voltage	1400 V
Width	20 ms
Puls number	2 pulses

For crRNA/tracrRNA duplex formation, 0.44 µl of the crRNA (200 µM) and 0.44 µl of the tracrRNA were transferred to a PCR tube containing 1.12 µl of IDT duplex buffer. The mixture was incubated at 95 °C for 5 min and then cooled down to RT. Cas9 nuclease was prepared separately by mixing 1.8 µl of Cas9 stock solution with 0.8 µl of buffer R. Subsequently, the pre-formed RNA duplex was mixed with Cas9 nuclease at volume ratio of 1:1. For electroporation, a 10 µl pipette tip was used. The electroporation mixture consisted of 1 µl of duplex/Cas9 mixture, 2 µl of the diluted enhancer (10 µM), and 0.5 x 10^6 cells resuspended in 9 µl of buffer R. After electroporation, the cells were transferred into 1 ml of RPMI medium containing 20% FCS devoid of antibiotics.

3.2.3.6 Isolation of single *ACTN4*$^{-/-}$ clones

Due to the high efficiency of this novel CRISPR/Cas9 approach, no sorting of cells that received both the RNAs and Cas9 protein was necessary. Instead, the electroporated cells were counted using a Neubauer improved counting chamber and diluted in RPMI medium containing 20 % FCS to a concentration of 0.6 cells per well in a 96-well plate. This corresponds to approximately 60-70 cells diluted in 20 ml of RPMI medium. After 48 of electroporation, single clones were cultured and expanded at 37 °C up to 6 weeks before the screening process for an *ACTN4*$^{-/-}$ clone took place.

3.2.3.7 Screening process for *ACTN4*$^{-/-}$ clones

Cell lysates of isolated clones were subjected to Western blot (WB) analysis. If no protein band was observed, further gene analyses were performed. Hence, genomic DNA was extracted from those clones, and the targeted exon was amplified by PCR using suitable primers. Amplicons were then cloned into pCR.2.1 vector *via* TA-cloning and sequenced using M13 forward and reverse primers. Clones were considered to be ACTN4-deficient, only when the sequencing of the targeted exon of both alleles showed a premature stop codon resulting from indel mutations.

3.2.3.8 Electroporation of human primary B cells

To diminish *ACTN4* expression in human primary B cells, 0.5 x 10^6 cells were electroporated with the same crRNA/tracrRNA duplex, that was used to generate *ACTN4*$^{-/-}$ in P493.6 cells, together with Cas9 endonuclease. As a positive control for this experiment, the *CD79B* gene locus was targeted because CD79B together with CD79A form the BCR signaling heterodimer which is essential for the initiation of tonic BCR signaling. Hence, targeting CD79B would be one of the perfect positive controls for this experiment. As a negative control, cells were only electroporated with the non-targeting portion of the sgRNA (tracrRNA) and Cas9 nuclease. For electroporation, the following parameters were used (table 23).

Table 23: Electroporation parameters used for primary B cells.

Electroporation program	
Voltage	1700 V
Width	10 ms
Puls number	1 pulse

3.2.3.9 shRNA PiggyBac electroporation

To diminish *ACTN1* expression (ACTN1 KD) in P493.6 WT as well as in *ACTN4*$^{-/-}$ cells, the PiggyBac vector PB-CMV-GreenPuro-H1-MCS which unconditionally drives shRNA expression, was utilized. To this end, *ACTN1* shRNA-expressing template (sh*ACTN1*) was cloned into the multiple cloning site (MCS) located under the control of the H1 promotor. This vector also expresses GFP which is driven by a CMV promotor. Before electroporation was conducted, the vector was amplified by Midi Preparation to minimize endotoxin contents and to increase DNA concentration. Subsequently, 2 x 10^6 cells of each cell line were washed once with 1x PBS and then resuspended in 100 µl of buffer R containing 5 µg of vector DNA and 1.5 µg of transposase vector. For electroporation, the same program as described in section 3.2.3.5 was used. As a negative control, each cell line was electroporated with 5 µg of the

PiggyBac vector expressing a non-targeting shRNA control (shCtrl). After electroporation, cells were transferred into a 6-well plate containing 2 ml RPMI medium supplemented with 20% FCS and devoid of antibiotics. 72 h after electroporation, cells were selected with 1 µg/ml puromycin for 48 h and then left to rest for another 7-10 days before cell line characterization took place.

Table 24: P493.6 cell lines that express *ACTN1* shRNA.

WT	shCtrl
	sh*ACTN1*
ACTN4$^{-/-}$	shCtrl
	sh*ACTN1*

3.2.3.10 PiggyBac transposon vector system

A PiggyBac transposon vector system (cat#: PB531A-1) was used to permanently reconstitute *ACTN4*$^{-/-}$. The transposon vector comprises a multiple cloning site (MCS) and GFP template under the control of a CMV promotor. ACTN4 cDNA was cloned into the MCS in-frame with GFP, and cells were electroporated with both vectors: the transposon vector encoding ACTN4-GFP and the transposase vector (cat#: PB210PA-1) encoding the transposase. Electroporation parameters depicted in 3.2.3.5 were used. The mechanism by which this transfection system integrates foreign DNA elements into the genome is a cut-paste mechanism, and there is no cargo limit according to the manufacturer (System Biosciences) (Figure 6).

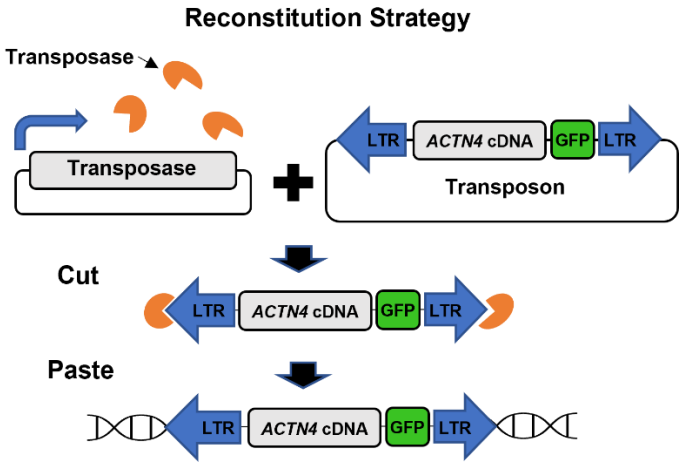

Figure 6: Schematic illustration of the PiggyBac Transposon System.
In electroporated cells that receive both vectors, the transposon and transposase, the transposase recognizes the long terminal repeats (LTRs) of the transposon vector. Subsequently, the transposase excises the LTRs flanking the gene of interest (GOI) in-frame with GFP and integrates the excised fragment into TTAA chromosomal sites.

3.2.3.11 Cell selection and cell sorting

Cells that were transfected with vectors encoding fluorescent proteins were either selected with 1 µg/ml puromycin or sorted using flow cytometry-based cell sorting. The cell sorting procedure was performed at the Core Facility Cell-Sorting in the Clinic for Hematology and Medical Oncology at Universitätsmedizin Göttingen.

3.2.3.12 Flow cytometry

Expression analysis of fluorescent proteins

To analyze the expression of ectopically expressed fluorescent proteins, such as GFP- or mCherry-tagged proteins, 1 x 10^6 cells were washed once with 1x PBS and resuspended in 300 µl of 1x PBS. Subsequently, the cells were subjected to flow cytometry analysis using 488 nm and 561 nm laser to excite GFP and mCherry, respectively.

Expression analysis of surface IgM

The expression level of surface IgM was assessed by staining 1 x 10^6 cells with APC-conjugated anti-IgM antibodies for 30 min on ice. For the staining, 1 µl of antibody stock solution was diluted in 1 ml of staining solution (2% BSA in PBS). Upon staining, cells were washed twice with PBS, resuspended in 300 µl of PBS, and analyzed by flow cytometry.

F-Actin cytoskeletal labeling

F-Actin was labeled by using the jasplakinolide-based dye SiR-actin (Spirochrome). SiR-actin is a cell permeable dye suitable for live cell staining. To perform the staining, 1 x 10^6 cells were washed once with 1x PBS prior to their incubation in 1 ml RPMI medium containing SiR-actin dye at a final concentration of 250 nM at 37 °C for 4 h. After staining, cells were washed once with 1x PBS, resuspended in 300 µl of 1x PBS and analyzed by flow cytometry. The Emission spectrum of SiR-actin dye was detected in Cy-5 channel.

Intracellular staining

A total number of 1.5 x 10^6 cells were resuspended in 100 µl of prewarmed RPMI medium devoid of FCS. An equal volume of Cytofix™ Fixation Buffer (BD) was added to each sample, and samples were incubated at 37 °C for 10 min under constant agitation. The cells were then centrifuged at 500 g for 5 min, and the cell pellet was resuspended in 400 µl of Perm/Wash Buffer (BD) diluted at a 1:10 ratio, followed by incubation for 20 min at RT. After permeabilization, the cells were stained with 100 µl of diluted Perm/Wash Buffer containing (x) µl of the antibody stock solution for 45 min at RT (table 25). Subsequently, 1 ml of diluted Perm/Wash Buffer was added, and cells were thoroughly vortexed. Finally, the cells were centrifuged for 5 min at 500 g, resuspended in 300 µl of Perm/Wash Buffer, and analyzed by flow cytometry.

Table 25: Antibodies used for intracellular staining.

Antibody	Dilution in (2% BSA in PBS)
α-pCD79A (Y188)	1:200
α-pSYK (Y525, 526)	1:200
α-pBLNK (Y84)	1:20
α-pAKT (S473)	1:100

Ca^{2+} mobilization assay

To determine intracellular calcium concentrations, 1.2 x 10^6 cells were washed once with 1x PBS. The cell pellet was then resuspended in 700 µl RPMI medium containing 5% FCS. Subsequently, cells were loaded with 1 µM Indo-1-AM and pluronic F-127 to a final concentration of 0.015% and incubated at 30 °C for 25 min under mild agitation. Indo-1-AM is a cell-permeable, ratiometric, and UV-light-excitable Ca^{2+} indicator. Its emission shifts from 475 nm (blue) to 400 nm (violet) due to Ca^{2+} binding. After dye loading, 800 µl of RPMI medium containing 10% FCS was added for another 10 min under mild agitation. The cells were then centrifuged for 4 min at 400 g and washed once with 400 µl of Krebs-Ringer buffer containing 1 mM $CaCl_2$. The cell pellet was then resuspended in 300 µl of Krebs-Ringer buffer containing 1mM $CaCl_2$ and left to rest at 25-30 °C for 20-30 min prior to the measurement. Before adding anti-human IgM $F(ab')_2$ at concentrations 1-5 µg/ml, a baseline was detected for 25 s and calcium flux was measured up to 5 min.

Apoptosis assay

Cells were seeded in RPMI medium containing 10% FCS at a density of 0.75 x 10^6 cells/ml and treated with doxycycline at a concentration of 500 ng/ml for 48 h. To assess apoptosis, 1 x 10^6 cells were centrifuged for 4 min at 400 g and then stained in 100 µl of Annexin V Binding buffer containing 1 µl of the APC-conjugated annexin V and 3 µl of the 7-AAD dye for 20-30 min. This staining allows for discrimination between early (APC Annexin V^{pos}/7-AAD^{neg}) and late apoptotic cells (APC Annexin V^{pos}/7-AAD^{pos}). After staining, another 300 µl of the annexin V Binding buffer was added to a final volume of 400 µl, and cells were analyzed by flow cytometry.

BH3 profiling

BH3 profiling assay was conducted in collaboration with Dr. Jens Löber. For the analysis, P493.6 cells were seeded at 0.25 x 10^6 cells/ml and treated with doxycycline for 48 h. 384-well plates were coated in quadruplicates per condition with 15 µl of BH3-peptides in MEB2 buffer containing 0.002% digitonin (Sigma Aldrich), including the controls DMSO and alamethicin (Enzo Life Sciences). The concentrations of the used peptides (JPT Peptide Technologies) were as follows: BIM 10/1/0.1 µM, BAD 10/1 µM, HRKγ 10/1 µM, MS1 10/1 µM, FS1 10/1 µM, PUMA 10 µM. DMSO (1%) was used as vehicle control for full retention of Cytochrome c, while alamethicin (25 µM) served as a control for complete Cytochrome c release. To trigger Cytochrome c release, cells were washed and suspended in MEB2 buffer (1 x 10^6 cells/ml). Then, 15 µl cell suspension were added to the plated peptides and controls and incubated for 1 h at 25°C. After incubation, the cells were fixed for 10 min at 25°C by adding 10 µl of 4 % formaldehyde in PBS (Suesse). The fixation process was quenched by the addition of 10 µl N2 buffer for 10 min at 25°C. The cells were then stained overnight by adding 10 µl staining solution (10% BSA, 2% Tween20 in PBS), containing 25 µg/ml Hoechst 33342 (Sigma Aldrich) and 1.25 µg/ml AF647 anti-Cytochrome c antibody (6H2.B4, Biolegend). Cells were analyzed at the next day by flow cytometry (BD LSRFortessa X-20). The DMSO control was used to determine cells with retention of Cytochrome c indicating no apoptosis.

3.2.3.13 Imaging flow cytometry

Co-localization analysis of ACTN4 and F-Actin

To directly analyze the co-localization of F-Actin and ACTN4-GFP without the need for cytoskeletal prestaining, I electroporated 2 x 10^6 cells of indicated cell lines (table 26) with 5 µg of a PiggyBac vector system encoding mCherry-tagged LifeAct and 1.5 µg transposase. 72 h upon electroporation, cells were selected with 1 µg/ml puromycin for another two days resulting in the generation of cell lines that permanently express LifeAct-mCherry. Subsequently, co-localization was analyzed by imaging flow cytometry using IDEAS software. For the analysis, 5 x 10^6 cells were washed once with 1x PBS, then resuspended in 60-80 µl 1x PBS. Only focused, single, and fluorophore double positive cells were gated and analyzed. Dyes were excited by lasers 488 nm and 561 nm for GFP and mCherry, respectively. Co-localization was defined as the percentage of cells that have a bright detail similarity ≥ 1.5.

Table 26: P493.6 cell lines that express LifeAct-mCherry.

WT LifeAct-mCherry
ACTN4$^{-/-}$ LifeAct-mCherry
ACTN4$^{-/-}$ + ACTN4-GFP LifeAct-mCherry
ACTN4$^{-/-}$ + ACTN4Δaa(100-252)-GFP LifeAct-mCherry
ACTN4$^{-/-}$ + K255E ACTN4-GFP LifeAct-mCherry

Analysis of LifeAct-mCherry fluorescence intensity

LifeAct-mCherry mean fluorescence intensity (MFI) was assessed for the WT and *ACTN4*$^{-/-}$ cell lines by imaging flow cytometry. To conduct this, 5 x 10^6 of the WT and *ACTN4*$^{-/-}$ cells expressing LifeAct-mCherry were washed once with 1x PBS and only single, focused, and fluorescent positive cells were analyzed. Of note, only the WT and *ACTN4*$^{-/-}$ were completely positive for LifeAct-mCherry expression because they were not resistant to puromycin and hence could be selected. In contrast, GFP-expressing cells were resistant to puromycin, and therefore only 10-20 % of the total cell population was positive for LifeAct-mCherry.

Co-localization analysis of ACTN4 and IgM-BCR

To analyze the co-localization of ACTN4-GFP and IgM, 5 x 10^6 cells were stained with 10 µg AZDye-568 conjugated IgM-specific nanobody (NanoTag Biotechnologies) for 30 min on ice. Upon staining, cells were washed once with 1x PBS, resuspended in 60 µl 1x PBS, and analyzed by imaging flow cytometry. Only single, focused, and ACTN4-GFP/LifeAct-mCherry fluorescent double positive cells were gated for the analysis. Dyes were excited using lasers 488 nm and 561 nm for GFP and mCherry, respectively. Co-localization was defined as the percentage of cells that have a bright detail similarity ≥ 1.5.

Co-localization analysis of IgM-BCR and F-Actin

To assess the co-localization of IgM and F-Actin, 5 x 10^6 cells of WT and *ACTN4*$^{-/-}$ cells were stained with 500 nM SiR-actin dye and incubated for 1 h on ice. Subsequently, cells were washed once with PBS and stained with 10 µg of AZDye-568-conjugated IgM-specific nanobody for another 30 min on ice. After staining, cells were washed twice with 1x PBS, resuspended in 60 µl 1x PBS, and analyzed by

imaging flow cytometry. Only single, focused, and fluorescent double positive cells were gated for the analysis. Dyes were excited by 561 nm and 641 nm lasers for AZDye-568 and SiR-actin, respectively. Co-localization was defined as the percentage of cells that have a bright detail similarity ≥ 1.5.

3.2.3.14 Microscopy

Confocal microscopy

ACTN4$^{-/-}$ and *ACTN4*$^{-/-}$+ ACTN4-GFP cells were incubated with 250 nM SiR-actin (Spirochrome, cat#: SC001) for 1 h at 4 °C. The samples were washed three times for 5 min each, to remove the excess SiR-actin. After staining, cells were resuspended in 400 µl of Krebs-Ringer buffer and analyzed by Confocal laser scanning microscopy (CLSM) (LSM 510 Meta, Zeiss). Acquired images were analyzed using Fiji/ImageJ (v. 1.53o).

Stimulated Emission Depletion (STED) microscopy

STED microscopy analysis was conducted in collaboration with the group of Prof. Dr. Silvio Rizzoli in Göttingen. For the analysis, WT and *ACTN4*$^{-/-}$ cells were incubated with 500 nM SiR-actin (Spirochrome, cat#: SC001) for 1 h at 4°C. The samples were washed three times for 5 min each, to remove the excess of SiR-actin. Cells were fixed with 4% PFA for 30 min at 4 °C and the remaining aldehydes were quenched with 0.1 M Glycine (Merck) for 15 min at RT. Glycine was removed, and cells were resuspended in Mowiol (12 ml of 0.2 M Tris buffer, 6 ml distilled water, 6 g glycerol, 2.4 g Mowiol 4-88, Merck Millipore) and mounted on microscopy slides with glass coverslips. STED microscopy of mounted samples in Mowiol took place with a STED Expert line microscope (Abberior Instruments, Göttingen, Germany). The microscopy setup was comprised of an IX83 inverted microscope (Olympus, Hamburg, Germany) equipped with UPLSAPO 100x 1.4 NA oil immersion objective (Olympus). Super-resolution STED images were obtained using 2 µW of 640 nm laser for excitation and 10 mW of 775 nm pulsed depletion laser. Images were analyzed in Fiji/ImageJ.

3.2.3.15 Single particle tracking (SPT) analysis

SPT analysis was conducted in collaboration with the group of Prof. Dr. Michael Gold in Vancouver.

Preparation of coverslips

35 mm dishes with #1.5 coverslip (Mattek, P35G-1.5-14-C) were incubated with 300 µl of 0.001% Poly-L-Lysine (Sigma, P4707) for 20 min. The Poly-L-Lysine was then aspirated, and the coverslip was washed three times with MilliQ water. Coverslips were then coated with 300 µl of 1x PBS and stored at RT until used.

IgM receptor labeling

1 x 10^6 cells of each line were incubated in 3 ml of media, supplemented with 500 ng/ml doxycycline for 48 h. Cells were then pelleted at 1500 rpm for 5 min and resuspended in 1 ml of phenol red free RPMI (Gibco, 11835) supplemented with 50 mM HEPES (Sigma, H3375) (4 °C). Cells were then counted, and 1 x 10^6 cells were resuspended and blocked in 50 µl ice cold 1x PBS (Gibco, 10010) supplemented with 5% rat serum (Stemcell technologies, 13551) for 20 min on ice. A solution containing 5 ng/ml

anti-IgM-Cy3 Fab (Jackson Immunoresearch, 109-167-003) was made in ice cold PBS containing 5% rat serum and 50 µl was added to each cell suspension and incubated on ice for 10 min. Cells were pelleted at 800 g for 5 min at 4 °C before washing in ice cold phenol red free RPMI supplemented with 50 mM HEPES. This wash step was repeated a total of three times. The cells were then resuspended at a concentration of 5 x 10^5/ml and incubated on ice until used.

Total internal reflection fluorescence (TIRF) microscopy

All single particle tracking was carried out using TIRF microscopy on a Leica super-resolution ground state depletion (SR-GSD) microscope using a 160x 1.43 NA oil immersion objective and a back-illuminated, electron-multiplying, charge-coupled device camera (iXon Ultra 697, Andor) with a 180 × 180 pixel cropped field of view utilizing a theoretical pixel size of 100 × 100 nm. 1 x 10^5 (in 200 µl) cells were added to slides along with 200 µl of phenol red free RPMI with 50 mM HEPES. Slides were equilibrated on the stage for 20 min to allow cells to settle and spread as well as to minimize drift during acquisition. Individual cells were identified using a 532 nm laser and imaged using the following settings: Exposure – 30 ms, Gain – 300, Gain List – 5, Frames – 5000, TIRF penetration depth – ~150 nm. Eight cells were imaged per condition per experimental repeat. The order in which the conditions were imaged was changed for each repeat to prevent order effects.

Image Analysis

Each stack of 5000 frames was opened in ImageJ and cropped to 1000 frames to ensure that SPT was carried out on images with optimal labeling density. Particle detection, tracking, thresholding, and analysis were carried out as previously described [131]. Briefly, individual particles were detected using the Spot Detector plugin in Icy (version 1.9.2.0, [132]). The UnDecimated Wavelet Transform detector was configured to detect bright spots, with a sensitivity to spots ~3 pixels (Scale 2) set to 50% and a size filter to ensure all spots were between 2 and 3000 pixels. The detected spots were then tracked with parameters set to recognize particles with either diffusive or directed motion using the multiple hypothesis tracking method. The saved tracks were then imported into MATLAB where immobile particles were removed using an immobility threshold, as calculated previously [131]. The tracks were then assumed to have a single state, indicating that particle displacement arises from 2-dimensional Brownian diffusion, and a trajectory analysis was carried out to calculate the diffusion coefficient for each track. This analysis used a maximum likelihood estimation as described by Berglund [133]. The calculated diffusion coefficients were then plotted as cumulative frequency graphs with all tracks from all cells from each condition in a single experiment pooled together.

4 Results

Tonic BCR signaling is a steady-state, low intensity signaling emitted by the BCR and is essential for human primary B cell survival, but the molecular details of tonic BCR signal transduction are still unclear [24]. It is known that BL cells exploit a dysregulated form of tonic BCR signaling for their survival [134]. Recently, phospho-proteome analysis of tonic BCR signaling in BL cells revealed that the F-Actin cross-linking protein ACTN4 is part of the tonic BCR signal network and essential for BL cell survival [68]. Since these data indicate a crucial role for ACTN4 in tonic BCR signaling, I elucidated its role in tonic BCR signaling transduction in the primary-like B cell line P493.6 [122].

4.1 BCR signaling properties of the primary-like P493.6 B cell model

In this study, the primary-like B cell line P493.6 was utilized to investigate tonic BCR signaling. The P493.6 cell line was generated from umbilical cord B cells that were transfected with a vector allowing for a conditional abrogation of *MYC* expression. These cells constitutively express *MYC* without doxycycline (-Dox) treatment, which drives their proliferation, thus showing all characteristics of BL cells. However, upon treatment with doxycycline (+Dox), *MYC* expression becomes repressed, and cells are arrested in the G0/G1 phase, thus resembling resting primary B cells [122].

To see if *MYC* abrogation changes BCR signaling intensity, the phosphorylation intensity of the indispensable BCR-proximal signaling kinase SYK in both an antigen-independent (tonic) and antigen-dependent (activated) manner was analyzed. To this end, P493.6 WT cells were treated with doxycycline for 48 h or left untreated, optionally followed by their stimulation with 5 µg/ml of anti-human IgM $F(ab')_2$. Cells were stained with fluorophore-conjugated anti-phospho-SYK (pY525/pY526) antibodies and analyzed by flow cytometry. Since proliferating P493.6 cells represent the BL state of this cell line, I included the BL cell lines DG75, Ramos, and Daudi, which are commonly used as human B cell model cell lines, in the analysis to compare their BCR signaling efficiency.

As indicated by MFI values, resting P493.6 cells exhibit the highest phosphorylation level for SYK in the tonic BCR state among the analyzed cell lines, which show similar levels of SYK phosphorylation (Figure 7 A). In response to BCR engagement, MFI values of phospho-SYK increase, with the strongest signal in activated resting P493.6 cells (Figure 7 B).

Moreover, the cell lines were tested for their capacity to induce Ca^{2+} mobilization in response to BCR engagement (see 3.2.3.12). Upon stimulation with low doses of anti-IgM, resting P493.6 cells show both earlier kinetics and stronger intracellular Ca^{2+} mobilization compared to their proliferative counterparts and the BL cells Daudi and Ramos (Figure 7 C). While DG75 mounts a similar BCR-induced Ca^{2+} profile, the kinetics is delayed when compared to resting P493.6 cells. After stimulating the cells with high doses of anti-IgM, these differences in Ca^{2+} mobilization were less pronounced but still detectable, except for DG75 cells, which mobilized Ca^{2+} more efficiently than all other cell lines (Figure 7 D).

These results strongly imply that BL as well as BL-like cell lines differ in the transduction efficiency of tonic and activated BCR signals, hence emphasizing the need for a B cell model that is more related to primary B cells.

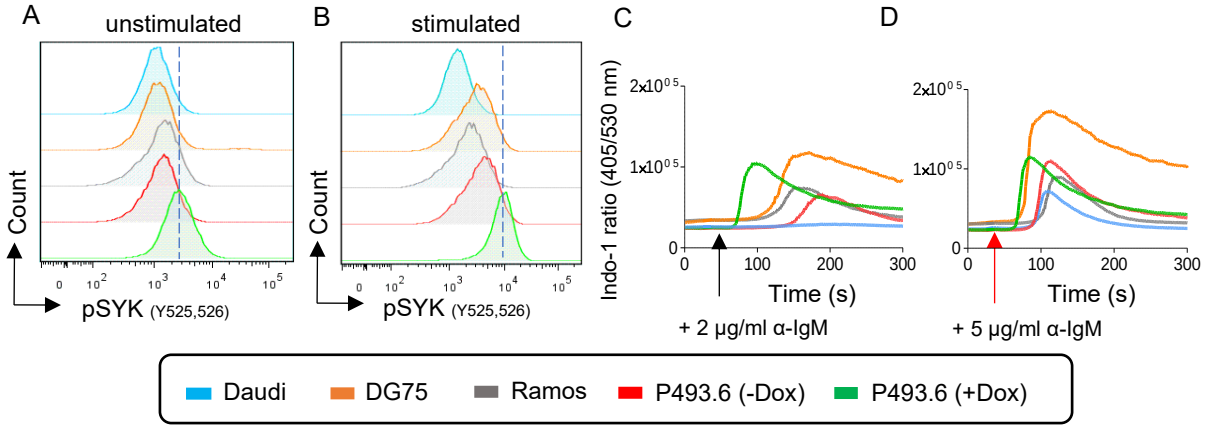

Figure 7: Resting P493.6 cells differ in the intensities of tonic and activated BCR signaling from their proliferative state and BL cell lines.
P493.6 parental cells were treated with doxycycline for 48 h (green line) or left untreated (red line) prior to the experiment. BL cell lines Daudi (blue line), Ramos (grey line), and DG75 (orange line) served as controls. Cells were subjected to intracellular staining for phosphorylated SYK using Alexa-647 conjugated α-human phospho-SYK (A & B). Before staining, cells were left unstimulated (A) or stimulated for 3 min with 5 µg/ml α-human-IgM F(ab')$_2$ fragments (B). (C & D) Cells were loaded with the Ca^{2+}-sensitive fluorophore Indo-1 AM. After recording of the basal Ca^{2+} levels for 25 s, cells were stimulated with 2 µg/ml of α-human-IgM F(ab')$_2$ fragments (black arrow) (C) or with 5 µg/ml α-human-IgM F(ab')$_2$ fragments (red arrow) (D), and the ratio of fluorescence signals at 405 nm and 530 nm was monitored for a total time of 5 min.

4.2 Generation of an ACTN4-deficient P493.6 cell line

CRISPR/Cas9 was used to target exon 2 of the *ACTN4* gene locus, *via* electroporation of sgRNA (crRNA/tracrRNA duplex) together with Cas9 endonuclease into P493.6 parental cells. The utilized sgRNA was chosen to have minimal off-target activity. 48 h after electroporation, single clones were isolated and expanded up to three weeks (see 3.2.3.4-7).

By subjecting CCLs of 50 single clones to anti-ACTN4 WB analysis, I identified 34 clones showing no detectable protein expression. In figure 8 A, a selection of the screening result is shown. From two of these clones, clone #3 and clone #5, the genomic region covering exon 2 of *ACTN4* was amplified by PCR, and the resulting amplicons were cloned into a pCR2.1 vector and subjected to Sanger sequencing. Blasting of sequenced clones against the WT ACTN4-encoding sequence revealed that clone #3 has a 1 base pair (bp) insertion on one allele and a 17 bp deletion on the other, while clone #5 exhibits a 2 bp deletion on one allele and an 11 bp deletion on the other allele. Induced indel mutations led to premature stop codons in both clones (Figure 8 B-E).

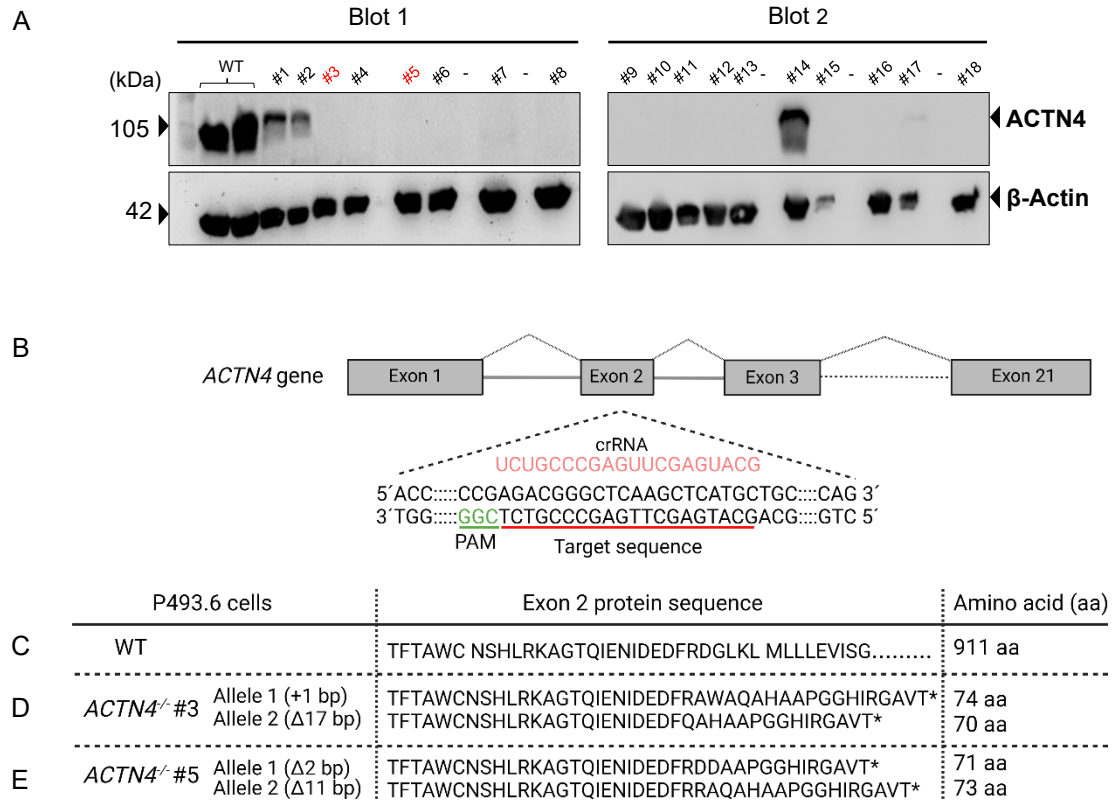

Figure 8: Generation and genetic characterization of ACTN4-deficient P493.6 clones #3 and #5.
(A) Cleared cellular lysates (CCLs) of the screened *ACTN4*$^{-/-}$ cells were subjected to WB analysis using antibodies specific for ACTN4 and β-Actin. (B-E) To genetically characterize *ACTN4*$^{-/-}$ P493.6 clones #3 and #5 (red), their genomic DNA was extracted, and exon 2 of ACTN4 was amplified, cloned into pCR2.1 vector, and subjected to Sanger sequencing. Using the Basic Local Alignment Search Tool (BLAST), the sequenced DNA was blasted against the WT ACTN4 sequence and translated into a protein sequence using BLASTx. (B) Scheme of ACTN4-encoding gene. The crRNA (light red) that was used to target exon 2 (red) and the PAM sequence for Cas9 is depicted in green. (C) The translated amino acid sequence referring to exon 2 in P493.6 WT cells, (D) the *ACTN4*$^{-/-}$ clone #3, and (E) the *ACTN4*$^{-/-}$ clone #5.

To exclude clonal and off-target effects, I reconstituted ACTN4-deficient cells by electroporation with a PiggyBac vector encoding ACTN4-GFP. Cells were analyzed for protein expression by subjecting their CCLs to WB analysis. ACTN4-GFP was expressed in both reconstituted clones and showed the correct apparent molecular weight compared to non-tagged ACTN4 expressed in WT cells (Figure 9 A). Flow cytometry analysis confirmed GFP expression in both reconstituted clones compared to WT and ACTN4-deficient cells that served as a negative control (Figure 9 B).

To visualize protein localization, I analyzed the reconstituted cells using Confocal laser scanning microscopy (CLSM). Confocal images revealed ACTN4-GFP localization near the plasma membrane of P493.6 cells in spot-like structures. ACTN4-GFP was very weakly present in the cytosol and not detectable in the nucleus (Figure 9 C).

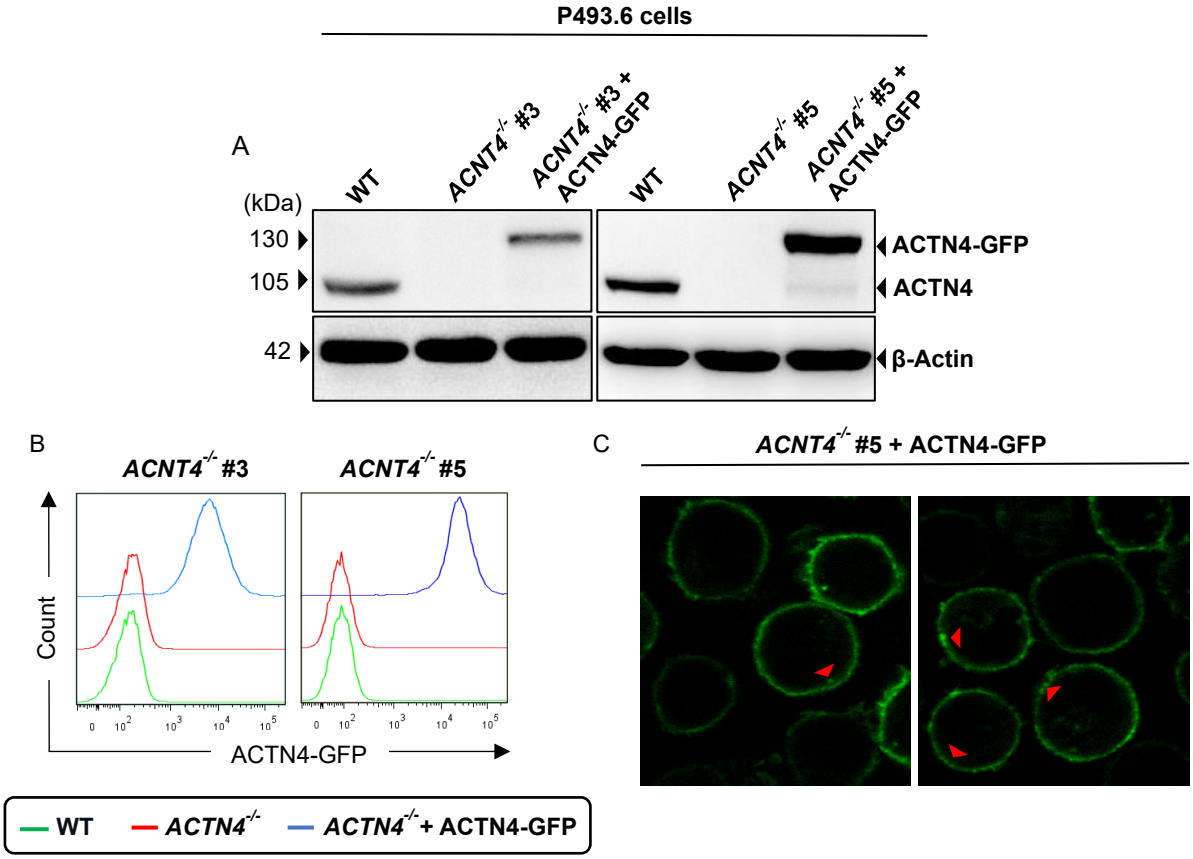

Figure 9: Reconstitution and characterization of ACTN4-deficient clones #3 and #5.
ACTN4$^{-/-}$ clones #3 and #5 were reconstituted with a vector encoding GFP-tagged ACTN4. (A) CCLs of P493.6 parental, *ACTN4*$^{-/-}$ #3 & #5, and *ACTN4*$^{-/-}$ *#3 & #5* + ACTN4-GFP cells were subjected to WB analysis using antibodies specific for ACTN4 and β-Actin. (B) Flow cytometry analysis of *ACTN4*$^{-/-}$ *#3 & #5* + ACTN4-GFP cells (blue line) compared to WT and *ACTN4*$^{-/-}$ #3 & #5 cells (green and red lines, respectively). (C) Localization of GFP-tagged ACTN4 in the reconstituted cells of ACTN4-deficient clones was visualized by Confocal LSM. ACTN4 localization in spot-like structures (red arrows).

4.3 Alpha-Actinin-4 positively regulates Ca^{2+} mobilization of resting P493.6 cells

To assess whether ACTN4-deficiency in the generated cell lines alters BCR expression levels, which might interfere with tonic and activated BCR signaling intensity [67], I stained for IgM surface expression with an APC-conjugated anti-human IgM. This approach revealed unaltered IgM surface expression levels in *ACTN4*$^{-/-}$ cells compared to WT and reconstituted cells (Figure 10 A & B).

To examine the BCR signaling efficiency in the generated *ACTN4*$^{-/-}$ cells, Ca^{2+} mobilization analyses were applied. After recording the baseline signal for 25 s, I stimulated the cells with 2 µg/ml (clone #5) or 5 µg/ml (clone #3) of anti-IgM F(ab')$_2$ fragments. Ca^{2+} profiles of clone #3 and clone #5 were compared to WT and reconstituted *ACTN4*$^{-/-}$ cells. In line with previous results (Figure 7), resting P493.6 cells showed Ca^{2+} levels up to 3-fold higher than their proliferative counterpart cells (Figure 10 C *vs.* D & E *vs.* F). Regardless of different anti-IgM concentrations for stimulation, *ACTN4*$^{-/-}$ cells of both clones showed an attenuated BCR-induced Ca^{2+} response compared to WT cells, which was most pronounced in the resting states. Upon reconstitution, Ca^{2+} mobilization was restored in clone #3 and reconstituted cells of clone #5 exhibited a slight increase in Ca^{2+} mobilization compared to parental cells (Figure 10 D & F).

In summary, my results reveal that the established P493.6 cell lines have similar surface IgM expression levels to parental cells and are in general capable of mounting BCR signal transduction. Moreover, the data indicate that ACTN4 positively regulates BCR-induced Ca^{2+} mobilization in resting P493.6 cells.

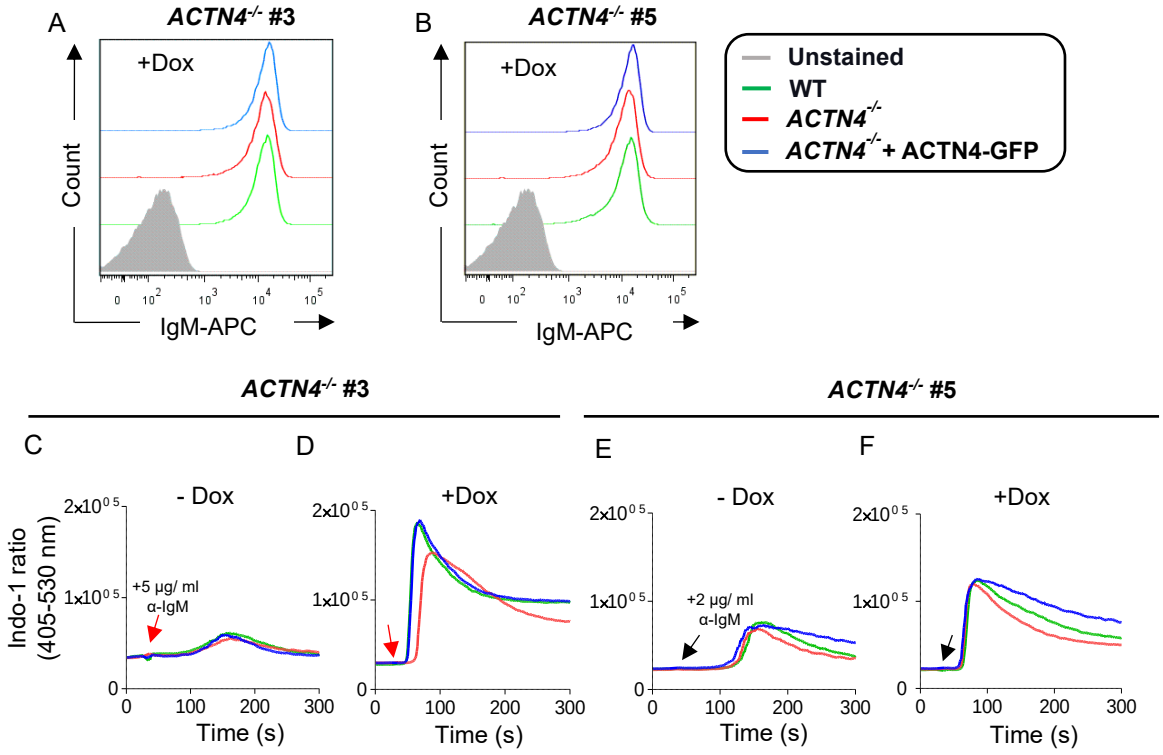

Figure 10: ACTN4 positively regulates BCR-induced Ca^{2+} mobilization in resting P493.6 cells.
WT (green line), *ACTN4*$^{-/-}$ (red line; clone #3 (A, C, & D) and clone #5 (B, E, & F)), and ACTN4-GFP reconstituted cells (blue line) were treated with doxycycline for 48 h or left untreated. (A & B) Flow cytometric analysis of resting P493.6 cells that were stained with APC-conjugated α-human IgM antibodies. Non-stained WT cells served as a negative control (grey). (C-F) Cells were loaded with the Ca^{2+}-sensitive fluorophore Indo-1-AM. After the recording of the basal signal for 25 s, cells were stimulated with 5 µg/ml (red arrows) (C & D) or 2 µg/ml (black arrows) (E & F) of α-human IgM $F(ab')_2$ fragments, and the fluorescence was monitored for a total time of 5 min. The graphs are representative of three independent experiments.

4.4 Alpha-Actinin-4 supports the survival of resting P493.6 cells

To assess whether ACTN4 is involved in tonic BCR survival signaling of resting P493.6 cells, I performed apoptosis assays after culturing the cells in the presence of doxycycline for a duration of up to a week. To discriminate between live, early apoptotic, and late apoptotic cells, they were stained with Annexin V and 7-ADD prior to flow cytometry analyses.

Dot plots (Figure 11 A) show the gating strategy used to evaluate apoptosis after two and seven days of doxycycline treatment. Each dot plot represents three segregated cell populations: the living cells (Annexin V^{neg}/7-AAD^{neg}), the early apoptotic cells (Annexin V^{pos}/7-AAD^{neg}), and the late apoptotic cells (Annexin V^{pos}/7-AAD^{pos}). Flow cytometry analysis showed that the apoptosis was mildly augmented in *ACTN4*$^{-/-}$ cells compared to WT and reconstituted cells, at day zero, which still represents the proliferative state of P493.6 cells. As expected, apoptotic cell levels increased with prolonged culturing time with doxycycline because of the lack of *MYC* expression (resting state). Compared to WT cells, the apoptosis of *ACTN4*$^{-/-}$ clone (#3) did not change after two days of doxycycline treatment (Figure 11 B), while in the case of *ACTN4*$^{-/-}$ clone #5, apoptosis levels were augmented after one and two days of doxycycline treatment (Figure 11 C).

After one week of proliferation arrest, WT cells survived slightly better than *ACTN4*$^{-/-}$ (clone #5) and exhibited approximately 10% less apoptosis than *ACTN4*$^{-/-}$ cells of clone #3. Consistently, reconstitution led to better survival than their *ACTN4*$^{-/-}$ counterpart cells (Figure 11 B & C).

In conclusion, these results indicate that ACTN4 contributes to resting P493.6 cell survival, suggesting a role in tonic BCR survival signaling. Since both analyzed *ACTN4*$^{-/-}$ clones showed similarly increased sensitivity to apoptosis with slightly faster kinetics in clone #5, I used clone #5 for further analyses and hereinafter referred to it as *ACTN4*$^{-/-}$.

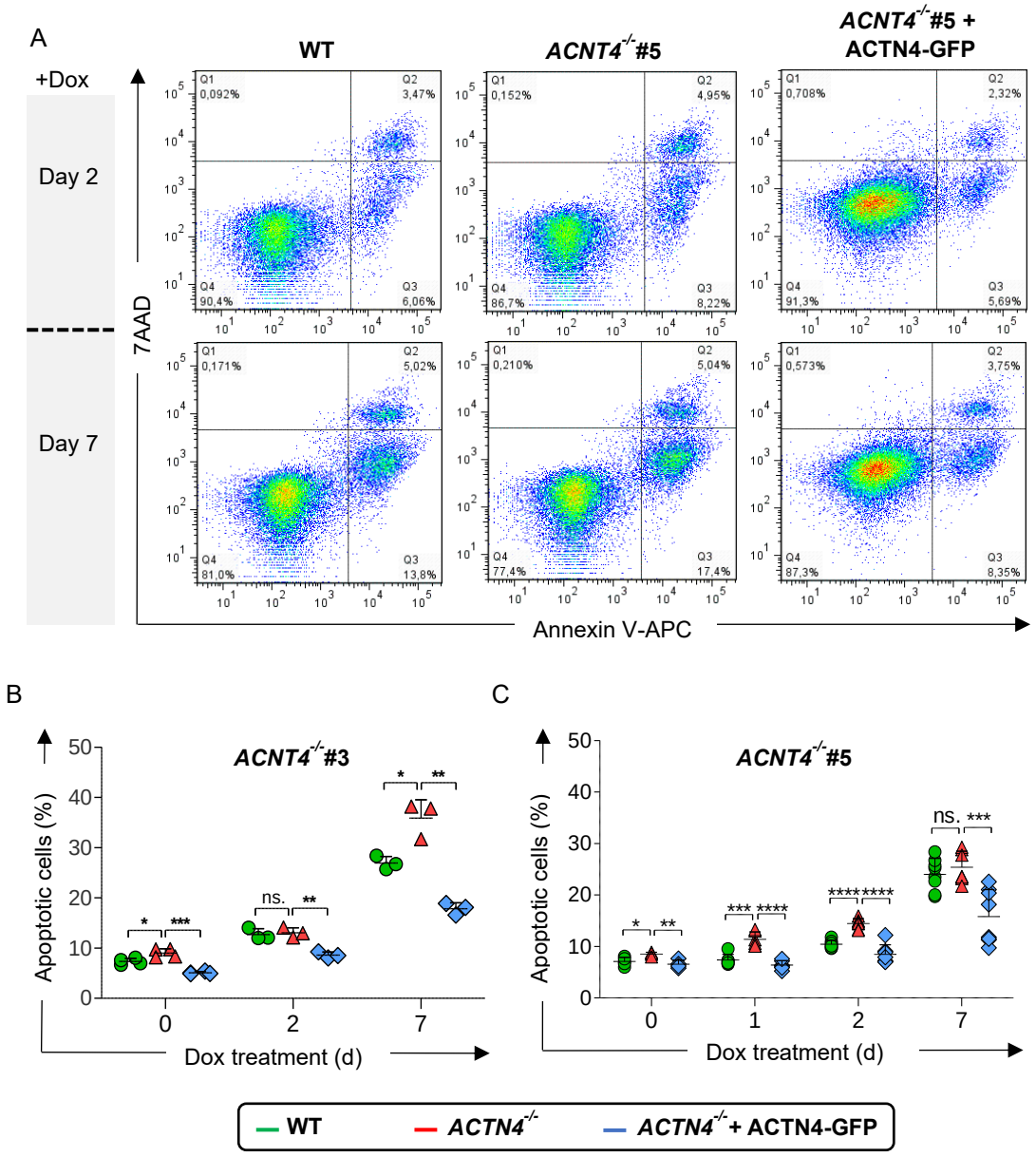

Figure 11: ACTN4 supports the survival of resting P493.6 cells.
WT, *ACTN4*$^{-/-}$ #3 & #5, and the ACTN4-GFP reconstituted *ACTN4*$^{-/-}$ cells were treated with 500 ng/ml doxycycline for the indicated times. Flow cytometric analysis to assess apoptosis was conducted after staining the cells with Annexin V-APC and 7-AAD. (A) Dot plots illustrate the gating strategy to distinguish between living, early, and late apoptotic cells for the different cell lines after two and seven days of proliferation arrest. (B & C) The graphs represent the total apoptosis (early + late) at indicated times after doxycycline treatment in clone #3 (B) and clone #5 (C). The graphs depict the mean ± SD of at least three independent experiments. Individual values are plotted. P-values are determined by a two-tailed t-test. ****: p<0.0001, ***: p<0.001, **: p<0.01, *: p<0.05, ns.: not significant.

4.5 Alpha-Actinin-1 is dispensable for the survival of resting P493.6 cells

While phospho-proteome analysis of tonic BCR signaling in BL cells identified ACTN4 as an effector protein, the role of ACTN1, which is also expressed in B cells, remains unclear [68]. But since ACTN4 and ACTN1 are highly homologous F-Actin cross-linking proteins [99], I assessed whether ACTN1 also regulates tonic BCR survival signals. Hence, I electroporated WT and *ACTN4*$^{-/-}$ cells with shRNA vectors co-expressing GFP with either *ACTN1* shRNAs (sh*ACTN1*) or control shRNAs (shCtrl) (see 3.2.3.9).

As indicated by WB analysis of CCLs, expression of sh*ACTN1* in WT and *ACTN4*$^{-/-}$ cells markedly reduced ACTN1 protein levels, compared to shCtrl cells (Figure 12 A & B). Indicated by comparable GFP expression levels, WT and *ACTN4*$^{-/-}$ cells express similar amounts of sh*ACTN1* and shCtrl. WT cells served as a negative control (Figure 12 C & D). ACTN1 reduction did not interfere with BCR surface expression, as revealed by flow cytometric analysis of APC-conjugated anti-human IgM-stained cells. Unstained WT cells served as a negative control (Figure 12 E & F).

Taken together, the *ACTN1* expression was downregulated in resting P493.6 cells using an shRNA expression vector. The reduced expression of ACTN1 did not interfere with surface IgM expression.

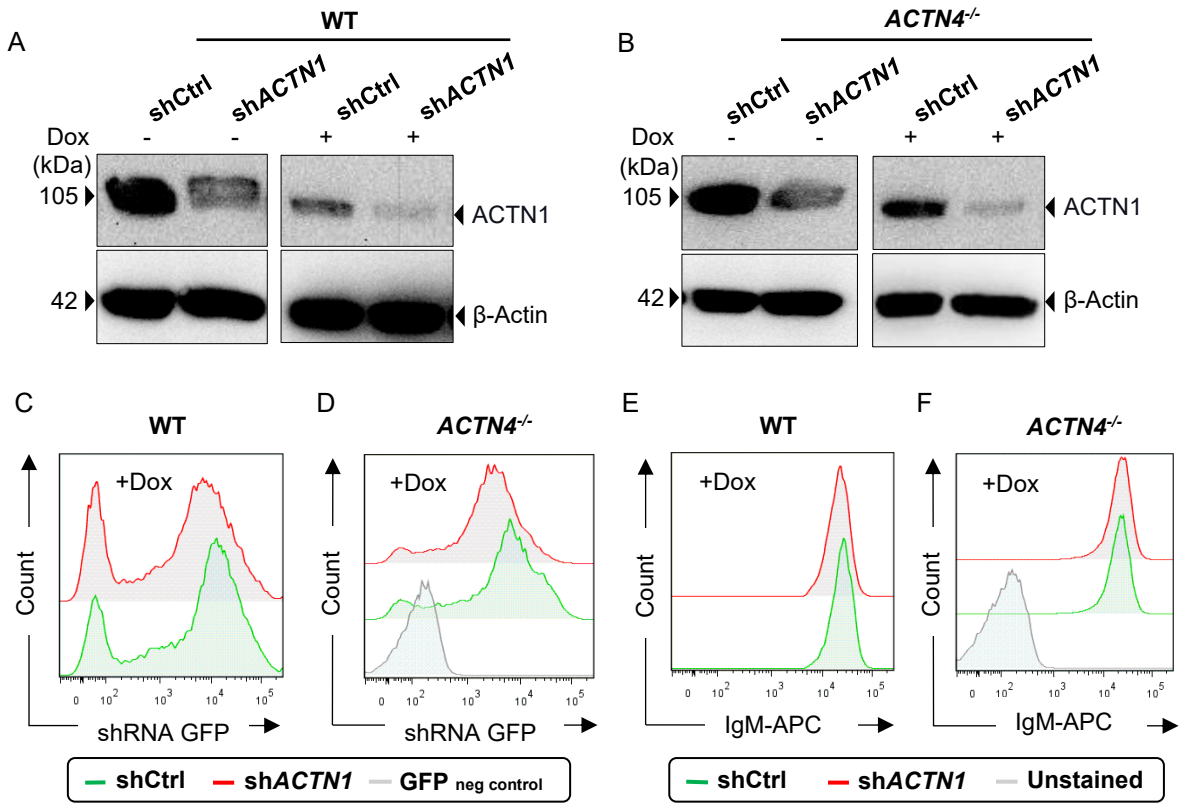

Figure 12: Generation of cell lines with downregulation of *ACTN1* expression.
P493.6 WT (A, C & E) and *ACTN4*$^{-/-}$ cells (B, D & F) were electroporated with a vector encoding an shRNA targeting *ACTN1* (sh*ACTN1*, green tinted) or non-targeting shRNA (red tinted) as a negative control (shCtrl). Cells were then treated with doxycycline for 48 h or left untreated. (A & B) CCLs were subjected to WB analysis using antibodies specific for ACTN1 and β-Actin. (C & D) Flow cytometry analysis was conducted to assess GFP, which was co-expressed with shRNAs. (E & F) IgM expression of indicated cells. Unstained WT cells expressing shCtrl were used as a negative control.

To assess whether ACTN1 contributes to the survival of resting P493.6 cells, WT and *ACTN4*$^{-/-}$ cells expressing either shCtrl or sh*ACTN1* were treated with doxycycline for 48 h, followed by Annexin V-APC and 7-AAD-based apoptosis assays.

The downregulation of *ACTN1* expression affected neither WT nor *ACTN4*$^{-/-}$ cell survival compared to their control counterparts (Figure 13).

In summary, these data suggest that unlike ACTN4, ACTN1 seems to be dispensable for resting P493.6 cell survival.

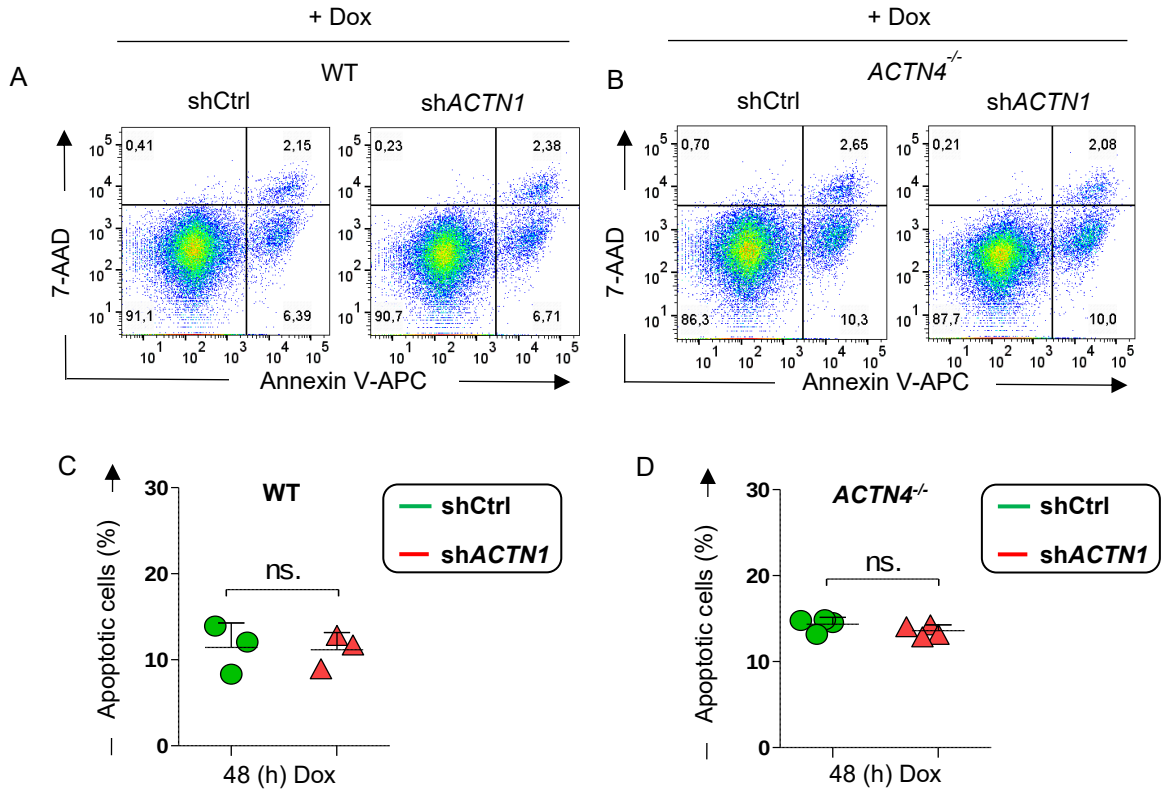

Figure 13: Downregulation of ACTN1 expression in resting WT and *ACTN4*$^{-/-}$ cells does not affect their survival.
WT (A & C) and *ACTN4*$^{-/-}$ cells (B & D) expressing sh*ACTN1* or non-targeting control shRNA (shCtrl) were treated with doxycycline for 48 h. Apoptotic cells were identified after staining with Annexin V-APC and 7-AAD. (A & B) Dot plots depict the different apoptotic states. (C & D) The aligned dot plots represent the mean ± SD of the total apoptosis (early + late) of three independent experiments. P-values were determined by a two-tailed t-test. ns.: not significant.

4.6 Alpha-Actinin-4 supports the survival of primary human B cells

My previous results imply that ACTN4, but not ACTN1, is involved in P493.6 cell survival. However, since resting P493.6 cells are only a model for primary B cells, I assessed whether the observed ACTN4-phenotype is applicable to primary human B cells.

To this end, 30-40 million primary human B cells were isolated from buffy coat using a pan-B cell negative selection kit to avoid pre-stimulation of purified cells. To confirm purity, B cells were labeled with APC-Cy7-conjugated anti-CD19 antibodies and analyzed by flow cytometry. Analysis showed that

more than 95% of purified cells expressed CD19 compared to unstained cells, indicating a sufficiently enriched B cell population (Figure 14 A).

To target *ACTN4* expression in isolated primary B cells, I electroporated them with the same CRISPR sgRNAs, which were used to generate P493.6 *ACTN4*$^{-/-}$ cell lines. As a negative control, I electroporated the cells with the non-targeting portion of the sgRNA (tracrRNA) in combination with Cas9. Since *CD79B* expression is essential for tonic BCR survival signals, cells were electroporated with sgRNAs that targeted the *CD79B* gene locus and served as a positive control to monitor the maximal decrease of survival in this approach (Figure 14 B & C).

CCLs derived from each population were subjected to WB analysis using antibodies specific for ACTN4, CD79B, and β-Actin, respectively, and signal intensities were normalized to β-Actin signals. Although cells have received the same sgRNA concentrations, *CD79B* expression was downregulated to around 60%, while *ACTN4* expression was only reduced by 25-30% (Figure 14 D & E). Despite the different efficiencies, genes targeting in primary human B cells was successful, allowing for the study of whether reduced expression of *ACTN4* affects their survival.

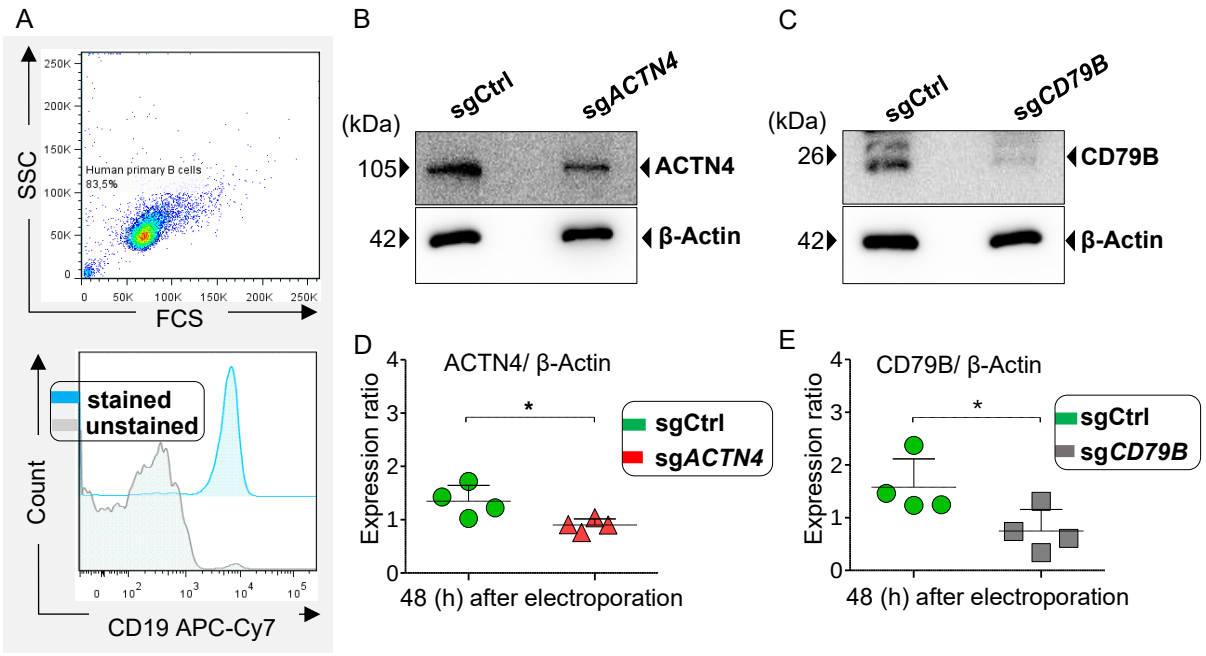

Figure 14: CRISPR/Cas9-based targeting of the ACTN4-encoding gene in human primary B cells.
Human primary B cells were isolated from buffy coat and electroporated with pre-formed (tracrRNA/crRNA)/Cas9 complexes either targeting *ACTN4* (sg*ACTN4*) or *CD79B* (sg*CD79B*) or serving as a non-targeting control (sgCtrl). (A) Flow cytometry analysis of purified B cells after APC-Cy7-conjugated α-human CD19 staining (blue tinted). Unstained cells served as negative control (grey-tinted). (B & C) WB analysis of CCLs from resulting primary B cells. (E & F) Quantifications of the relative expression level of ACTN4 and CD79B compared with the controls, normalized to β-Actin signals. Graphs represent the mean ± SD of three independent experiments. P-values were determined by a two-tailed t-test. *: $p<0.05$.

To assess whether reduced *ACTN4* expression affects primary B cell survival, apoptosis assays for the resulting cells were conducted and analyzed by flow cytometry up to 48 h after electroporation. Generally, after 18 h, 24 h, and 48 h of electroporation, the survival of primary B cells was compromised, which may be attributed to factors such as the transfection procedure itself and their generally poor

viability *ex vivo* (Figure 15 A). Nevertheless, since controls were included, the apoptosis rates could be monitored for up to 48 h after electroporation.

Up to 48 h after electroporation, reduced *ACTN4* expression rendered primary B slightly more prone to apoptosis, in a significant manner compared to control cells. Reduced *CD79B* expression also caused an augmented apoptosis sensitivity compared to the control cells, albeit more pronounced than in the ACTN4 approach (Figure 15 B).

In conclusion, these results corroborate the supportive function of ACTN4 in B cell survival and confirm the suitability of resting P493.6 cells as a primary-like B cell model.

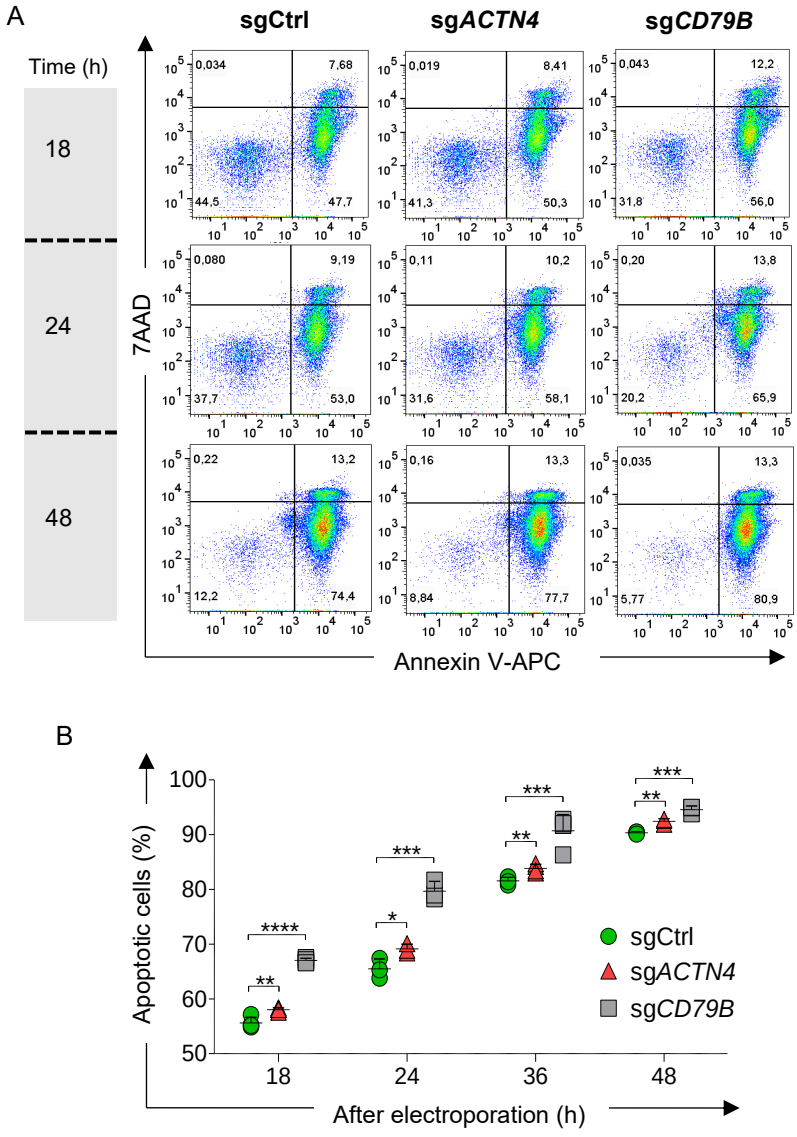

Figure 15: ACTN4 supports resting primary B cell survival.
Electroporated primary human B cells (sgCtrl, sg*ACTN4*, sg*CD79B*) were stained with Annexin V-APC and 7-AAD at the indicated times and analyzed by flow cytometry. (A) Dot plots illustrate the portions of viable, early, and late apoptotic cells after 18 h, 24 h, and 48 h of electroporation. (B) The aligned dot plot depicts the total apoptotic (early + late apoptotic) cells at the indicated times. Primary cells used for this experiment were from two different donors on a voluntary basis. P-values were determined by a two-tailed t-test. ***: p<0.001, **: p<0.01, *: p<0.05.

4.7 Alpha-Actinin-4 supports the survival of resting P493.6 cells *via* the BFL-1 survival axis

To gain insights into the details of how ACTN4 augments resting mature B cell survival, a BH3 profiling assay was conducted in collaboration with Dr. Jens Löber. To this end, the different P493.6 cell lines were treated with small pro-apoptotic peptides such as BIM or sensitizer BH3-only peptides such as PUMA, BAD, HRK, MS-1, and FS-1 that prime cells for apoptosis by engaging and thereby sequestering anti-apoptotic proteins (Figure 16 A), leading to Cytochrome c release, which is the point of no return of apoptosis signaling cascades [135].

For the analysis, DMSO was used as vehicle control for full retention of Cytochrome c, and alamethicin served as a positive control for complete Cytochrome c release induced by a chemical disruption of the mitochondrial membrane integrity. BIM served as a positive control to predict the total dynamic range of apoptosis induction. After treatment with the different BH3 peptides, cells were intracellularly stained with Alexa Fluor® 647-conjugated anti-Cytochrome c antibodies and analyzed by flow cytometry.

Regardless of *MYC* expression, treating the different P493.6 cells with BIM led to an almost complete release of Cytochrome c, indicating that P493.6 cells possess an intact apoptosis machinery. However, at lower concentrations, proliferative cells were more sensitive to BIM treatment than resting cells. Similarly, proliferative cells were more sensitive to PUMA treatment than resting cells (Figure 16 B & C). The lower sensitivity of resting cells for both treatments might be attributed to the more efficient tonic BCR survival signaling in resting compared to proliferative cells (Figure 7). Hence, it is possible that the increase in tonic BCR survival signals of resting P493.6 cells lowers their sensitivity for both treatments.

Interestingly, proliferative as well as resting P493.6 cells showed almost no sensitivity for BAD, HRK, and MS-1, indicating that P493.6 cells barely require BCL-2, BCL-xL, and MCL-1 for their survival. In contrast, treating the cells with FS-1, the inhibitor of BFL-1, resulted in Cytochrome c release of about 60% in proliferative and 20% in resting cells, respectively (Figure 16 B & C). Since PUMA sequesters BCL-2, BCL-xL, MCL-1, and BFL-1, it is plausible to propose that PUMA-triggered Cytochrome c release was solely due to the inhibition of BFL-1, as the inhibition of BCL-2, BCL-xL, and MCL-1 did not induce Cytochrome c release.

In resting P493.6 cells, while WT cells showed a slight reduction in their sensitivity for FS-1 and PUMA treatments compared to *ACTN4*$^{-/-}$ cells, the re-expression of *ACTN4* in *ACTN4*$^{-/-}$ cells rendered them half as sensitive to both treatments (Figure 16 C). Hence, this is consistent with the pro-survival phenotype which was more pronounced in reconstituted than WT cells.

In summary, results suggest that the apoptosis of P493.6 cells can be driven by apoptotic pathways and that ACTN4 renders resting P493.6 cells less sensitive to FS-1 pro-apoptotic peptide treatments that antagonize the BFL-1 survival axis.

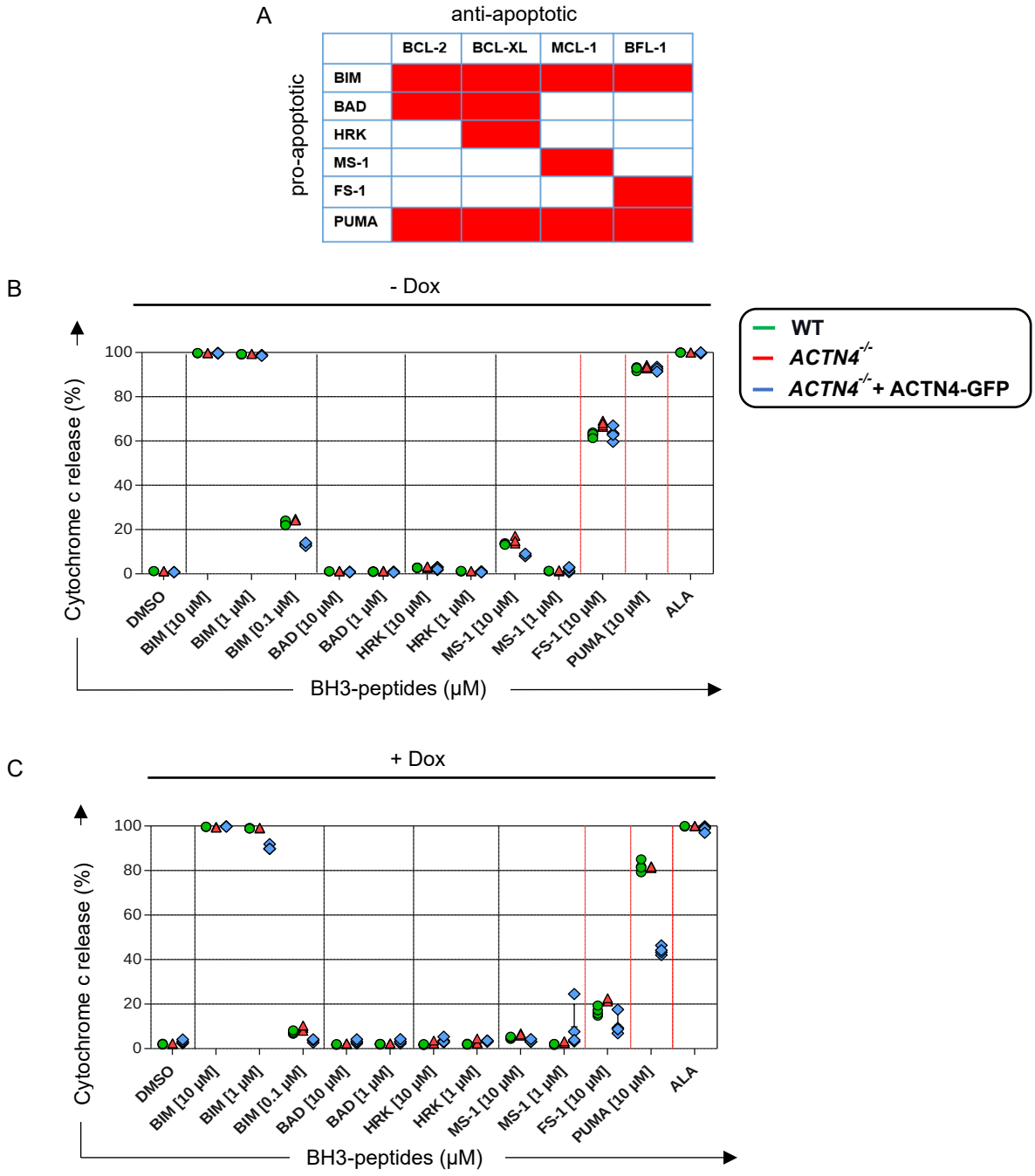

Figure 16: ACTN4 reduces the general sensitivity of resting P493.6 cells for apoptosis.
(A) The binding matrix depicts the selectivity of pro-apoptotic proteins to engage and inhibit anti-apoptotic proteins (red boxes). (B & C) WT (green circle), *ACTN4*$^{-/-}$ (red triangles), and reconstituted cells (blue diamonds) either without treatment (B) or doxycycline-treated for 48 h (C). Cells were then incubated with the indicated BH3-peptides, fixed, neutralized, intracellularly stained with AF647-labelled antibodies specific for Cytochrome c, and analyzed by flow cytometry. DMSO was used as vehicle control for full retention of Cytochrome c, while BIM served as a control for complete Cytochrome c release. The aligned dot plots represent one of two independent experiments that were conducted in quadruplicates and revealed the same results.

4.8 Alpha-Actinin-4-dependent stabilization of F-Actin correlates with P493.6 cell survival

4.8.1 Alpha-Actinin-4 alters the amount, but not the spatial organization of F-Actin

ACTN4's hallmark is to cross-link and organize F-Actin [96,99]. In addition, previous studies have shown that alteration in Actin remodeling can impact tonic BCR survival signals [136].

To examine whether ACTN4 loss impacts the overall spatial organization of F-Actin in P493.6 cells, I stained WT and *ACTN4*$^{-/-}$ cells with SiR-actin, which is a suitable dye for F-Actin labeling in living cells. Cells were visualized by STED and Confocal LSM, which was conducted in collaboration with the group of Prof. Dr. Silvio Rizzoli in Göttingen.

Confocal and STED microscopy revealed that resting P493.6 cells possess a ring-shaped condensed F-Actin network localized in their cortical area (Figure 17 A), which is in line with previous studies that visualized the F-Actin network in the cortical area of B cells [137,138]. ACTN4 loss did not impact the general structure of F-Actin in P493.6 cells. Apparently, ACTN4 loss reduces SiR-actin fluorescence intensity compared to WT cells, indicating an overall attenuated F-Actin amount. The abundance of F-Actin extrusions was variable and not significantly different in the WT compared to *ACTN4*$^{-/-}$ cells (Figure 17 A & B).

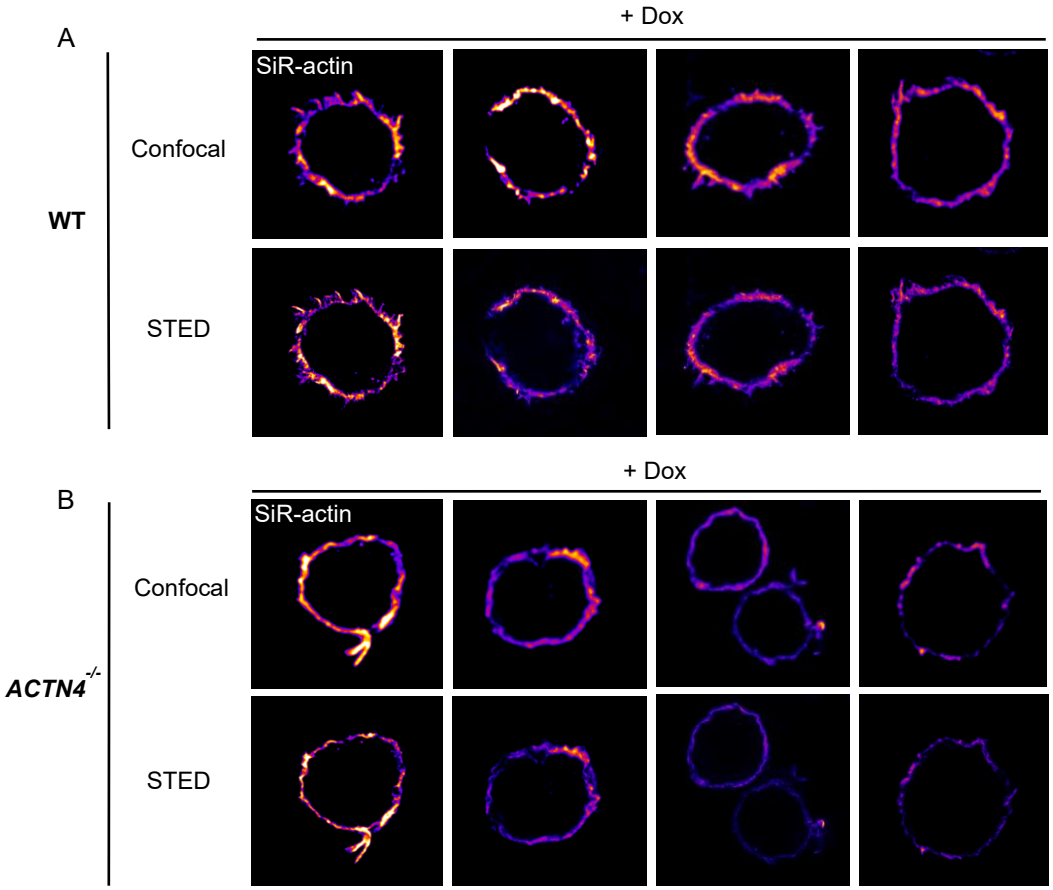

Figure 17: ACTN4-deficiency does not alter the spatial organization of filamentous Actin.
WT (A) and *ACTN4*$^{-/-}$ (B) cells were treated with doxycycline for 48 h, fixed and stained with 500 nM SiR-actin, and visualized by Confocal (upper row) and STED microscopy (lower row). Single images were processed and analyzed using Image J. Images are representative of 10-12 images for the WT as well as *ACTN4*$^{-/-}$ cells.

To clarify whether ACTN4 loss has an impact on the amount of F-Actin, SiR-actin-stained WT and *ACTN4*$^{-/-}$ cells were analyzed by flow cytometry (Figure 18 A & B). As indicated by the normalized SiR-actin MFI values, proliferative as well as resting *ACTN4*$^{-/-}$ cells exhibit 10-15% less overall amount of F-Actin compared to WT cells (Figure 18 E & F).

Taken together, my results show that the F-Actin network is localized at the cortical area of resting P493.6 cells. Although ACTN4 does not alter the general F-Actin spatial organization, results indicate that it does stabilize cortical F-Actin.

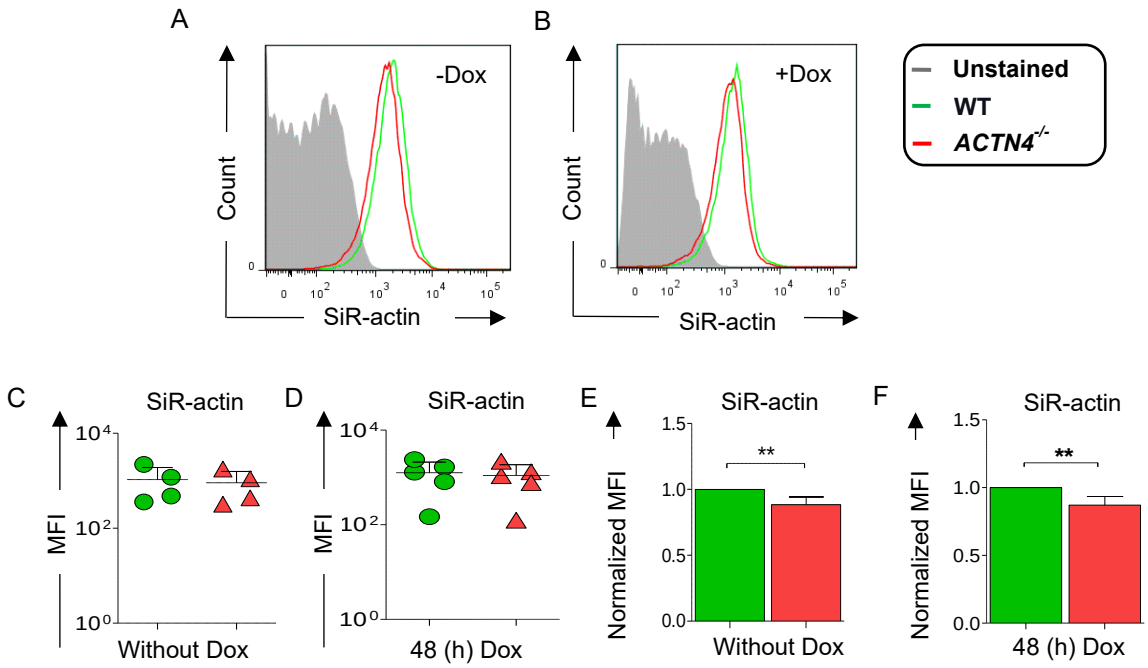

Figure 18: ACTN4 loss slightly reduces the overall amount of F-Actin.
WT (green line/circle) and *ACTN4*$^{-/-}$ cells (red line/triangle) were either left untreated (A, C & E) or treated with doxycycline for 48 h (B, D & F), stained with 250 nM of SiR-actin, and analyzed by flow cytometry. (A & B) The overlay histograms exhibit the MFI values of SiR-actin-stained WT compared to *ACTN4*$^{-/-}$ cells. Unstained *ACTN4*$^{-/-}$ cells served as a negative control. (C & D) The aligned dot plots depict the MFI values for each experimental repetition. (E & F) MFI values of *ACTN4*$^{-/-}$ cells were normalized to that of the WT cells for each repetition. The diagrams show the mean ± SD of at least three independent experiments. P-values were determined by a two-tailed t-test. **: $p<0.01$.

To examine whether the re-expression of *ACTN4* in *ACTN4*$^{-/-}$ cells re-establishes the amount of F-Actin, SiR-actin-stained *ACTN4*$^{-/-}$ and *ACTN4*$^{-/-}$ + ACTN4-GFP cells were analyzed by flow cytometry (Figure 19 A & B).

Indicated by the normalized MFI values of SiR-actin, the re-expression of *ACTN4* in *ACTN4*$^{-/-}$ increases F-Actin by approximately 2-fold in proliferative and 1.6-fold in resting reconstituted cells compared to their *ACTN4*$^{-/-}$ counterpart cells (Figure 19 E & F). Notably, the ACTN4-mediated impact on F-Actin was more pronounced in reconstituted than WT cells, suggesting a correlation with its observed pro-survival phenotype.

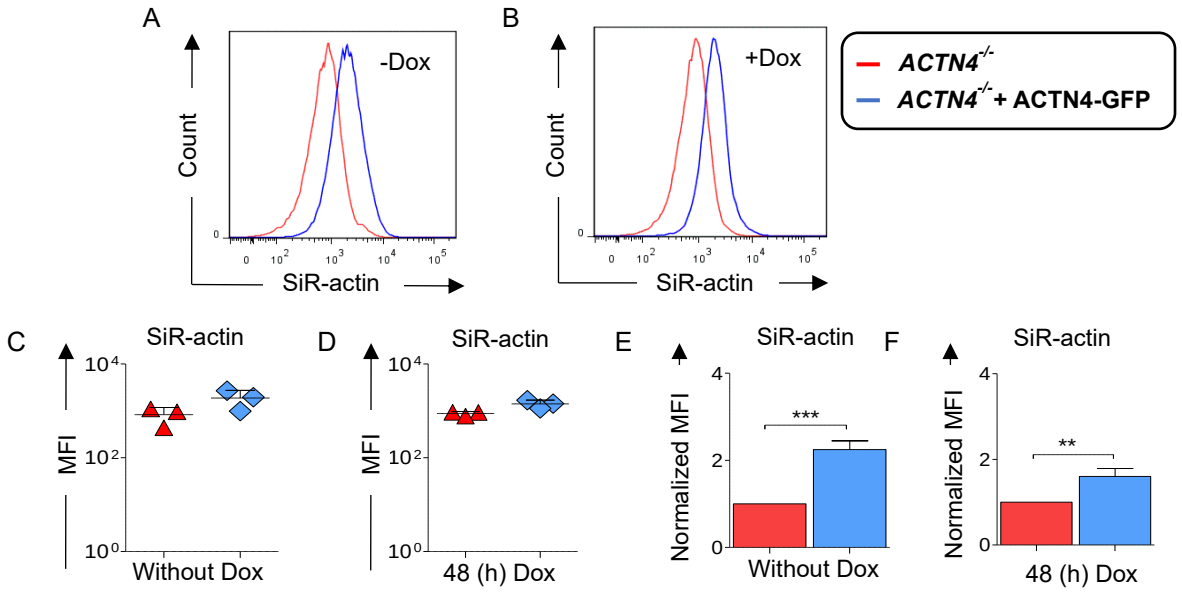

Figure 19: ACTN4 reconstitution increases F-Actin overall amount in ACTN4-deficient cells.
ACTN4$^{-/-}$ (red line/triangle), and *ACTN4*$^{-/-}$+ ACTN4-GFP cells (blue line/diamond) were either left untreated (A, C, & E) or treated with doxycycline for 48 h (B, D & F), stained with 250 nM of SiR-actin, and analyzed by flow cytometry. (A & B) The overlay histograms show SiR-actin MFI values of *ACTN4*$^{-/-}$ + ACTN4-GFP compared to *ACTN4*$^{-/-}$ cells. (C & D) The aligned dot plots depict the MFI values for each experimental repetition. (E & F) MFI values of *ACTN4*$^{-/-}$+ ACTN4-GFP were normalized to that of the *ACTN4*$^{-/-}$ cells for each repetition. The diagrams depict the mean ± SD of three independent experiments. P-values were determined by a two-tailed t-test. ***: p<0.001, **: p<0.01.

Complementary to SiR-actin staining, WT and *ACTN4*$^{-/-}$ cells were electroporated with a construct encoding for LifeAct-mCherry. LifeAct is a 17-aa-long polypeptide that specifically labels F-Actin in living cells and does not interfere with F-Actin dynamics, both *in vitro* and *in vivo* [139]. The resulting cells were either left untreated (Figure 20 A & B) or stimulated with anti-IgM F(ab')$_2$ fragment for 1 h (Figure 20 C & D) and analyzed by imaging flow cytometry.

Regardless of *MYC* state and stimulation, *ACTN4*$^{-/-}$ cells exhibited up to 25% reduced LifeAct-mCherry MFI values compared to WT cells, indicating reduced F-Actin amount, which is consistent with results revealed by SiR-actin labeling.

Taken together, the different F-Actin labeling approaches suggest a positive correlation between the indicated F-Actin amount and survival among the different P493.6 cell lines. Based on these data, it is plausible to propose that the ACTN4-manifested pro-survival phenotype might underlay F-Actin remodeling.

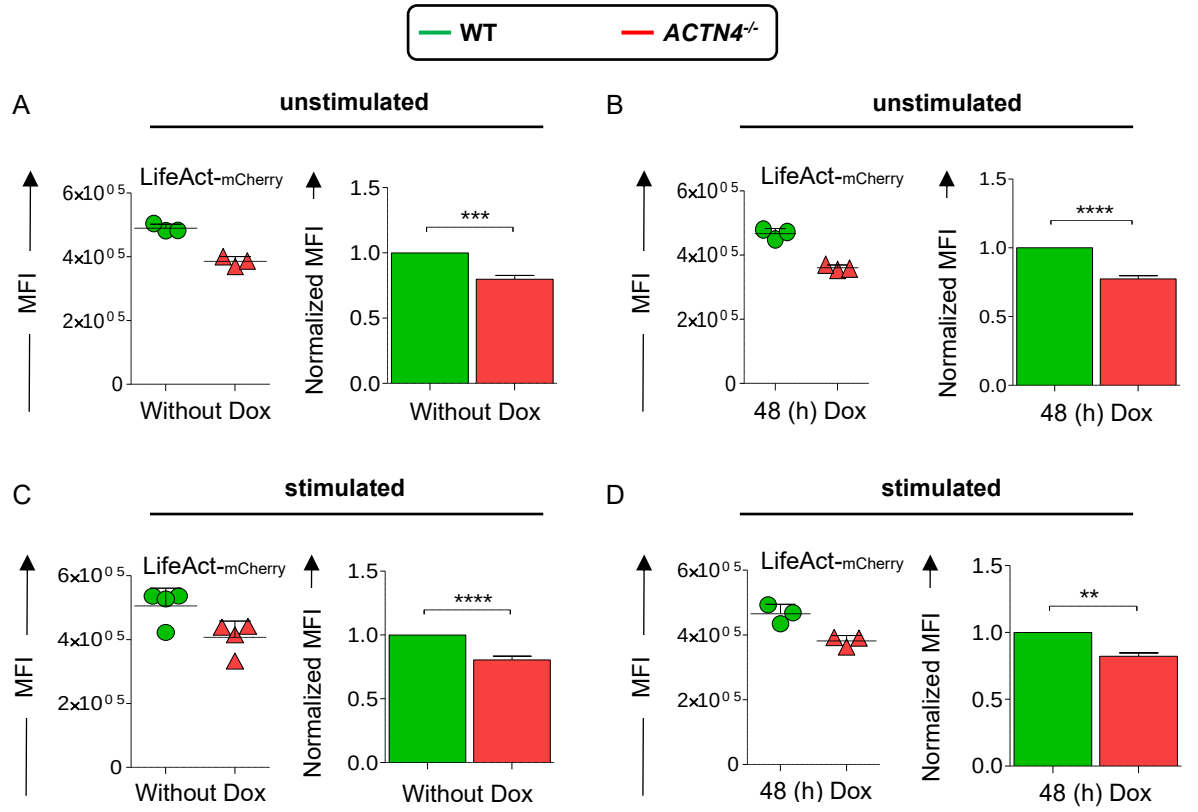

Figure 20: ACTN4 loss reduces LifeAct-mCherry intensity in tonic and activated BCR signaling.
WT (green line/circle) and *ACTN4*$^{-/-}$ cells (red line/triangle) expressing LifeAct-mCherry were either left untreated or treated with doxycycline for 48 h, stained with 250 nM of SiR-actin, and analyzed by imaging flow cytometry. Before analysis, cells were left either without stimulation (A & B) or stimulated with α-IgM for 1 h (C & D). (A-D) The aligned dot plots depict the determined MFI values for each repetition. MFI values of *ACTN4*$^{-/-}$ cells were normalized to that of the WT cells for each repetition. The diagrams depict the mean ± SD of at least three independent experiments. P-values were determined by a two-tailed t-test. ****: p<0.0001, ***: p<0.001, **: p<0.01.

4.8.2 Generation of alpha-Actinin-4 variants with altered F-Actin binding properties

As my data suggest a positive correlation between F-Actin amount and survival and since the ABD of ACTN4 is indispensable for F-Actin binding [99,140], I assessed whether the pro-survival function of ACTN4 depends on its F-Actin binding capacity.

For this purpose, I generated constructs encoding two different variants of ACTN4. The first variant harbors a deletion, which covers the amino acids 100 to 252 within the ABD of ACTN4 and is therefore F-Actin binding-incapable (ACTN4Δaa(100-252)-GFP) [140]. In the second construct, I introduced a single point mutation in the ABD of ACTN4, thereby substituting the amino acid lysine (K) at position 255 by glutamic acid (E) (K255E ACTN4-GFP), since it has been shown that this exchange increases the ACTN4 F-Actin binding capacity [108] (Figure 21 A). Generated vectors encoding GFP-tagged ACTN4 variants were then electroporated into *ACTN4*$^{-/-}$ cells. Based on WB analysis, both variants were successfully expressed in *ACTN4*$^{-/-}$ cells and showed the correct molecular weight. However, their expression levels were markedly low compared to WT expression levels (Figure 21 B). As indicated by the GFP signal, K255E ACTN4-GFP is expressed to a higher extent than ACTN4Δaa(100-252)-GFP (Figure 21 C). Notably, expression of ACTN4Δaa(100-252)-GFP in *ACTN4*$^{-/-}$ cells decreased during culturing, indicating reduced tolerance for a truncated form of ACTN4.

Collectively, the ACTN4 variants K255E ACTN4-GFP and ACTN4Δaa(100-252)-GFP were successfully expressed in *ACTN4*$^{-/-}$ cells.

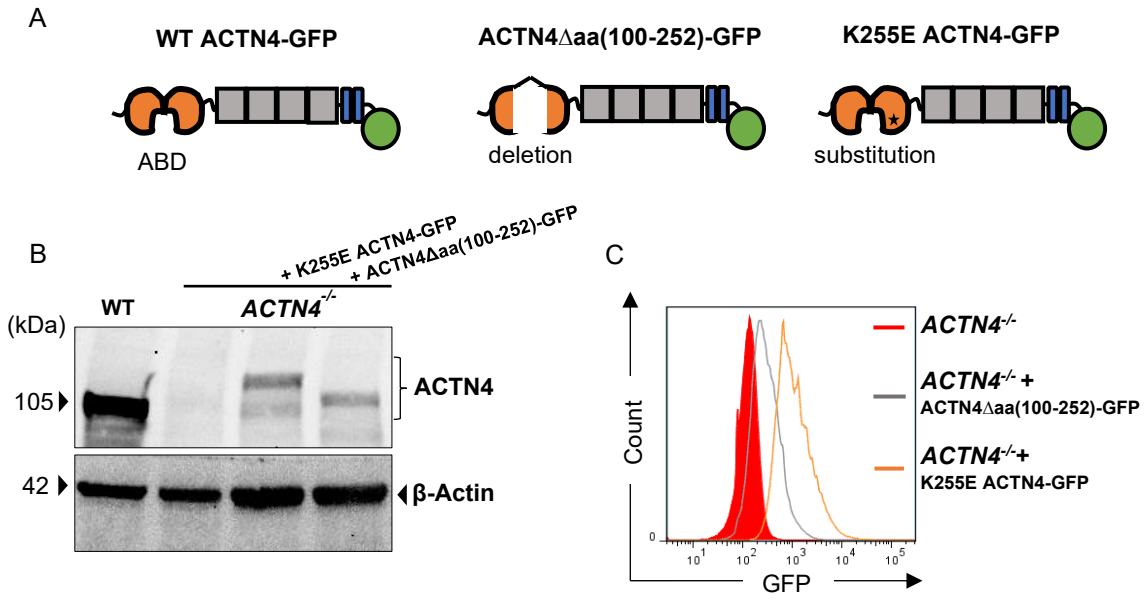

Figure 21: Generation of ACTN4 variants with modified F-Actin binding capacity.
(A) Scheme of WT ACTN4-GFP, ACTN4Δaa(100-252)-GFP, and K255E ACTN4-GFP. (B) CCLs of WT, *ACTN4*$^{-/-}$, *ACTN4*$^{-/-}$ + K255E ACTN4-GFP, and *ACTN4*$^{-/-}$ + ACTN4Δaa(100-252)-GFP cells were subjected to WB analysis using antibodies specific for ACTN4 and β-Actin. Protein's apparent molecular weight is shown in kilodaltons (kDa). (C) Flow cytometry analysis indicates GFP expression in K255E ACTN4-GFP (orange line) and ACTN4Δaa(100-252)-GFP (grey line). *ACTN4*$^{-/-}$ (red filled) served as a negative control for GFP expression.

4.8.3 The localization of alpha-Actinin-4 at F-Actin requires its Actin-binding domain

To examine the localization of the expressed ACTN4 variants, *ACTN4*$^{-/-}$ cells expressing either ACTN4Δaa(100-252)-GFP or K255E ACTN4-GFP were stained with SiR-actin and visualized using Confocal LSM. WT ACTN4-GFP (ACTN4-GFP) served as a positive control.

As indicated by the SiR-actin signal, ACTN4-GFP co-localizes with F-Actin in a spotted ring-shaped ACTN4/F-Actin structure near the plasma membrane of resting P493.6 cells (Figure 22 A). The co-localization extent was only calculated for regions across the plasma membrane (yellow lines) by plotting the relative distance between ACTN4-GFP and SiR-actin signals against their determined fluorescence intensities.

Compared to ACTN4-GFP, ACTN4Δaa(100-252)-GFP is distributed within the cytoplasm and does not co-localize with F-Actin (Figure 22 B). In line with several studies [108,110,140], K255E ACTN4-GFP forms aggregates with F-Actin near and at the plasma membrane of resting P493.6 cells (Figure 22 C).

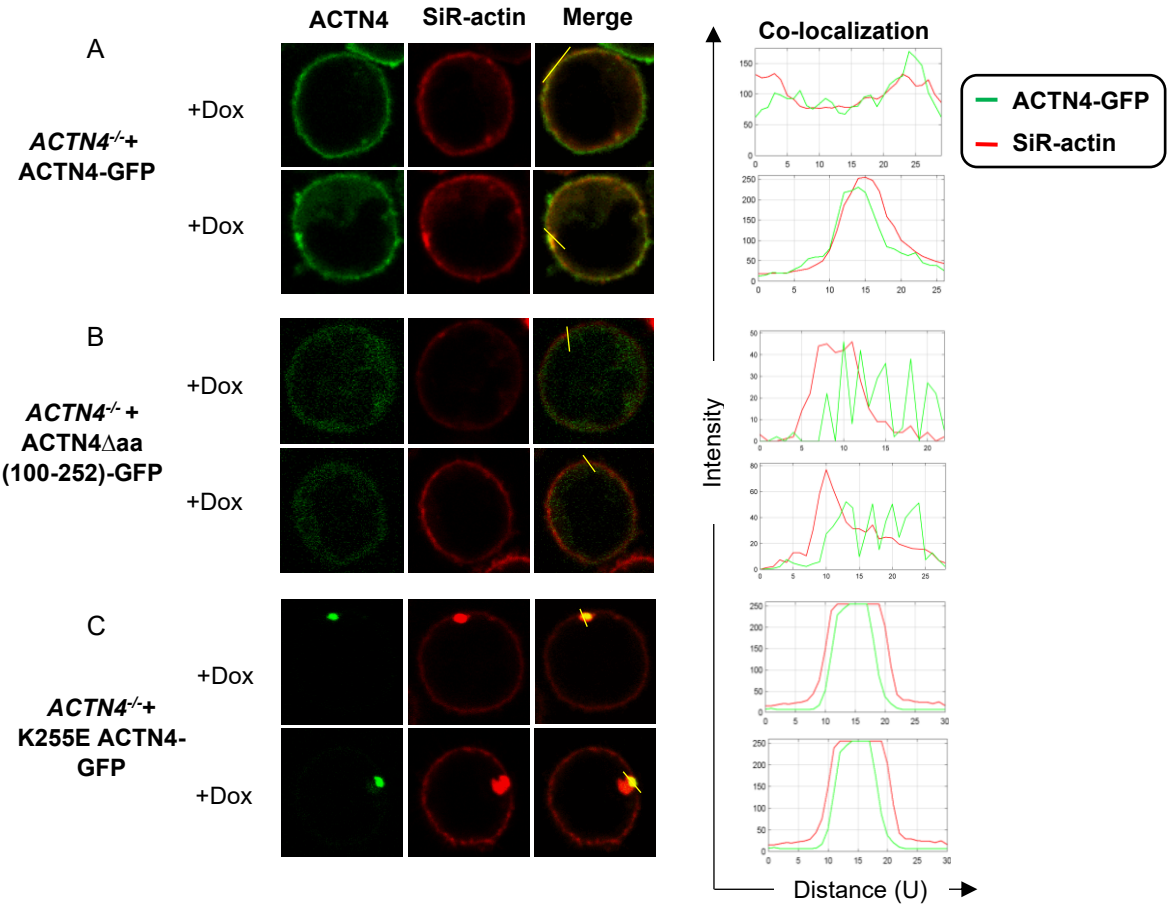

Figure 22: The ABD of ACTN4 is necessary for its co-localization with F-Actin.
ACTN4$^{-/-}$ cells expressing WT ACTN4-GFP(A), ACTN4Δaa(100-252)-GFP (B), or K255E ACTN4-GFP(C) were treated with doxycycline for 48 h, stained with 250 nM SiR-actin, and visualized by Confocal LSM. Channels showing ACTN4-GFP and SiR-actin were merged in Image J, and co-localization of GFP/SiR-actin was determined for the selected areas (yellow line) and represented as RGB Profile Plots, which show the intensities of ACTN4-GFP (green line) and SiR-actin (red line) over the indicated distance in unit (U).

To corroborate the SiR-actin co-localization studies, I electroporated the different P493.6 cell lines with the LifeAct-mCherry vector and analyzed the cells using imaging flow cytometry (Figure 23 A-C).

As indicated by the calculated bright similarity detail score (Figure 23 D & E), ACTN4-GFP co-localized with LifeAct-mCherry by approximately 60% in proliferative and 80% in resting P493.6 cells. In contrast, ACTN4Δaa(100-252)-GFP co-localized with LifeAct-mCherry neither in proliferative nor in resting cells. Despite its aggregated appearance, K255E ACTN4-GFP co-localized with LifeAct-mCherry by approximately 20% in proliferative as well as in resting cells compared to ACTN4Δaa(100-252)-GFP. Hence, this analysis confirmed the co-localization results obtained by Confocal microscopy of SiR-actin-stained cells (Figure 22 A-C).

In summary, my results indicate that ACTN4-GFP and K255E ACTN4-GFP are F-Actin binding-competent, whereas ACTN4Δaa(100-252)-GFP is incapable of F-Actin binding. This allows for investigating the impact of modified ACTN4 F-Actin binding properties on survival.

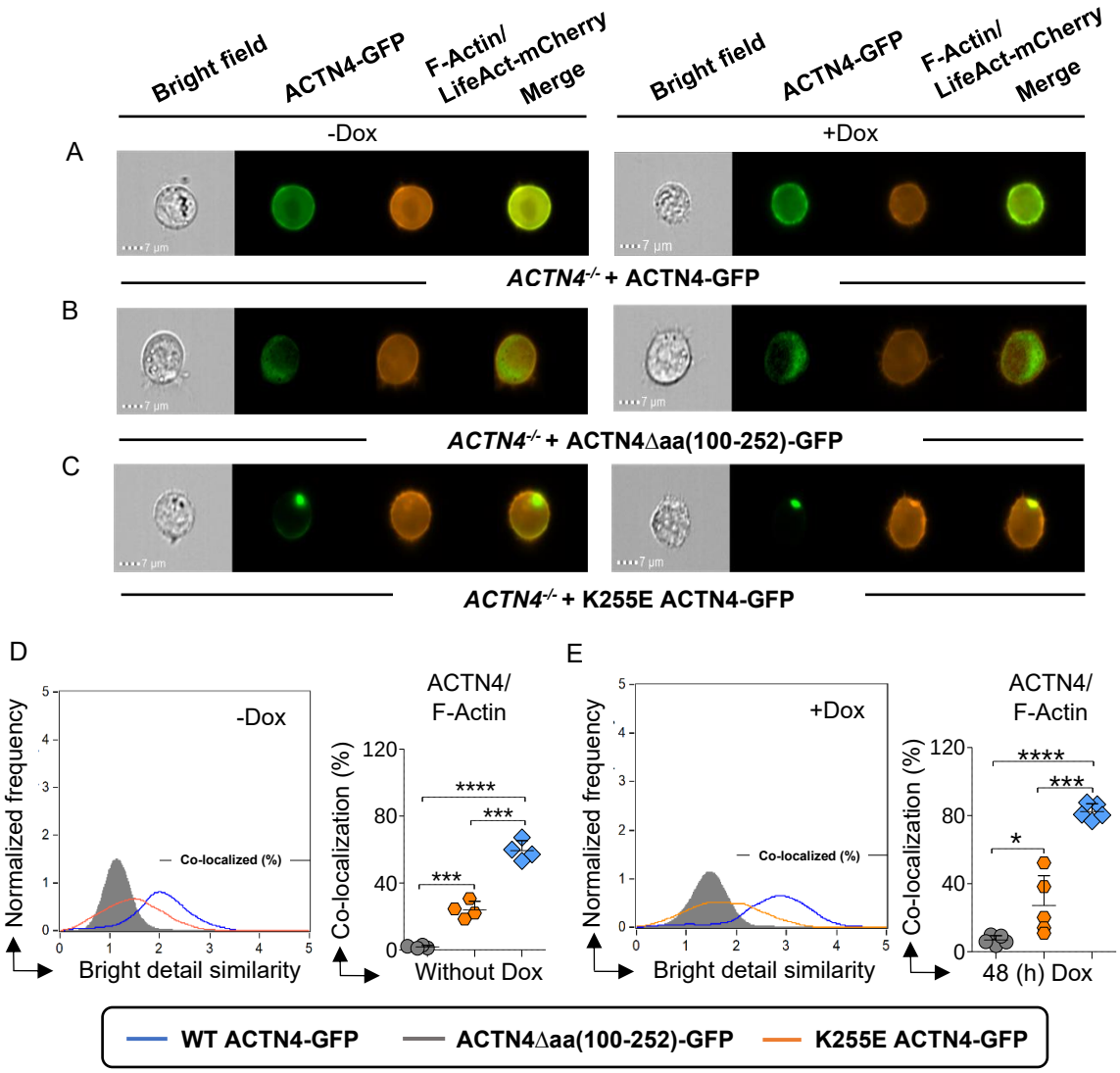

Figure 23: Only F-Actin binding-competent ACTN4 has the capacity to co-localize with F-Actin.
ACTN4$^{-/-}$+ WT ACTN4-GFP(A), *ACTN4*$^{-/-}$ + ACTN4Δaa(100-252)-GFP (B), or *ACTN4*$^{-/-}$ + K255E ACTN4-GFP (C) cells expressing LifeAct-mCherry were either left untreated (left column) or treated with doxycycline for 48 h (right column). (A-C) Object images show the bright field and ACTN4-GFP/LifeAct-mCherry merged channels of single cells. (D & E) The bright detail similarity score indicates ACTN4-GFP/LifeAct-mCherry co-localization and was calculated by IDEAS software, and co-localization was defined as the percentage of cells that have a bright detail similarity score ≥ 2. The aligned dot plots depict the mean ± SD of five independent experiments. P-values were determined by a two-tailed t-test. ****: p<0.0001, ***: p<0.001, *: p<0.05.

4.8.4 Only F-Actin binding-competent alpha-Actinin-4 supports survival of resting P493.6 cells

To investigate whether ACTN4 depends on its F-Actin binding capacity to support the survival of resting P493.6 cells, *ACTN4*$^{-/-}$ cells either expressing K255E ACTN4-GFP or ACTN4Δaa(100-252)-GFP were stained with Annexin V-APC and 7-AAD and analyzed by flow cytometry. *ACTN4*$^{-/-}$ and *ACTN4*$^{-/-}$ + ACTN4-GFP cells served as a negative and positive control, respectively.

Up to one week after induction of cell proliferation arrest, expression of K255E ACTN4-GFP in *ACTN4*$^{-/-}$ cells re-established their survival to a similar extent to *ACTN4*$^{-/-}$ + ACTN4-GFP cells, while ACTN4Δaa(100-252)-GFP did not improve survival. Apoptotic rates manifested by

ACTN4$^{-/-}$ + ACTN4-GFP and K255E ACTN4-GFP were half as much as *ACTN4*$^{-/-}$ and *ACTN4*$^{-/-}$ expressing ACTN4Δaa(100-252)-GFP (Figure 24).

Collectively, these results demonstrate that only F-Actin binding-competent ACTN4 has the capacity to support the survival of resting *ACTN4*$^{-/-}$ P493.6 cells, suggesting that the cortical F-Actin contributes to the survival of resting B cells.

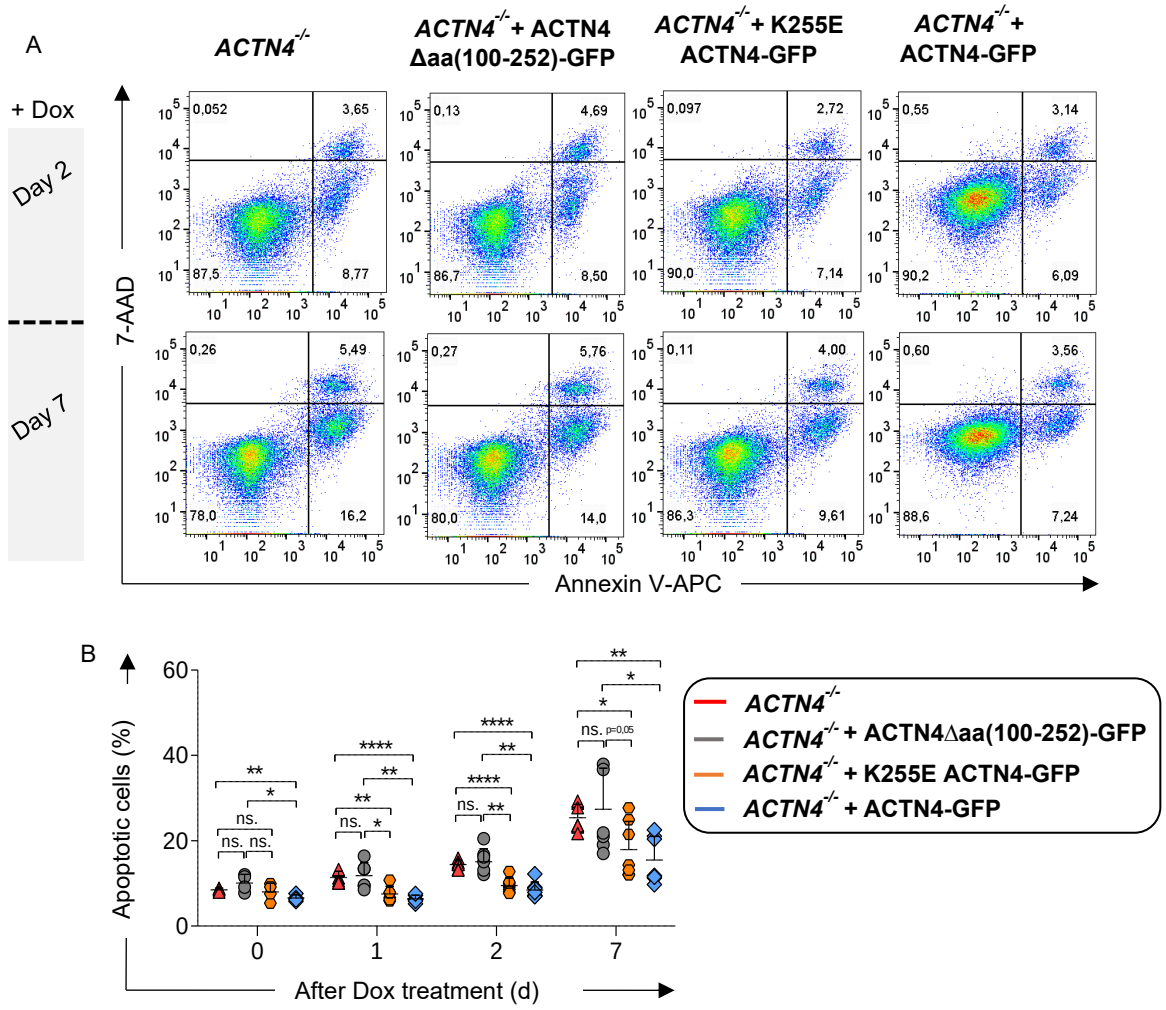

Figure 24: ACTN4 requires its ABD to support resting P493.6 cell survival.
ACTN4$^{-/-}$, *ACTN4*$^{-/-}$ + ACTN4-GFP, *ACTN4*$^{-/-}$ + K255E ACTN4-GFP, and *ACTN4*$^{-/-}$ + ACTN4Δaa(100-252)-GFP were treated with 500 ng/ml doxycycline for the indicated times. Flow cytometric analysis to assess apoptosis was conducted after staining the cells with Annexin V-APC and 7-AAD. (A) Dot plots illustrate the strategy to distinguish between living, early, and late apoptotic cells for the different cell lines after two and seven days of proliferation arrest. (B) The aligned dot plot represents the total apoptosis (early + late) at indicated times after doxycycline treatment and depicts the mean ± SD of at least three independent experiments. Individual values are plotted. P-values are determined by a two-tailed t-test. ****: p<0.0001, ***: p<0.001, **: p<0.01, *: p<0,05, ns.: not significant.

4.9 Alpha-Actinin-4-dependent F-Actin remodeling regulates lateral BCR mobility and tonic BCR signaling

4.9.1 The Actin-binding domain of alpha-Actinin-4 is required for its co-localization with the BCR

As only F-Actin binding-competent ACTN4 supported resting P493.6 cell survival and since studies have reported that the cortical cytoskeleton in B cells creates F-Actin barriers that restrict BCR diffusion and might affect emitted BCR signaling [81], I assessed whether ACTN4 co-localizes with BCRs and affects their lateral diffusion.

To examine ACTN4 co-localization with the IgM-BCR, *ACTN4*$^{-/-}$ cells expressing ACTN4-GFP or either of both ACTN4 variants were stained with AZDye-568-conjugated anti-IgM nanobody to avoid BCR stimulation and analyzed by imaging flow cytometry.

In comparison to only GFP-expressing negative control cells (Figure 25 A), ACTN4-GFP (Figure 25 B) strongly co-localized with the BCR. ACTN4∆aa(100-252)-GFP (Figure 25 C) exhibited co-localization values that were similar to that of the negative control. Notably, K255E ACTN4-GFP (Figure 25 D) co-localized with the BCR to a similar extent to ACTN4-GFP, particularly in the areas with K255E ACTN4-GFP accumulation (Figure 25 E & F).

In summary, these results suggest that the F-Actin binding capacity of ACTN4 is required for its co-localization with the BCR. The positive correlation between ACTN4/IgM co-localization and survival reinforces the hypothesis that the ACTN4 pro-survival phenotype might be manifested *via* the BCR.

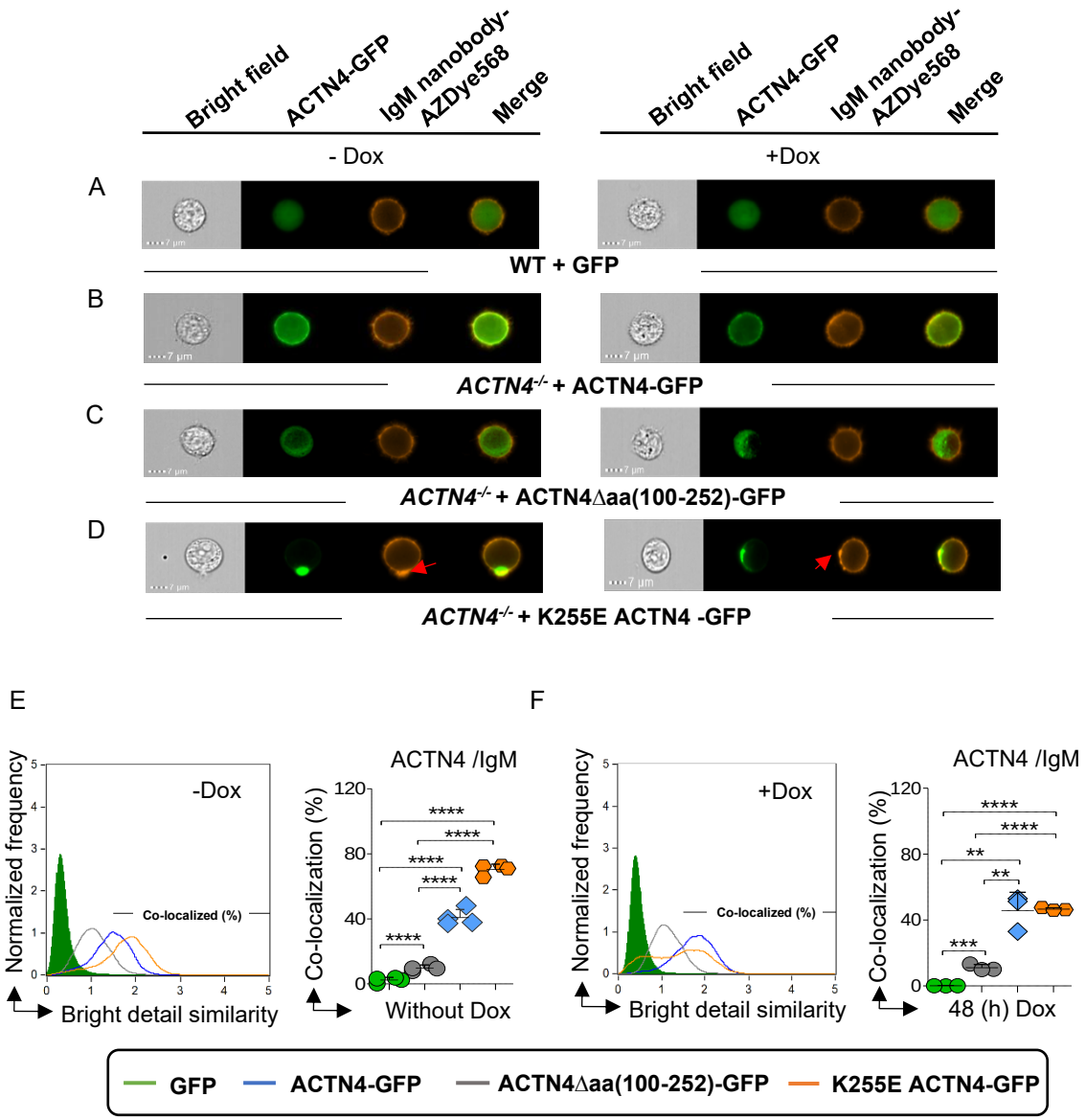

Figure 25: The ABD of ACTN4 is indispensable for its co-localization with the IgM-BCR.
WT + GFP (A), *ACTN4*$^{-/-}$ + WT ACTN4-GFP(B), *ACTN4*$^{-/-}$ + ACTN4Δaa(100-252)-GFP (C), and *ACTN4*$^{-/-}$ + K255E ACTN4-GFP cells (D) were either left untreated (left column) or treated with doxycycline for 48 h (right column), stained with AZDye-568-tagged IgM-specific nanobody, and analyzed by imaging flow cytometry. (A-D) Object images show the bright field and ACTN4-GFP/IgM-AZDye-568 merged channels of single cells. (D) Red arrows show BCR aggregation. (E & F) The bright detail similarity score indicates ACTN4/IgM co-localization and was calculated by IDEAS software and defined as the percentage of cells that have a score of ≥ 1.5. The aligned dot plots depict the mean ± SD of ≥ 3 independent experiments. P-values were determined by a two-tailed t-test. ****: p<0.0001, ***: p<0.001, **: p<0.01, *: p<0.05.

4.9.2 F-Actin co-localizes with the BCR in tonic and activated BCR signaling

As my results suggest that ACTN4 co-localization with the BCR correlates with the survival outcome of resting P493.6 cells, I aimed to confirm that the cortical F-Actin cytoskeleton co-localizes with the BCR. For this purpose, proliferative and resting WT as well as *ACTN4*$^{-/-}$ cells were stained with SiR-actin, followed by BCR staining using a AZDye-568-conjugated anti-IgM nanobody to avoid BCR stimulation, and analyzed by imaging flow cytometry.

Regardless of *MYC* expression, ACTN4 loss did not impact BCR distribution, and the F-Actin shape remained unchanged (Figure 26 A & B). As indicated by the calculated bright detail similarity score, the F-Actin/IgM-BCR co-localization increased in proliferative cells by 10% compared to resting counterparts. In addition, ACTN4 loss did not impact the F-Actin/BCR co-localization score compared to WT cells (Figure 26 C & D).

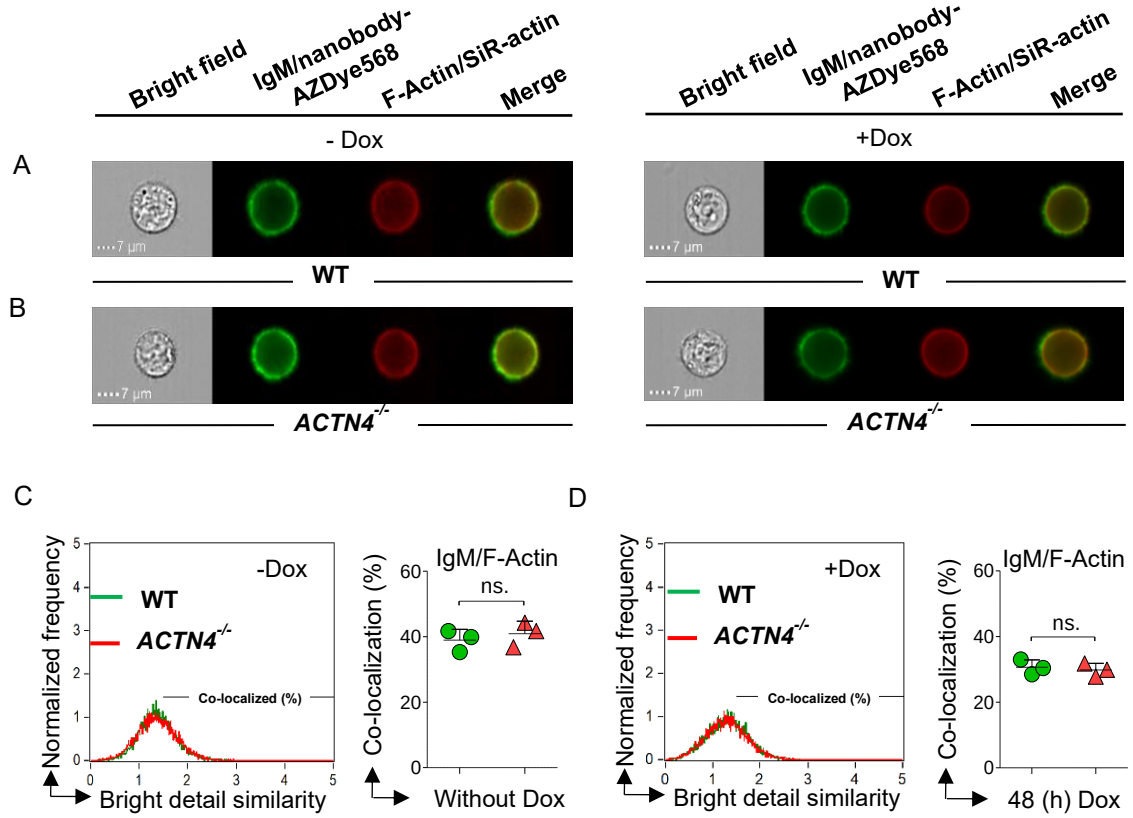

Figure 26: F-Actin/IgM-BCR co-localization analysis in tonic BCR signaling.
WT (A) and *ACTN4*$^{-/-}$ cells (B) were either left untreated (left column) or treated with doxycycline for 48 h (right column), stained with SiR-actin and AZDye-568-tagged IgM-specific nanobody, and analyzed by imaging flow cytometry. (A & B) Object images show the bright field and SiR-actin/IgM-AZDye-568 merged channels of single cells (C & D) The bright detail similarity score indicates F-Actin/IgM co-localization and was calculated by IDEAS software. Co-localization was defined as the percentage of cells that have a bright detail similarity score ≥ 1.5. The aligned dot plots depict the mean ± SD of three independent experiments. P-values were determined by a two-tailed t-test; ns.: not significant.

In addition, I examined whether IgM-BCR stimulation changes F-Actin/IgM-BCR co-localization compared to unstimulated cells. Hence, WT and *ACTN4*$^{-/-}$ cells expressing LifeAct-mCherry were stimulated with an FITC-conjugated anti-IgM F(ab')$_2$ fragment and analyzed by imaging flow cytometry.

Imaging flow cytometry analysis revealed similar images to those of unstimulated cells, with no alteration in IgM distribution or F-Actin shape (Figure 27 A & B). However, as indicated by the calculated bright detail similarity score, F-Actin/IgM-BCR co-localization was generally increased in BCR-stimulated compared to unstimulated cells (Figure 26). Upon stimulation, *ACTN4*$^{-/-}$ cells exhibited a reduced F-Actin/IgM-BCR co-localization compared to WT cells in their proliferative and resting states (Figure 27 C & D).

In summary, my results indicate that the cortical F-Actin cytoskeleton co-localizes with IgM-BCR regardless of *MYC* expression. Although ACTN4 does not impact the F-Actin/IgM-BCR co-localization score in the tonic BCR state, it does increase it upon BCR engagement.

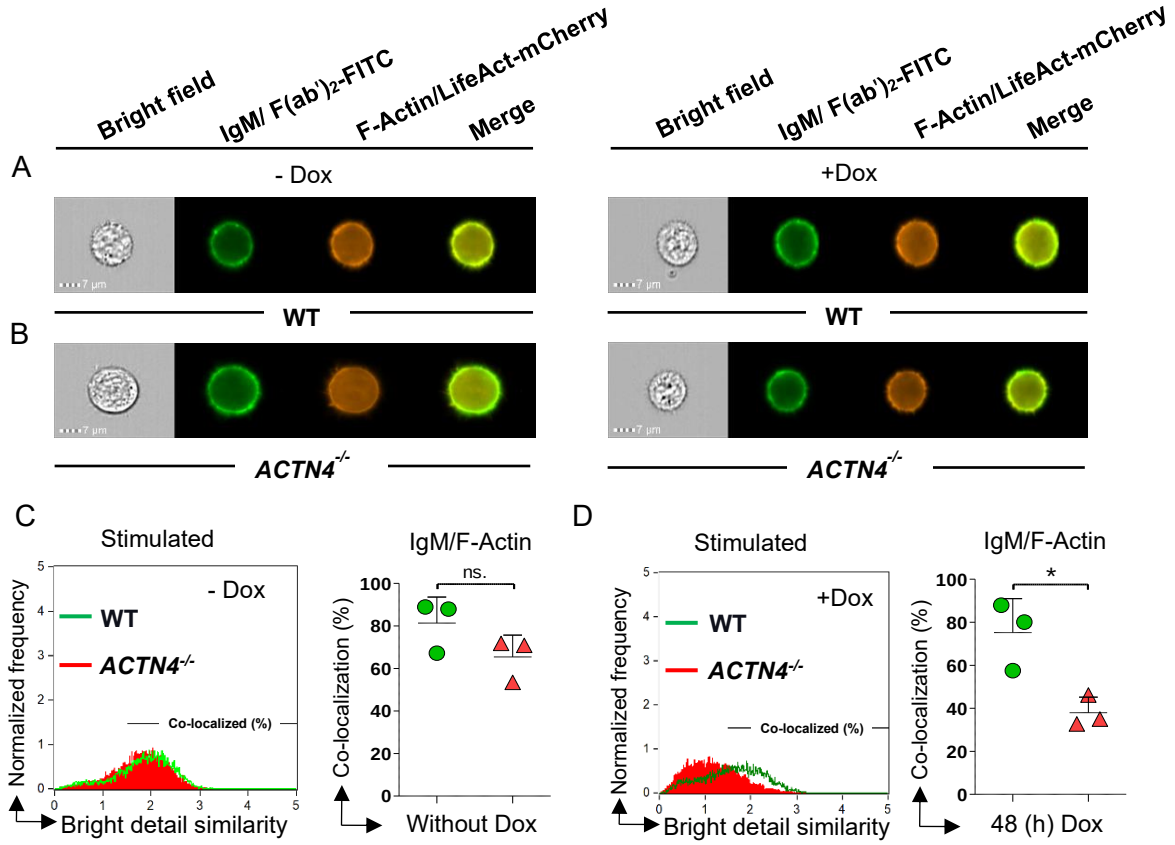

Figure 27: F-Actin/IgM-BCR co-localization analysis upon BCR stimulation.
WT (A) and *ACTN4*$^{-/-}$ (B) cells expressing LifeAct-mCherry were left untreated (left column) or treated with doxycycline for 48 h (right column), stimulated with FITC-conjugated α-IgM F(ab')$_2$, and analyzed by imaging flow cytometry. (A & B) Object images show the bright field and LifeAct-mCherry/IgM-FITC merged channels of single cells. (C & D) The bright detail similarity score indicates F-Actin/IgM co-localization and was calculated by IDEAS software. Co-localization was defined as the percentage of cells that have a bright detail similarity score ≥ 1.5. The aligned dot plots depict the mean ± SD of three independent experiments. P-values were determined by a two-tailed t-test. *: p<0.05, ns.: not significant.

4.9.3 Alpha-Actinin-4 confines lateral BCR diffusion of resting P493.6 cells

To assess whether ACTN4 affects BCR diffusion, resting WT, *ACTN4*$^{-/-}$, and *ACTN4*$^{-/-}$ + ACTN4-GFP cells were stained with low doses of Fc-specific Cy-3-conjugated anti-IgM monomeric Fab fragments and analyzed using single particle tracking (SPT) by total internal reflection (TIRF) microscopy (see 3.2.3.15), which was conducted in collaboration with the group of Prof. Dr. Michael Gold in Vancouver.

While the upper row of images displays single frames from single cells lasting 30 ms, the lower row represents BCR tracks from the next three seconds (100 frames) (Figure 28 A). ACTN4 loss substantially increased BCR diffusion by approximately 7.5-fold (0.2399 μm^2/s) compared to WT and reconstituted cells, where BCRs were relatively immobile, with similar BCR diffusivities ranging from 0.03163 to 0.04833 μm^2/s (Figure 28 B & C).

In summary, SPT analysis of IgM-BCR demonstrates that ACTN4 confines BCR diffusion of resting P493.6 cells in tonic BCR signaling.

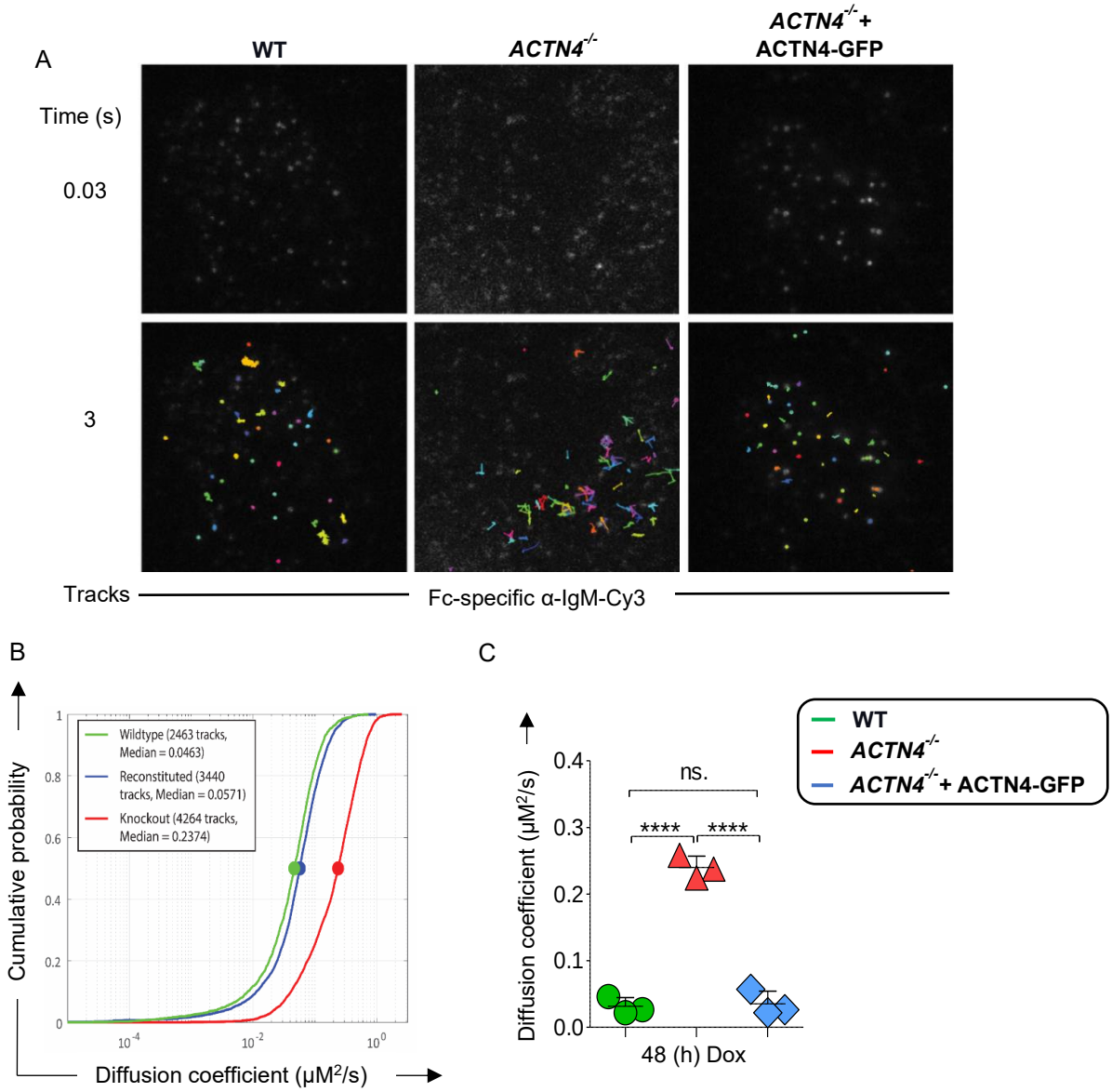

Figure 28: ACTN4 loss increases BCR diffusion in resting P493.6 cells.
WT (green line/circle), *ACTN4*$^{-/-}$ (red line/triangle), and *ACTN4*$^{-/-}$ + ACTN4-GFP cells (blue line/diamond) were treated with doxycycline for 48 h, stained with very low doses of IgM-Cy3 Fab, and imaged using TIRF microscopy. (A) Images show the recorded IgM-BCR tracks after 0.03 s (upper row) and 3 s (lower row). The tracks are colored randomly to allow adjacent tracks to be distinguished from one another. (B) The calculated diffusion coefficients are plotted as cumulative frequency graphs with all tracks from eight different cells from each condition. (C) The aligned dot plot depicts the mean ± SD of three independent experiments. P-values were determined by a two-tailed t-test. ****: p<0.0001, ns.: not significant.

4.10 Alpha-Actinin-4-dependent control of BCR diffusion correlates with efficient tonic BCR signaling

4.10.1 Alpha-Actinin-4 augments ITAM-tyrosine phosphorylation of CD79A

To assess whether an altered BCR diffusion affects tonic BCR signaling, I examined the efficiency of tonic BCR signaling by analyzing ITAM phosphorylation. Studies have shown that the phosphorylation

of tyrosine residue 188 in CD79A ensures appropriate tonic BCR signaling initiation [141]. Since tonic BCR signaling has a very low intensity, its analysis is challenging, and differences are expected to be mild.

To assess the effect of *ACTN4* expression on tonic signaling efficiency, WT, *ACTN4*$^{-/-}$, and ACTN4-GFP reconstituted cells were either left untreated or treated for 48 h with doxycycline, intracellularly stained with Alexa Fluor® 647-conjugated anti-pCD79A (Y188) antibodies and analyzed by flow cytometry (Figure 29 A & B).

As indicated by MFI values (Figure 29 C & D), resting P493.6 cells showed a 2-fold increase in CD79A phosphorylation intensity compared to their proliferative counterpart cells, which is in line with previous results showing that P493.6 cells have more efficient tonic BCR signaling compared to their proliferative counterpart cells (Figure 7).

Based on the normalized MFI values (Figure 29 E & F), proliferative and resting *ACTN4*$^{-/-}$ cells exhibited slightly reduced levels of CD79A phosphorylation at Y188 compared to their counterpart WT cells. The re-expression of *ACTN4* in *ACTN4*$^{-/-}$ cells restored Y188 phosphorylation, to a WT-comparable level in their proliferative state and by approximately 20-30% higher than WT cells in their resting state, which is thus consistent with its more pronounced impact on survival in resting reconstituted cells (Figure 11).

In conclusion, my results suggest that ACTN4 supports the efficiency of the proximal BCR signaling indicated by efficient ITAM phosphorylation of CD79A.

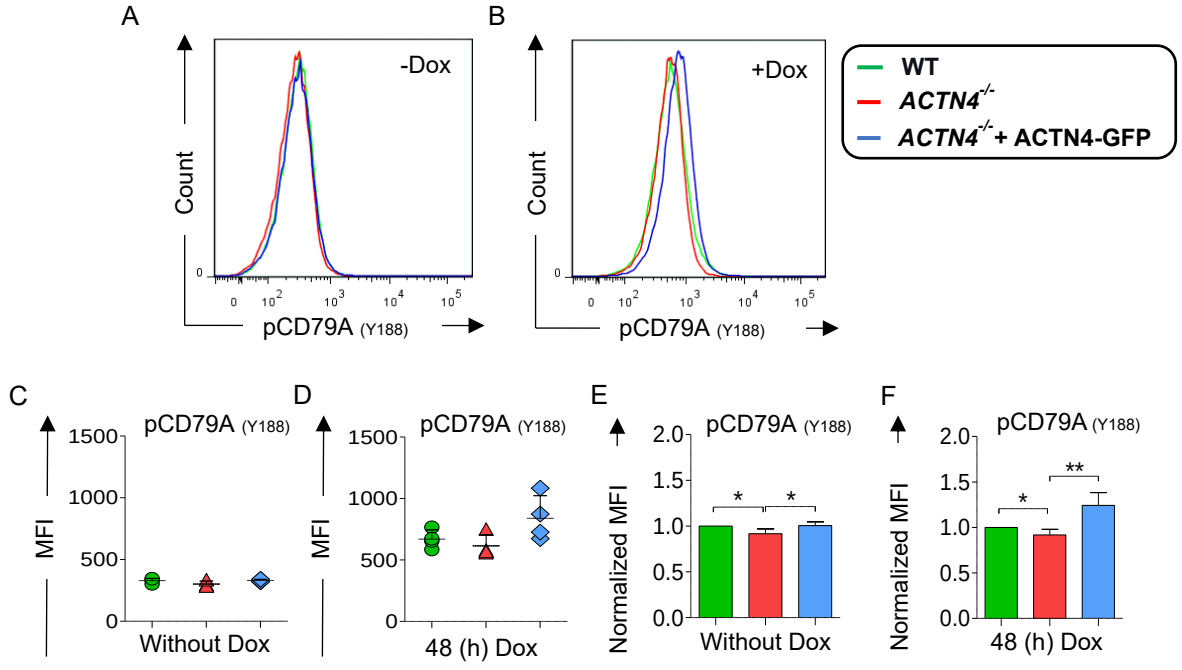

Figure 29: ACTN4 supports the phosphorylation intensity of ITAM-containing tyrosine residues of CD79A. WT (green line/circle), *ACTN4*$^{-/-}$ (red line/triangle), and reconstituted cells (blue line/diamond) were either left untreated (A, C & E) or treated with doxycycline for 48 h (B, D & F), then intracellularly stained with Alexa-fluor-647-tagged α-phospho-CD79A (Y188) antibodies and analyzed by flow cytometry. (A-D) The overlay histograms and the aligned dot plots depict the determined MFI values for each cell line. (E & F) MFI values shown in (C & D) were normalized to MFI values of WT cells for each repetition. The diagrams depict the mean ± SD of at least three independent experiments. P-values were determined by a two-tailed t-test. **: p<0.01, *: p<0.05.

4.10.2 Alpha-Actinin-4 positively regulates the activities of the proximal BCR kinases SYK and LYN

It is known that BCR utilizes PTKs such as SYK and LYN for efficient signaling transduction [21]. To examine whether the phosphorylation of CD79A correlates with the activity of SYK and/or LYN, I assessed their phosphorylation on key tyrosine residues. To this end, CCLs derived from the different P493.6 cell lines were subjected to WB analysis using phospho-specific antibodies.

According to WB analysis, LYN as well as SYK were barely phosphorylated in proliferative P493.6 cells compared to their resting counterpart cells, which is in line with the compromised BCR signaling in proliferative P493.6 cells (Figure 30 A & B). In resting cells, while ACTN4 loss resulted in an increase of approximately 20% in LYN phosphorylation on the inhibitory tyrosine residue Y508 (Figure 30 A), it decreased SYK phosphorylation on tyrosine residues Y525 and Y526 by approximately 40% compared to WT cells (Figure 30 B). In both cases, this indicates reduced activities for both kinases in the absence of ACTN4. In reconstituted cells, phosphorylation of LYN and SYK was restored to WT-comparable levels.

Complementary to the WB analysis, the phosphorylation levels of SYK were also measured by flow cytometry using Alexa fluor-647 conjugated anti-phospho-SYK (pY525 and pY526) antibodies. Consistent with the WB analysis, WT and reconstituted cells showed MFI values approximately 30-40% higher than *ACTN4*$^{-/-}$ cells, indicating efficient SYK phosphorylation in the presence of ACTN4 (Figure 30 C). Hence, efficient CD79A phosphorylation results in the efficient activity of SYK and LYN.

In conclusion, these data suggest that ACTN4 supports the activity of the tonic BCR-proximal effectors SYK and LYN and provide evidence that ACTN4-dependent control of lateral BCR mobility correlates with efficient tonic BCR-proximal survival signaling of resting P493.6 cells.

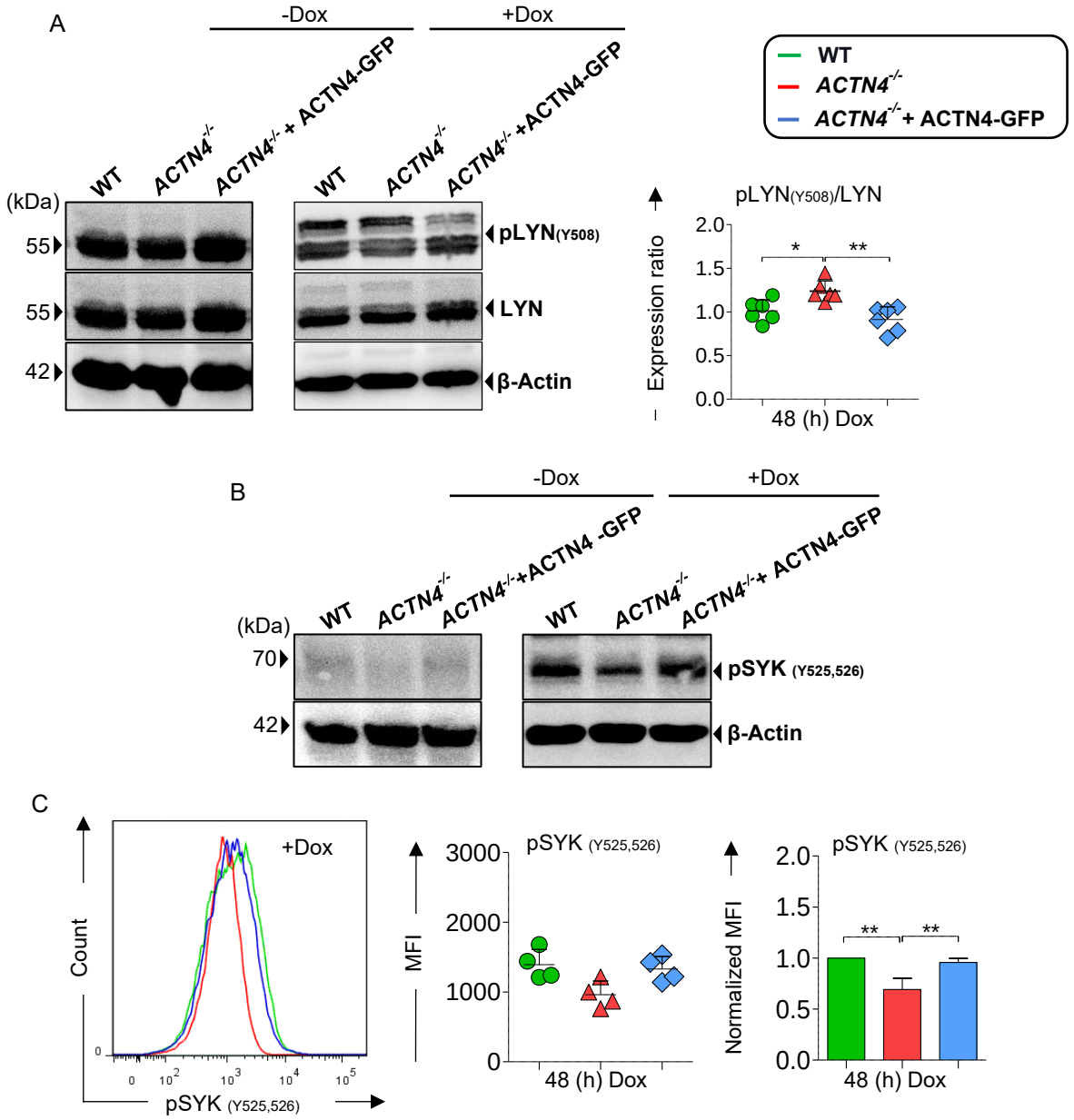

Figure 30: Analysis of the proximal BCR effectors SYK and LYN in resting P493.6 cells.
(A & B) CCLs derived from doxycycline-treated and non-treated WT (green line/circle), *ACTN4*$^{-/-}$ (red line/triangle), and reconstituted cells (blue line/diamond) were subjected to WB analysis using rabbit α-phospho-LYN (Y508), rabbit α-pan-LYN, rabbit α-phospho-SYK (Y525,526) and α-β-Actin antibodies for loading control. The molecular weights of the proteins are depicted in kilodaltons (kDa). LYN (pY508) was normalized to pan-LYN. (C) Doxycycline-treated cells were intracellularly stained with Alexa fluor-647-conjugated α-phospho-SYK (Y525,526) antibodies and analyzed by flow cytometry. The overlay histogram and the aligned dot plot illustrate the MFI values for each cell line. MFI values were normalized to the MFI values of WT cells for each repetition. The graphs depict the mean ± SD of at least three independent experiments. P-values were determined by a two-tailed t-test **: p<0.01.

4.10.3 Alpha-Actinin-4 mildly augments the phosphorylation of SLP65

The *bona fide* SYK substrate is SLP65. The phosphorylation of SLP65 on multiple tyrosine residues constitutes docking sites for other signaling molecules required for signaling propagation [38,40].

To examine whether augmented tonic SYK activity results in efficient phosphorylation of SLP65, I intracellularly stained the different P493.6 cell lines in their proliferative and resting states with Alexa Fluor® 647-conjugated anti-phospho-SLP65 (pY84) antibodies and used flow cytometry for analyses.

As indicated by the overlay histograms and normalized MFI values (Figure 31), SLP65 phosphorylation was not significantly changed among P493.6 cell lines in their proliferative state. In resting cells, however, its phosphorylation showed a slight increase of approximately 10% in WT and 10-15% in *ACTN4*$^{-/-}$ + ACTN4-GFP compared to *ACTN4*$^{-/-}$ cells, which is consistent with the more pronounced impact of ACTN 4 on survival in *ACTN4*$^{-/-}$ + ACTN4-GFP cells.

In summary, these data suggest that ACTN4-dependent effects on SYK result in more efficient tonic BCR-proximal processes, leading to a slight increase in the phosphorylation of the pivotal adapter protein SLP65.

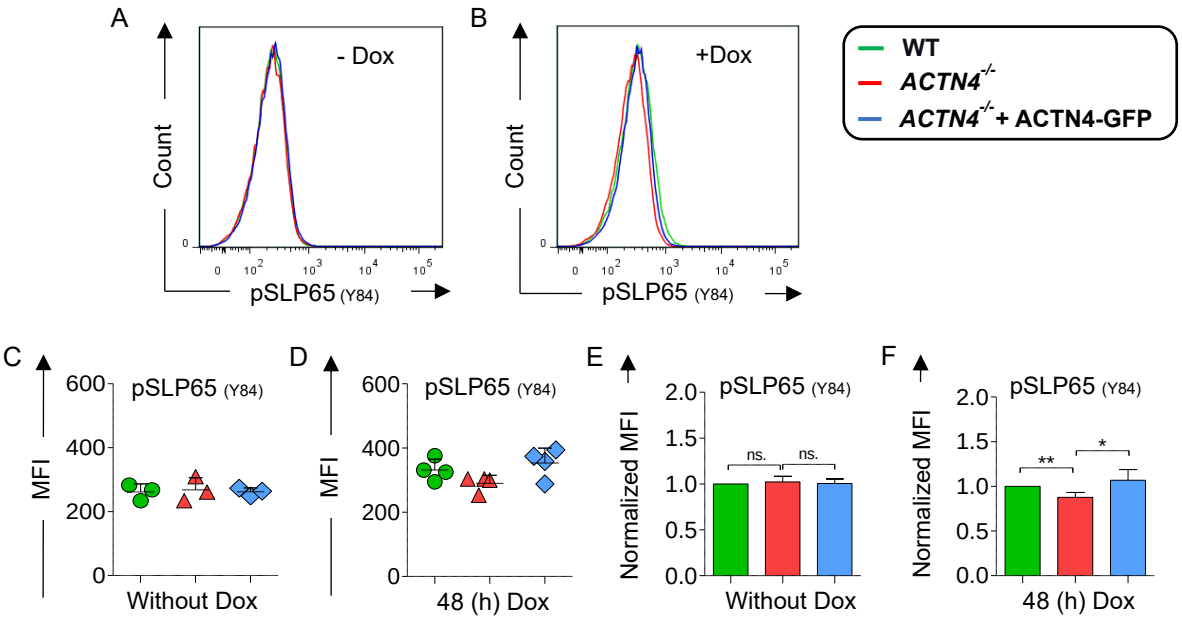

Figure 31: ACTN4 slightly augments SLP65 phosphorylation intensity in resting P493.6 cells.
WT (green line/circle), *ACTN4*$^{-/-}$ (red line/triangle), and reconstituted cells (blue line/diamond) were either left untreated (A, C & E) or treated with doxycycline for 48 h (B, D & F), intracellularly stained with Alexa Fluor®647-tagged α-phospho-SLP65 (Y84) antibodies and analyzed by flow cytometry. (A-D) The overlay histograms and the aligned dot plots depict the determined MFI values for each cell line. (E & F) MFI values shown in C & D were normalized to MFI values of WT cells for each repetition. The diagrams depict the mean ± SD of at least three independent experiments. P-values were determined by a two-tailed t-test. **: p<0.01, *: p<0.05, ns.: not significant.

4.10.4 Alpha-Actinin-4 supports the phosphorylation of AKT

To see whether efficient phosphorylation of proximal BCR effectors translates into efficient tonic BCR-distal signaling, I assessed the activity of AKT. The PI3K/AKT signaling axis constitutes the central mediator of tonic BCR survival signals in resting B cells [57]. In tonic BCR signaling, AKT becomes phosphorylated on serine residue 473 [142]. To this end, CCLs derived from proliferative and resting P493.6 WT cells were subjected to WB analysis using anti-AKT and anti-phospho-AKT (pS473) antibodies.

In line with the weak tonic BCR signaling in proliferative P493.6 cells, AKT is barely phosphorylated at S473 in proliferative compared to resting cells, where AKT is efficiently phosphorylated (Figure 32 A). Hence, I only used resting cells for further AKT analysis and subjected the different P493.6 cell lines to intracellular staining using phospho-AKT-specific antibodies (Figure 32 B). Resting WT and reconstituted cells showed MFI values that are approximately 10% and 10-15% significantly higher, respectively, compared to *ACTN4*$^{-/-}$ cells, indicating augmented phosphorylation of AKT in the presence of ACTN4 (Figure 32 B).

In conclusion, these results suggest that ACTN4 marginally increases the activity of distal BCR effectors, such as AKT, by supporting the efficiency of proximal tonic BCR signaling.

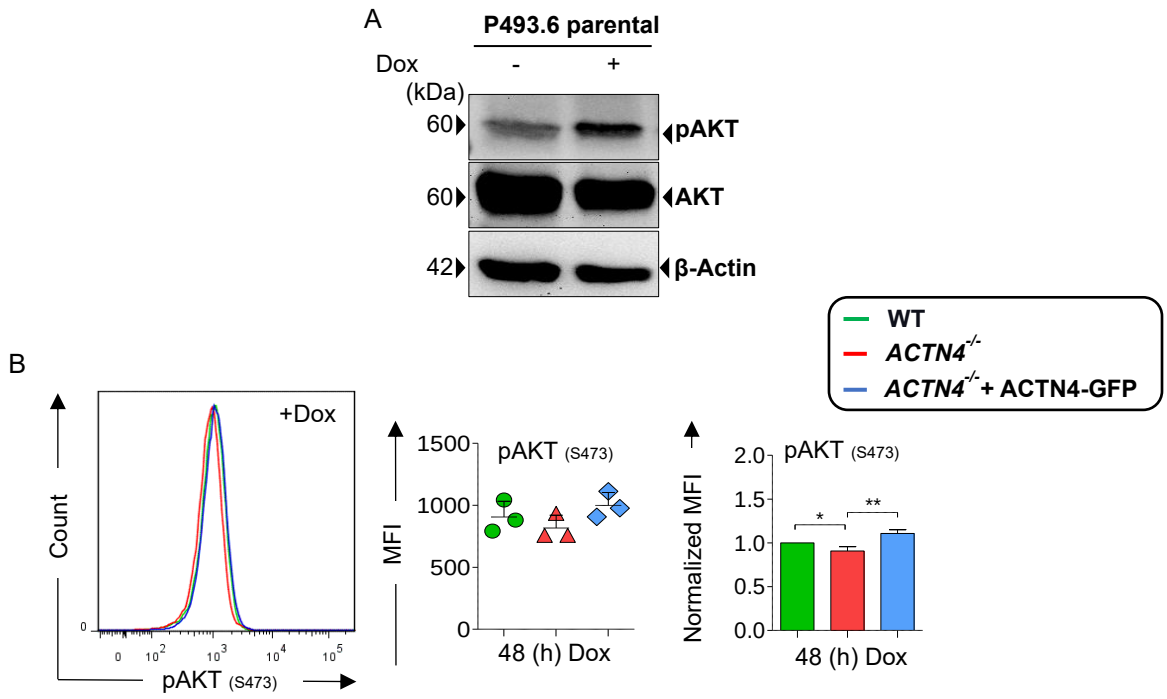

Figure 32: ACTN4 mildly augments AKT phosphorylation intensity in resting P493.6 cells.
(A) CCLs derived from doxycycline-treated and non-treated WT cells were subjected to WB analysis using rabbit α-human pAKT (S473) and mouse α-human pan-AKT. (B) Doxycycline-treated WT (green line), *ACTN4*$^{-/-}$ (red line), and *ACTN4*$^{-/-}$ + ACTN4-GFP (blue line) were intracellularly stained with Alexa Fluor®647-tagged α-pAKT (S473) antibodies and analyzed by flow cytometry. The overlay histogram and the aligned dot plot indicate phospho-AKT MFI for each cell line. MFI values were normalized to the MFI values of WT cells for each repetition. The diagrams depict the mean ± SD of at least three independent experiments. P-values were determined by a two-tailed t-test. **: p<0.01, *: p<0.05.

4.10.5 Alpha-Actinin-4 moderately increases phosphorylation events of the MAPK ERK

Besides the BCR-dependent PI3K/AKT activation, the MAPKs ERK, JNK, and p38 are hallmarks of BCR signaling. The different MAPKs have been shown to be phosphorylated in BL cells in an antigen-independent manner [49]. To assess which of these MAPKs is more likely to be phosphorylated in tonic BCR signaling of resting P493.6 cells, CCLs derived from doxycycline-treated or non-treated cells were subjected to WB analysis using phospho-specific antibodies that detect key tyrosine and threonine phosphorylation sites.

According to WB analysis, only the MAPK kinase ERK exhibited efficient phosphorylation in tonic BCR signaling of resting P493.6 cells, whereas JNK and p38 were efficiently phosphorylated in proliferative but not in resting P493.6 cells (Figure 33 A-C). This suggests that tonic BCR-dependent MAPK signals are more likely to be transduced through ERK rather than JNK or p38 in resting P493.6 cells. Hence, I further examined phospho-ERK by subjecting CCLs of resting WT, *ACTN4*$^{-/-}$, and *ACTN4*$^{-/-}$ + ACTN4-GFP to WB analysis. According to WB analysis, *ACTN4*$^{-/-}$ cells showed a reduction in phosphorylation intensity for ERK of 50% compared to WT and reconstituted counterpart cells (Figure 33 D), indicating reduced ERK activity. Collectively, my results suggest that the ACTN4-dependent effects on BCR-proximal signaling events contribute to the efficient phosphorylation of ERK.

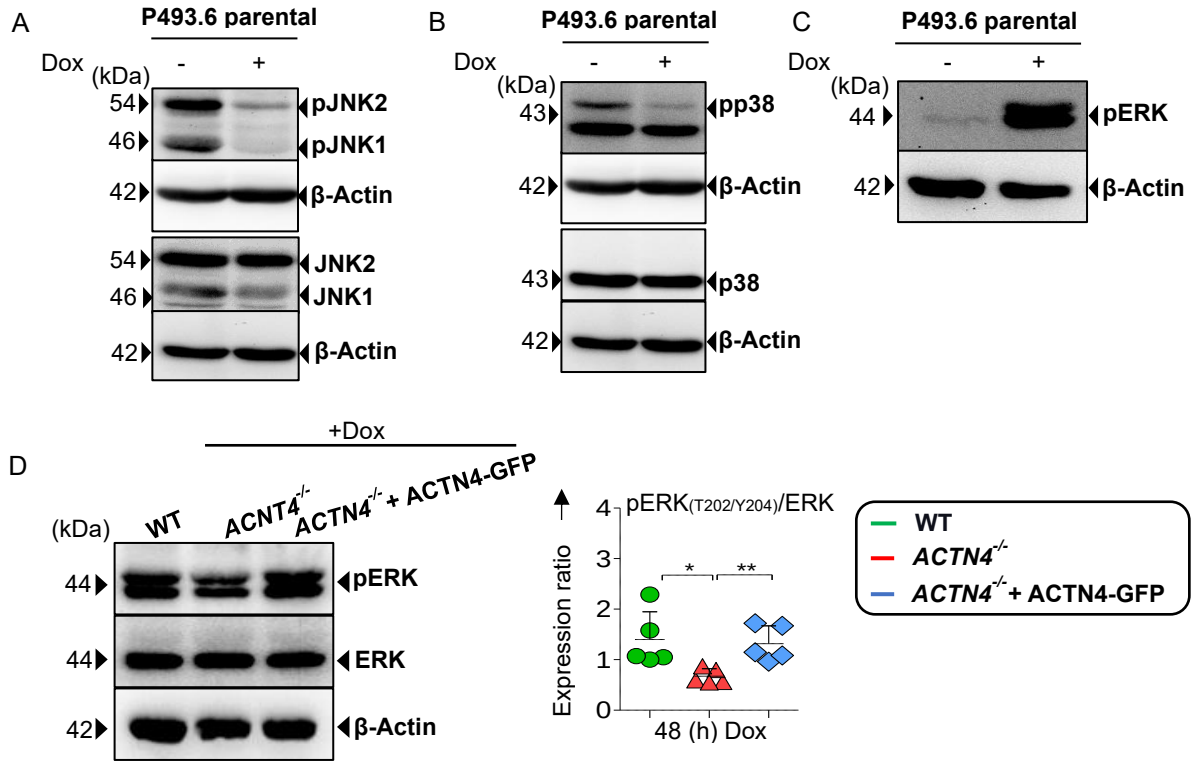

Figure 33: Analysis of tonic MAPKs singling in resting P493.6 cells.
(A & B) CCLs derived from doxycycline-treated or non-treated WT cells were subjected to WB analysis using rabbit α-human pJNK (T183/Y185), mouse α-pan-JNK, rabbit α-human pp38 (T180/Y182), rabbit α-pan-p38, rabbit α-human pERK (T202/Y204), mouse α-pan-ERK, and α-β-Actin antibodies as loading control. The molecular weights of the proteins are indicated in kilodaltons (kDa). (C) Phospho-ERK was analyzed by subjecting CCLs derived from doxycycline-treated WT (green line), *ACTN4*$^{-/-}$, and reconstituted cells to WB analysis. For quantification, phospho-ERK was normalized to pan-ERK in each repetition. The graphs depict the mean ± SD of at least three independent experiments. P-values were determined by a two-tailed t-test. **: p<0.01, *: p<0.05.

4.11 Analysis of tonic BCR signaling cascades in *ACTN4*$^{-/-}$ P493.6 cells by mass spectrometry

To corroborate the initial analysis of tonic BCR signaling, I examined changes in phosphorylation events in tonic BCR signaling using a more comprehensive approach, by subjecting both clones #3 and #5 of *ACTN4*$^{-/-}$ P493.6 cells and their reconstituted counterparts to MS-based phospho-proteome analysis.

For this purpose, I utilized the stable isotope labeling with amino acids in the cell culture (SILAC) approach. While *ACTN4*$^{-/-}$ cells were cultured in SILAC media supplemented with “light” (L) non-labeled amino acids (K0/R0), reconstituted cells were cultured in SILAC supplemented with “intermediate” (M) ($^{13}_{6}$C, $^{14}_{4}$N)-L-arginine and 4,4,5,5-d4-L-lysine (K+4/R+6). To ensure sufficient incorporation rates of added amino acid isotypes, cells were cultured for a duration of up to 10 days. Subsequently, lysates were prepared and mixed at a 1:1 ratio. Since incorporated amino acids will increase the overall molecular mass of peptides compared to non-labeled light amino acids, the shift in protein mass can be used to distinguish the intensities of phosphorylation. MS analysis was performed in collaboration with the group of Prof. Dr. Thomas Oellerich at the DKTK Proteomics Core Facility, University Hospital Frankfurt.

The obtained results (table 27) confirmed the initial analyses, revealing the impact of ACTN4 on tonic BCR signals. This was indicated by dysregulated phosphorylation of pivotal tonic BCR effectors such as CD79B, SYK, and LYN/HCK as well as negative regulators of BCR signaling such as CD22. Similarly, the phosphorylation of the signaling molecule RASAL3, a negative regulator of the ERK pathway in B cells, was dysregulated due to the loss of ACTN4 [143]. Moreover, ACTN4 also impacted the phosphorylation of several Actin cytoskeleton-related proteins. Notably, the F-Actin severing protein Cofilin exhibited efficient phosphorylation at tyrosine residue Y68, which leads to its degradation, indicating efficient F-Actin polymerization in the presence of ACTN4 [144]. The phosphorylation of transcription factors, such as the BCL-2 associated transcription factor 1 (BCLAF1, also known as BTF), was downregulated in the presence of ACTN4. BCLAF1 is described as a positive regulator of the intrinsic apoptotic signaling pathways [145].

In summary, phospho-proteome analysis of P493.6 cell lines suggests that ACTN4 affects tonic BCR signaling, indicated by dysregulated phosphorylation of pivotal tonic BCR effectors, cytoskeleton regulators, and transcription factors.

Table 27: Overview of phospho-proteome analysis of resting P493.6 cells.
While *ACTN4*$^{-/-}$ + ACTN4-GFP cells were cultured in an intermediate (M) SILAC medium (K4/R6), *ACTN4*$^{-/-}$ cells were grown in a light (L) SILAC medium (K0/R0). Phosphorylation of proteins that have a log2 M/L ratio ≥ 0.5 were considered to be enriched in *ACTN4*$^{-/-}$ + ACTN4-GFP cells.

BCR signaling	**Gene**	**P-sites**	**log2 (M/L)**
B cell antigen receptor complex-associated protein beta chain	*CD79B*	Y196	0.70
Tyrosine-protein kinase SYK	*SYK*	Y352/Y323	2.08/1.81
Tyrosine-protein kinase LYN	*LYN*	S11	-1.50
B cell receptor CD22	*CD22*	S717	-0.70
Protein kinase C beta type; alpha type; gamma type	*PRKCA;B;C*	T500	-1.00
Protein kinase C delta type	*PRKCD*	S664/S654	-0.86/-0.86
NF-kappa-B essential modulator	*IKBKG*	S387	-1.59
Tyrosine-protein kinase LYN;Tyrosine-protein kinase HCK	*LYN; HCK*	Y397	0.82
Other signaling proteins			
RAS protein activator like-3	*RASAL3*	S224/S228/S231	-1,11/-1,11/-1,11
Cytoskeleton regulator and trafficking molecules			
Cofilin-1	*CFL1*	Y68/Y140	2.13/1.75
L-plastin	*LCP1*	S5/S7	1.04/1.04
Microtubule-associated protein 1A	*MAP1A*	S526/S527	0.88/0.88
Microtubule-associated serine/threonine-proteine kinase 3	*MAST3*	S792/S793	0.91/0.91
Pleckstrin	*PLEK*	S117	0.86
Leupaxin	*LPXN*	Y22	1.17
Vesicle-trafficking protein SEC22b	*SEC22B*	S137	-0.86
1-phosphatidylinositol 3-phosphate 5-kinase	*PIKFYVE*	S307	-1.23
Proteins involved in apoptotic processes			
BCL-2-associated transcription factor 1	*BCLAF1*	S512	-1.77
RNA-binding protein 25	*RBM25*	S703	1.54
SAFB-like transcription modulator	*SLTM*	S289	0.81

5 Discussion

The survival of B cells relies on tonic signals that are transduced by BCRs in the absence of antigen binding, but the molecular details of this process remain elusive. Based on studies of BL cells, I investigated the impact of F-Actin cytoskeleton dynamics in tonic BCR survival signals, specifically the role of the F-Actin cross-linking protein ACTN4. For this purpose, I established a cellular model that allows for studying signal transduction and survival in a primary-like B cell state and shows that ACTN4 contributes to the survival of B cells because it limits the lateral mobility of BCR complexes by controlling the F-Actin cytoskeleton dynamics. Hence, my study reveals ACTN4 as a tonic BCR effector protein in resting mature B cells and sheds light on a mechanism by which F-Actin remodeling regulates B cell survival, which might be exploited by tonic BCR signaling-dependent B cell malignancies.

5.1 The primary-like B cell model P493.6 for the analysis of tonic BCR signals

A general obstacle to analyze tonic BCR processes in human B cells is the fact that the vast majority of available human B cell lines are derived from lymphoma cells. Previous studies in mice imply that tonic BCR signaling is mainly governed by the PI3K/AKT signaling pathway and ensures cell survival through the inhibition of transcription factors involved in apoptosis induction such as FOXO1 [57]. FOXO1 inhibition usually diminishes the transcription of the *BCL2L11* gene (encoding the BCL-2 family member BIM), thus reducing the pool of the pro-apoptotic protein BIM *vs.* the pool of anti-apoptotic proteins such as BCL-2 and BCL-xL [56,57]. This process, however, is exploited by aggressive GC B cell lymphomas such as BL cells, which are characterized by enhanced expression of the oncogene *MYC* through translocation of the gene to the *IGH* locus [72,146]. In normal B cells, *MYC* overexpression usually induces apoptosis [147]. BL cells, however, have acquired a centroblast-like transcription profile to counterbalance this effect by enforcing the PI3K/AKT survival axis [134,148]. Further studies demonstrated that aberrant activities of the PI3K/AKT pathway in BL cells underlie mutations in the transcription factor E2A (*TCF3*) or its negative regulator ID3, as mutations in either of both result in promoted cell survival through the PI3K/AKT axis [75].

Recently, a comprehensive phospho-proteome analysis, which was conducted to elucidate the dysregulated tonic BCR signals in BL cells revealed a plethora of tonic BCR effectors [68]. According to this study, tonic BCR signaling cascades comprise not only kinases, phosphatases, and transcription factors but also membrane trafficking molecules and cytoskeleton regulators such as the F-Actin cross-linking protein ACTN4.

Because of the reported BL-specific characteristics, it is uncertain that the identified tonic BCR effector proteins resemble the situation in primary human B cells. However, studying the molecular mechanisms that underlay tonic BCR survival signaling of primary resting B cells is limited due to several reasons such as the purification procedure, a short life span, and limited options for genetic manipulation. Moreover, another drawback of primary B cells is that different donors with different genetic backgrounds might affect the reproducibility of the experiment.

Hence, I took advantage of the P493.6 B cell model, in which *MYC* expression can be conditionally switched off, thereby rendering cells in a resting primary-like state [122]. I could show that the BCR signaling properties of both states are distinct. The switch into the resting state increases the tonic BCR signaling intensity of P493.6 cells compared to the proliferative state, which is evident in BCR-proximal signaling and downstream signaling. Some effectors, such as the MAPKs p38 and JNK, were more strongly phosphorylated in proliferating P493.6 cells, while ERK is more active in the resting state, indicating complex changes in tonic BCR signaling by the expression of *MYC* (Figure 34). Hence, the permanent *MYC* expression in established BL-related B cell lines impedes the investigation of tonic BCR signals and emphasizes the need for a primary-like B cell model such as the P493.6 cell model. While the altered tonic BCR signaling properties *per se* are not sufficient to validate resting P493.6 cells as a primary-like B cell model, I could reproduce the survival analyses obtained from P493.6 cells in purified primary human B cells, further indicating the suitability of the established B cell model.

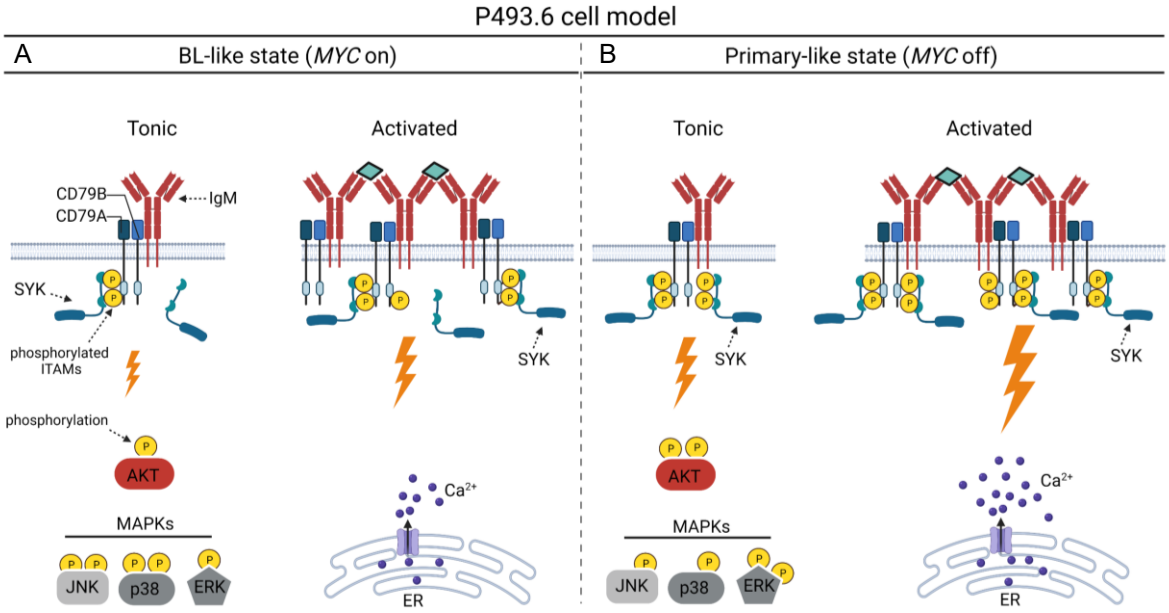

Figure 34: Graphical illustration of tonic and activated BCR signaling in P493.6 cells.
(A) Without doxycycline treatment, *MYC* is expressed and P493.6 cells exhibit low BCR signaling intensity indicated by less efficient phosphorylation levels of the BCR-proximal effectors CD79A and SYK, as well as BCR-distal effectors such as AKT and the MAPK ERK. (B) Upon doxycycline treatment, *MYC* expression is repressed and P493.6 cells show efficient BCR signaling intensity indicated by more efficient phosphorylation levels of the BCR-proximal effectors CD79A and SYK, as well as the BCR-distal effectors AKT and ERK, while JNK and p38 are barely phosphorylated in the absence of MYC. Created with BioRender.com.

5.2 Alpha-Actinin-4, but not alpha-Actinin-1, supports the survival of human B cells

In this study, I could show that ACTN4, but not ACTN1, supports the survival of resting mature P493.6 B cells. This is evident since only the loss of ACTN4 slightly augmented apoptosis, while ACTN1 downregulation neither affected the survival of WT cells nor increased the apoptosis in *ACTN4*$^{-/-}$ cells. Notably, ACTN4 augmented resting P493.6 cell survival in a dose-dependent manner since reconstituted cells with higher ACTN4-GFP expression survived more efficiently compared to cells that have moderate expression levels, which might provide an explanation for the more pronounced survival

in reconstituted cells than in WT P493.6 cells. Further evidence for ACTN4's contribution to resting P493.6 cell survival was revealed through the BH3 profiling, which indicated that ACTN4 protects from apoptosis through the BFL-1 survival axis, which inhibits P53-induced apoptosis [149,150]. In accordance with its survival-supporting function in resting P493.6 cells, ACTN4 downregulation rendered resting primary B cells slightly more prone to apoptosis compared to control cells. Thus, my results provide evidence for the specific contribution of ACTN4 for resting B cell survival, while a role of ACTN1 in survival processes is not supported, although both proteins are highly homologous [99].

This is also in line with previous findings in BL cells, which propose that ACTN4 but not ACTN1 is part of the tonic BCR survival signaling network [68]. Non-redundant functions for ACTN4 and ACTN1 were also illustrated in the literature with respect to cellular processes such as proliferation and survival [95]. In mouse kidney cells, a study has shown that although ACTN4 and ACTN1 have similar biochemistry and localization, they are not functionally redundant [151]. Furthermore, both proteins were reported to contribute to the malignant phenotype of cancer cells, even though an increasing body of evidence highlights ACTN4, rather than ACTN1's role in the tumorigenesis, as a dysregulated function of ACTN4 contributes to metastatic processes [96,99,100]. Hence, distinct roles for ACTN4 and ACTN1 have been unveiled across various contexts, extending beyond their impact on cell survival.

The specific contribution of ACTN4 but not ACTN1 to cell survival could be partially explained by different regulatory mechanisms such as unique tyrosine phosphorylation patterns and distinct interaction partners associated with each protein, marking their functional divergence [103_105]. Moreover, ACTN4 has been shown to be a part of signaling pathways that are involved in cell survival such as PI3K/AKT signaling, WNT/β-catenin signaling, and NF-κB signaling, while ACTN1's contribution to signaling pathways is barely described in the literature [97,152_154].

In conclusion, this study corroborates the existing reports implying that ACTN4 and ACTN1 are functionally non-redundant with respect to several cellular processes and highlights the importance of ACTN4 for resting mature B cell survival, while ruling out the relevance of ACTN1 for this process.

5.3 The survival-supporting function of alpha-Actinin-4 depends on its F-Actin binding capacity

According to the literature, the main function of ACTN4 is to cross-link and organize F-Actin [96,99]. Alterations in F-Actin remodeling have been shown to correlate with cell survival variations across different cell lines [136,155,156]. In this study, the visualization of F-Actin structures in resting P493.6 cells using STED microscopy revealed that ACTN4 loss does not alter the configuration of F-Actin, while resulting in a reduced F-Actin density. Consistently, ACTN4 co-localizes with F-Actin structures at the plasma membrane, and the detected amount of F-Actin positively correlates with survival among the different P493.6 cell lines. In fact, ACTN4 relies on its ABD to mediate its survival-supporting function. This was evident since ACTN4Δ(100-252)-GFP, which lacks a substantial portion of its ABD, could not reconstitute the survival deficits when expressed in *ACTN4*$^{-/-}$ cells. In contrast, the ACTN4 variant K255E exhibited comparable survival-supporting capacity to that of WT ACTN4-GFP. Previous reports have shown that ACTN4 variant K255E possesses an enhanced affinity to F-Actin, suggesting a functional dependency between cortical F-Actin and cell survival [108,110].

Although ACTN4 localization at F-Actin has never been visualized in B cells before, a previous study reported that the cortical F-Actin structures are the prevalent structures in B cells and that the B cell cortex is a prominent site of F-Actin remodeling [137]. Another study showed that the F-Actin cytoskeleton is uniformly distributed at the periphery of unstimulated B cells and undergoes a dramatic reorganization in response to BCR engagement [138]. In addition, ACTN4 was suggested as an F-Actin cross-linking protein contributing to cortical F-Actin dynamics and organization in B cells [78]. In BL cells, ACTN4 has been shown to be phosphorylated on Y265 upon BCR engagement [68]. Phosphorylation of this tyrosine residue, or alternatively substituting it with glutamic acid (E) as a phosphomimetic (Y265E), remarkably increases ACTN4's binding affinity to F-Actin, suggesting an augmented function as an F-Actin cross-linker [108]. Hence, my results align with previous studies regarding the visualized F-Actin structures and confirm the suggested localization of ACTN4 at cortical F-Actin structures in B cells.

The F-Actin cross-linking function of ACTN4 is dependent on its ABD, which harbors three ABSs [110,157]. The removal of amino acids 100-252 from the ABD, which encodes two ABSs, completely abolishes the ACTN4 F-Actin binding capacity [110,140]. Therefore, it is consistent with the results revealed in this study, which show that ACTN4Δ(100-252)-GFP localization was diverted from the plasma membrane to the cytosol and could not co-localize with F-Actin. In contrast, amino acid exchanges in the ABD of ACTN4 (for example, K225 to E, S262 to P, or T258 to I) increase the ACTN4 F-Actin binding affinity [108,110,140]. ACTN4 variants with amino acid substitutions at these sites have been shown to form aggregates in different cell lines, which is in accordance with the observed K255E ACTN4/F-Actin aggregates in resting P493.6 cells.

While my data imply that the stabilization of the cortical F-Actin supports B cell survival, the existing literature about the impact of F-Actin dynamics on B cell survival indicates a more complex interrelation. For example, a study investigating the role of WIP in BCR signaling revealed that less overall amount of F-Actin correlates with less efficient survival in B cells [136]. However, another report on the role of the downstream ARP2/3 complex in B cells implies that a reduced overall amount of F-Actin does not affect B cell fitness [91]. It is worth noting that while WIP and ARP2/3 are involved in branched F-Actin nucleation, ACTN4 forms parallel F-Actin bundles, indicating multifaceted regulatory mechanisms for cortical F-Actin structures. Therefore, the survival of B cells is not simply dependent on the cortical F-Actin amount *per se* but rather on the cortical F-Actin remodeling, which is tightly controlled by several F-Actin binding proteins with unique characteristics in B cell biology [78]. These findings further emphasize the importance of F-Actin dynamics in the regulation of many cellular processes, including the survival of B cells.

In conclusion, my data provide further evidence for the contribution of F-Actin remodeling to survival processes, support the suggested function of ACTN4 as an F-Actin cross-linking protein in B cells, and emphasize the necessity of ACTN4 binding to F-Actin for mediating its survival-supporting function in resting B cells.

5.4 Alpha-Actinin-4 at F-Actin confines BCR diffusion and supports tonic BCR signals

The elucidation of the molecular details that underlay the survival-supporting function of ACTN4 indicated that ACTN4-dependent cross-linking of F-Actin limits lateral BCR mobility and thereby supports tonic BCR survival signals. I could show that a substantial proportion of BCR complexes co-localizes with cortical F-Actin, which depends on the F-Actin binding capacity of ACTN4 and correlates to more efficient survival. Notably, while the presence of ACTN4 restricted the lateral mobility of IgM-BCR to diffusivities that are similar to literature reports [81], its loss markedly increased it. Thus, this study sheds light on the importance of F-Actin remodeling in controlling lateral BCR mobility and tonic BCR survival signaling.

As illustrated in the literature, the cortical F-Actin cytoskeleton of resting B cells is attached to the plasma membrane through Ezrin, Myosin, and Radixin and forms compartments created by F-Actin barriers that restrict lateral BCR mobility, which correlates with BCR signaling [83,158]. For example, the overexpression of a dominant-negative form of Ezrin, which cannot link the cortical F-Actin network to membrane proteins, increases BCR diffusion. Consistently, WT Ezrin overexpression increases F-Actin barriers and restricts BCR diffusion [81].

Similarly, cytoskeleton proteins that control F-Actin polymerization and depolymerization also have an impact on lateral BCR mobility and tonic BCR signaling. Studies showed that the inhibition of the ARP2/3 complex, a master regulator of branched Actin polymerization in B cells, reduces the overall amount of F-Actin and increases BCR mobility and tonic BCR signaling [91]. Also, the complete disruption of F-Actin polymerization in resting B cells using Cytochalasin D or Latrunculin A increases BCR diffusion and tonic BCR signaling [81]. Other studies have provided evidence that F-Actin remodeling affects tonic BCR signaling but without addressing the impact of F-Actin on BCR diffusion. For instance, the disruption of HEM1, a regulator of Actin polymerization and mTOR2 signaling in resting B cells, results in increased tonic BCR signaling [159]. These increases in tonic BCR signaling intensity are evidenced by higher phosphorylation levels of BCR downstream effectors, such as ERK and AKT, as indicated across the studies mentioned in this paragraph.

In contrast to the findings of the aforementioned studies, although ACTN4 loss increased BCR diffusion, it resulted in less efficient tonic BCR signaling, indicated by attenuated phosphorylation levels of ERK and AKT. These apparently conflicting results might be explained by a more complex interdependency between the cortical F-Actin and signaling capacities during different states of BCR signaling [84]. Previous reports showed that the cortical F-Actin remodeling of resting B cells is constantly influenced by the activity of BCR signaling components [81]. Hence, divergent effects of BCR diffusion on tonic BCR signaling could be attributed to the reciprocal impact mediated by BCR signaling on the F-Actin dynamics and *vice versa*.

Furthermore, BCR ligation triggers Actin polymerization, as well as the formation of Actin foci that stabilize the formation of BCR micro-clusters [160]. Thus, the cortical F-Actin not only hinders BCRs diffusion but also promotes interactions between membrane proteins through the regulation of their clustering. Recent advancements in super-resolution microscopy have provided insights into the organization of BCRs on the surface of resting mature B cells. It has been observed that BCRs exist as

monomers or dimers, while the presence of higher oligomeric BCR structures has been ruled out [28]. This finding suggests a correlation between BCR clustering and increased BCR signaling, indicating that dimeric BCRs are more likely to emit tonic signals in resting cells rather than monomeric BCRs [28]. Considering these data, it is reasonable to propose that the localization of ACTN4 at F-Actin supports tonic BCR signaling by increasing the probability of dimeric BCR formation. An alternative explanation could be that enhanced BCR mobility might also kinetically limit the ability of PTKs, such as SYK, to phosphorylate ITAMs located within CD79A/B heterodimer, which is crucial for signaling initiation (Figure 35).

Because the transition from tonic to activated BCR signaling requires F-Actin remodeling and is associated with changes in the intensity of BCR signaling, it is difficult to disentangle effects mediated by Actin remodeling on tonic BCR signaling from activated BCR signaling. Recently, a study classified lateral BCR mobility into eight different BCR diffusive states and correlated distinct BCR diffusive states with potential signaling states in response to BCR ligation [92]. According to their data, B cell activation leads to a reduction in the overall BCR mobility with an increase in BCR fractions with low diffusivity, suggesting that signaling BCRs possess low diffusivity. They also observed that low BCR diffusion correlates with a higher degree of BCR spatial clustering, suggesting that BCR clustering increases signaling. This observation is consistent with the aforementioned study regarding the relationship between BCR clustering and signaling [28]. Therefore, their study would also provide an explanation for why limited lateral BCR mobility, in the presence of ACTN4, supports the efficiency of tonic BCR signaling by facilitating the formation of BCR clusters.

Moreover, it seems that although some cytoskeletal proteins involved in Actin polymerization, such as ARP2/3 and Formin, have similar impacts on BCR diffusion, they differentially affect the various BCR diffusive states [92]. This might explain why, while some cytoskeletal proteins similarly affect BCR diffusion, they differentially affect BCR signaling, as their study linked distinct BCR diffusive states rather than the overall diffusivity to different signaling properties [92]. Therefore, this underscores the unique properties of lateral BCR mobility that require the dynamic regulation of the various F-Actin structures accomplished by multiple Actin cytoskeleton proteins [78]. Understanding the different modes of action by which F-Actin polymerization and depolymerization are accomplished, as well as whether certain BCR diffusive states are more affected than others, might provide valuable insights into the regulatory function of the different cytoskeletal proteins in relation to BCR signaling.

In summary, the finding that ACTN4 limits lateral BCR mobility contributes to a growing body of findings that highlight the significance of F-Actin remodeling in fine-tuning BCR diffusion and nanoscale organization, which influences the efficiency of tonic BCR signaling.

5.5 Efficient tonic BCR signaling correlates with efficient survival

As discussed above, controlling the lateral BCR mobility is pivotal for the tight regulation of BCR signal intensities. Despite the very weak intensity of tonic BCR signal transduction, I could provide some evidence that the ACTN4-dependent confinement of lateral BCR mobility corresponds with changes in tonic BCR signaling.

Previous reports have shown that phosphorylation of tyrosine residues within the ITAM of CD79A is required for tonic BCR signaling initiation, and depends on LYN and SYK activity because the BCR itself is incapable of signaling initiation [121,141]. Moreover, although it was suggested that CD79A and CD79B phosphorylation depends on F-Actin dynamics and density, which control the spatial organization of proximal BCR kinases, such as SYK and LYN, and their access to the ITAMs of CD79A and CD79B, mechanisms remain unclear [161,162]. In line with these reports, my data indicate that the efficient phosphorylation of CD79A is accompanied by reduced phosphorylation of LYN on the inhibitory key tyrosine residue and augmented phosphorylation of activatory tyrosine residues buried within the kinase domain of SYK [34,35,163]. Therefore, my results indicate an augmented activity of LYN and SYK in the presence of ACTN4. In a similar manner, SLP65 phosphorylation was augmented, which is compatible with the augmented activity of its upstream regulator protein SYK. In accordance with the efficient tonic BCR-upstream signaling, ACTN4 significantly supports the phosphorylation of the distal BCR effectors ERK and to a lesser degree AKT, even though AKT is seen as the guardian of tonic BCR survival signals in B cells. Thus, my results suggest that ACTN4 supports the phosphorylation of the tonic BCR-distal effectors ERK and AKT by maintaining tonic BCR-proximal signaling efficiency.

Further evidence that ACTN4 supports the efficiency of tonic BCR signaling of resting P493.6 cells was provided by comprehensive MS-based phospho-proteome analysis, indicated by augmented phosphorylation levels of CD79B, SYK, and LYN/HCK in the presence of ACTN4. Analyses also provided hints that the augmented phosphorylation of ERK might be a result of reduced phosphorylation of RASAL3, which is a negative regulator of the Ras/ERK pathway in B cells [143]. In addition, the impact of ACTN4 on tonic BCR signaling was also reflected by dysregulated tyrosine phosphorylation of several Actin cytoskeleton-related proteins, which is compatible with the previous study showing that numerous cytoskeleton regulators are a part of tonic BCR signaling in BL cells [68]. Particularly, the F-Actin severing protein Cofilin has been shown to be phosphorylated on tyrosine residue Y68 in the presence of ACTN4. Cofilin is described to have a role in BCR signaling, and phosphorylation at this tyrosine residue leads to its degradation [138,144,164]. Therefore, the results revealed by MS analysis suggest that increased F-Actin polymerization correlates with efficient signaling, thus emphasizing the positive correlation between the overall amount of F-Actin and the efficiency of tonic BCR signaling. Collectively, my data indicate that the ACTN4-mediated impact on tonic BCR signaling results from its impact on the cortical F-Actin, thereby confining lateral BCR mobility, which ultimately correlates with the survival of B cells.

In line with my data, which show that efficient tonic BCR signaling correlates with better survival, CD79A downregulation markedly reduces BL cell survival [68]. In a mouse strain in which *SYK* expression can be conditionally abrogated, the loss of SYK results in rapid mature B cell death, indicating impaired tonic BCR survival signaling [165,166]. In addition, the expression of an active form of SYK reduced the apoptosis in BL cells with defects in tonic BCR signaling [167]. Similarly, SYK-deficient B cells survived better in the absence of FOXO1, a downstream effector of AKT, indicating that SYK transduces tonic BCR survival signaling through AKT [168]. In primary B cells, higher phosphorylation levels of AKT and ERK significantly correlate with more survival potential [67]. The ectopic activation of the ERK pathway partially rescues the survival of SYK-deficient B cells, indicating that SYK also transduces survival signals through ERK

together with AKT [165]. This is also feasible since GRB2 has been shown to recruit ERK to the BCR, suggesting that its phosphorylation might take place by proximal BCR effectors [48].

Other studies revealed that the inhibition of SYK or the downregulation of *CD79A* expression reduces ERK phosphorylation in BL cells [68]. In WSU-DLCL2 lymphoma cells, it has been shown that the inhibition of phospho-ERK correlates with increased apoptosis, with EGR1 suggested as a downstream target for ERK in tonic BCR survival signals. While BTK-dependent B cell lymphomas with high phospho-ERK levels are sensitive to the BTK inhibitor ibrutinib (PCI-32765), cells with low phospho-ERK levels are not sensitive and their survival is not affected [169,170]. Taken together, these studies emphasize the importance of the MAPK ERK for B cell survival and suggest it as a downstream effector of SYK to mediate tonic BCR survival signals.

In conclusion, the data of this study highlight ACTN4 as an F-Actin cross-linking protein that supports resting B cell survival by improving the efficiency of tonic BCR signaling which is facilitated by limited lateral BCR mobility. Thus, this study emphasizes the already established role of cortical F-Actin remodeling in the regulation of lateral BCR mobility and tonic BCR survival signaling (Figure 35).

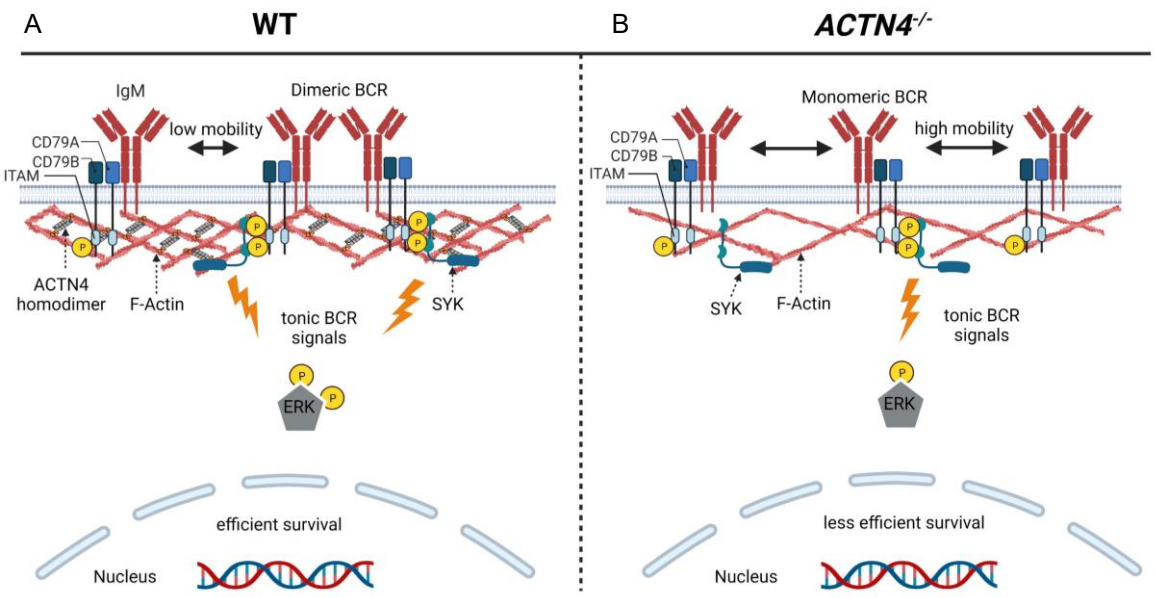

Figure 35: Schematic illustration of the proposed mechanism by which ACTN4 supports tonic BCR survival signals.
(A) ACTN4-dependent control of F-Actin remodeling confines lateral BCR mobility, is believed to support the formation of dimeric BCRs, and is associated with higher phosphorylation levels of tyrosine residues within the ITAMs of CD79A and CD79B. As a result, SYK is effectively recruited to the phosphorylated ITAMs and transduces efficient tonic signaling to ERK, thereby improving the survival of resting P493.6 cells. (B) In contrast, ACTN4 loss reduces F-Actin amount and increases lateral BCR mobility, which might reduce the probability of dimeric BCR formation, resulting in less augmented phosphorylation of tyrosine residues within the ITAM of CD79A and CD79B. Consequently, SYK is recruited to the phosphorylated ITAMs to a lesser degree, resulting in slightly attenuated tonic signaling of ERK and less efficient survival. Created with BioRender.com.

6 Conclusion and Outlook

My study provides molecular details of how the F-Actin cross-linking protein ACTN4 contributes to tonic BCR survival signals of resting mature B cells. Although previous studies revealed the PI3K/AKT pathway as the main pathway of tonic BCR survival signals, molecular mechanisms underlying tonic BCR survival signaling have still been largely unclear. The results of this study imply that ACTN4 contributes to mature resting B cell survival, which is in accordance with its identified role in BL cells. In addition, my data suggest that ACTN4 supports tonic BCR survival signaling in resting B cells mainly *via* the SYK-ERK survival axis through regulating F-Actin remodeling and thereby confining lateral BCR mobility. This study sheds light on a potential survival mechanism that may be co-opted by tonic BCR signaling-dependent B cell malignancies through the modulation of F-Actin dynamics.

Since the organization of the F-Actin-based cytoskeleton appears to be a pivotal aspect of controlled tonic BCR signals, it is necessary to understand the spatial characteristics of tonic BCR signaling orchestrated by a complex network of F-Actin structures that impact BCR diffusion and tonic BCR signaling. For this purpose, it would be feasible to determine whether certain F-Actin structures are required more than others for an appropriate efficiency of tonic BCR survival signals and to link these processes with BCR diffusion. Furthermore, it is imperative to assess the pivotal role of F-Actin dynamics in facilitating appropriate spatiotemporal stability as well as the dynamical organization of pre-formed macromolecular signaling complexes, which are unique characteristics of resting B cells [171].

Gaining a comprehensive understanding of the spatial aspects of tonic BCR signaling would shed light on how BL cells exploit F-Actin-regulating mechanisms to modulate tonic BCR survival signaling, which may uncover novel therapeutic possibilities to control the pathological tonic BCR signaling in BL cells.

7 References

1. Chaplin, D. D. 1. Overview of the human immune response. *The Journal of allergy and clinical immunology* **117,** S430-5; 10.1016/j.jaci.2005.09.034 (2006).
2. Murphy, K. M. & Weaver, C. *Janeway's immunobiology. An introduction to the immunobiology and innate immunity.* 9th ed. (GS, Garland Science, Taylor & Francis Group, New York, London, 2017).
3. Takeuchi, O. & Akira, S. Pattern recognition receptors and inflammation. *Cell* **140,** 805–820; 10.1016/j.cell.2010.01.022 (2010).
4. Abbas, A. K., Lichtman, A. H., Pillai, S. & Baker, D. L. *Cellular and molecular immunology* (Elsevier, Saunders, 2015).
5. Medzhitov, R. & Janeway, C. A. Innate immunity: the virtues of a nonclonal system of recognition. *Cell* **91,** 295–298; 10.1016/s0092-8674(00)80412-2 (1997).
6. Chaplin, D. D. Overview of the immune response. *The Journal of allergy and clinical immunology* **125,** S3-23; 10.1016/j.jaci.2009.12.980 (2010).
7. Von Behring, E. & Kitasato, S. Ueber das zuandekommen der diphtherie-immunität und der tetanus-immunitat bei thieren. Deutsche medizinische wochenschrift 16, 1113-1114, 1890.
8. Tiselius, A. & Kabat, E. A. AN ELECTROPHORETIC STUDY OF IMMUNE SERA AND PURIFIED ANTIBODY PREPARATIONS. *The Journal of experimental medicine* **69,** 119–131 (1939).
9. Fagraeus, A. The plasma cellular reaction and its relation to the formation of antibodies in vitro. *J. Immunol. 58, 1–13,* 1–13 (1948).
10. COOPER, M. D., PETERSON, R. D. & GOOD, R. A. DELINEATION OF THE THYMIC AND BURSAL LYMPHOID SYSTEMS IN THE CHICKEN. *Nature* **205,** 143–146; 10.1038/205143a0 (1965).
11. TILL, J. E. & McCULLOCH, E. A. A direct measurement of the radiation sensitivity of normal mouse bone marrow cells. *Radiation research* **14,** 213–222 (1961).
12. Kondo, M. Lymphoid and myeloid lineage commitment in multipotent hematopoietic progenitors. *Immunological reviews* **238,** 37–46; 10.1111/j.1600-065X.2010.00963.x (2010).
13. Pieper, K., Grimbacher, B. & Eibel, H. B-cell biology and development. *The Journal of allergy and clinical immunology* **131,** 959–971; 10.1016/j.jaci.2013.01.046 (2013).
14. Hozumi, N. & Tonegawa, S. Evidence for somatic rearrangement of immunoglobulin genes coding for variable and constant regions. *Proceedings of the National Academy of Sciences of the United States of America* **73,** 3628–3632 (1976).
15. Mårtensson, I.-L., Keenan, R. A. & Licence, S. The pre-B-cell receptor. *Current opinion in immunology* **19,** 137–142; 10.1016/j.coi.2007.02.006 (2007).
16. Teng, G. & Papavasiliou, F. N. Immunoglobulin somatic hypermutation. *Annual review of genetics* **41,** 107–120; 10.1146/annurev.genet.41.110306.130340 (2007).
17. Chaudhuri, J. & Alt, F. W. Class-switch recombination: interplay of transcription, DNA deamination and DNA repair. *Nature reviews. Immunology* **4,** 541–552; 10.1038/nri1395 (2004).
18. Muramatsu, M. *et al.* Pillars Article: Class Switch Recombination and Hypermutation Require Activation-Induced Cytidine Deaminase (AID), a Potential RNA Editing Enzyme. Cell. 2000. 102: 553-563. *Journal of immunology (Baltimore, Md. : 1950)* **201,** 2530–2540 (2018).

19. Muramatsu, M. *et al.* Specific expression of activation-induced cytidine deaminase (AID), a novel member of the RNA-editing deaminase family in germinal center B cells. *The Journal of biological chemistry* **274,** 18470–18476; 10.1074/jbc.274.26.18470 (1999).

20. Suan, D., Sundling, C. & Brink, R. Plasma cell and memory B cell differentiation from the germinal center. *Current opinion in immunology* **45,** 97–102; 10.1016/j.coi.2017.03.006 (2017).

21. Murphy, K. M. & Weaver, C. *Janway's immunobiology. Lymphocytes Receptor Signaling.* 9th ed. (GS, Garland Science, Taylor & Francis Group, New York, London, 2017).

22. Schroeder, H. W. & Cavacini, L. Structure and Function of Immunoglobulins. *The Journal of allergy and clinical immunology* **125,** S41-52; 10.1016/j.jaci.2009.09.046 (2010).

23. Reynolds, H. Y. Immunoglobulin G and its function in the human respiratory tract. *Mayo Clinic proceedings* **63,** 161–174; 10.1016/s0025-6196(12)64949-0 (1988).

24. Kraus, M., Alimzhanov, M. B., Rajewsky, N. & Rajewsky, K. Survival of resting mature B lymphocytes depends on BCR signaling via the Igalpha/beta heterodimer. *Cell* **117,** 787–800; 10.1016/j.cell.2004.05.014 (2004).

25. Treanor, B. B-cell receptor: from resting state to activate. *Immunology* **136,** 21–27; 10.1111/j.1365-2567.2012.03564.x (2012).

26. Yang, J. & Reth, M. The dissociation activation model of B cell antigen receptor triggering. *FEBS letters* **584,** 4872–4877; 10.1016/j.febslet.2010.09.045 (2010).

27. Tolar, P. & Pierce, S. K. A conformation-induced oligomerization model for B cell receptor microclustering and signaling. *Current topics in microbiology and immunology* **340,** 155–169; 10.1007/978-3-642-03858-7_8 (2010).

28. Gomes de Castro, M. A. *et al.* Differential organization of tonic and chronic B cell antigen receptors in the plasma membrane. *Nature communications* **10,** 820; 10.1038/s41467-019-08677-1 (2019).

29. Brown, M. T. & Cooper, J. A. Regulation, substrates and functions of src. *Biochimica et biophysica acta* **1287,** 121–149; 10.1016/0304-419x(96)00003-0 (1996).

30. Okada, M. Regulation of the SRC family kinases by Csk. *International journal of biological sciences* **8,** 1385–1397; 10.7150/ijbs.5141 (2012).

31. Nguyen, P.-H., Niesen, E. & Hallek, M. New roles for B cell receptor associated kinases: when the B cell is not the target. *Leukemia* **33,** 576–587; 10.1038/s41375-018-0366-8 (2019).

32. Xu, Y., Harder, K. W., Huntington, N. D., Hibbs, M. L. & Tarlinton, D. M. Lyn tyrosine kinase: accentuating the positive and the negative. *Immunity* **22,** 9–18; 10.1016/j.immuni.2004.12.004 (2005).

33. Ingley, E. Functions of the Lyn tyrosine kinase in health and disease. *Cell communication and signaling : CCS* **10,** 21; 10.1186/1478-811X-10-21 (2012).

34. Fütterer, K., Wong, J., Grucza, R. A., Chan, A. C. & Waksman, G. Structural basis for Syk tyrosine kinase ubiquity in signal transduction pathways revealed by the crystal structure of its regulatory SH2 domains bound to a dually phosphorylated ITAM peptide. *Journal of molecular biology* **281,** 523–537; 10.1006/jmbi.1998.1964 (1998).

35. Zhang, J., Billingsley, M. L., Kincaid, R. L. & Siraganian, R. P. Phosphorylation of Syk activation loop tyrosines is essential for Syk function. An in vivo study using a specific anti-Syk activation loop phosphotyrosine antibody. *The Journal of biological chemistry* **275,** 35442–35447; 10.1074/jbc.M004549200 (2000).

36. Wienands, J. *et al.* SLP-65: A New Signaling Component in B Lymphocytes which Requires Expression of the Antigen Receptor for Phosphorylation. *The Journal of experimental medicine* **188,** 791–795 (1998).

37. N Engels 1, B Wollscheid, J Wienands. Association of SLP-65/BLNK with the B cell antigen receptor through a non-ITAM tyrosine of Ig-alpha. *Eur J Immunol,* 1521–4141 (2001).

38. Fu, C., Turck, C. W., Kurosaki, T. & Chan, A. C. BLNK: a central linker protein in B cell activation. *Immunity* **9,** 93–103; 10.1016/s1074-7613(00)80591-9 (1998).

39. Grabbe, A. & Wienands, J. Human SLP-65 isoforms contribute differently to activation and apoptosis of B lymphocytes. *Blood* **108,** 3761–3768; 10.1182/blood-2006-02-005397 (2006).

40. Oellerich, T. *et al.* SLP-65 phosphorylation dynamics reveals a functional basis for signal integration by receptor-proximal adaptor proteins. *Molecular & cellular proteomics : MCP* **8,** 1738–1750; 10.1074/mcp.M800567-MCP200 (2009).

41. Minegishi, Y. *et al.* An essential role for BLNK in human B cell development. *Science (New York, N.Y.)* **286,** 1954–1957; 10.1126/science.286.5446.1954 (1999).

42. Jumaa, H. *et al.* Abnormal development and function of B lymphocytes in mice deficient for the signaling adaptor protein SLP-65. *Immunity* **11,** 547–554; 10.1016/s1074-7613(00)80130-2 (1999).

43. Oellerich, T. *et al.* The B-cell antigen receptor signals through a preformed transducer module of SLP65 and CIN85. *The EMBO journal* **30,** 3620–3634; 10.1038/emboj.2011.251 (2011).

44. Engelke, M., Engels, N., Dittmann, K., Stork, B. & Wienands, J. Ca(2+) signaling in antigen receptor-activated B lymphocytes. *Immunological reviews* **218,** 235–246; 10.1111/j.1600-065X.2007.00539.x (2007).

45. Su, Y. W. *et al.* Interaction of SLP adaptors with the SH2 domain of Tec family kinases. *European journal of immunology* **29,** 3702–3711; 10.1002/(SICI)1521-4141(199911)29:11<3702::AID-IMMU3702>3.0.CO;2-R (1999).

46. Hashimoto, S. Identification of the SH2 domain binding protein of Bruton's tyrosine kinase as BLNK - Functional significance of Btk-SH2 domain in B-cell antigen receptor- coupled calcium signaling. *Blood* **94,** 2357–2364 (1999).

47. Saijo, K. *et al.* Protein kinase C beta controls nuclear factor kappaB activation in B cells through selective regulation of the IkappaB kinase alpha. *The Journal of experimental medicine* **195,** 1647–1652; 10.1084/jem.20020408 (2002).

48. Vanshylla, K. *et al.* Grb2 and GRAP connect the B cell antigen receptor to Erk MAP kinase activation in human B cells. *Scientific reports* **8,** 4244; 10.1038/s41598-018-22544-x (2018).

49. Kruse, V. *Identification of therapeutic targets in the Burkitt's lymphoma specific B cell antigen receptor signaling network* (2018).

50. Xu, Y., Fairfax, K., Light, A., Huntington, N. D. & Tarlinton, D. M. CD19 differentially regulates BCR signalling through the recruitment of PI3K. *Autoimmunity* **47,** 430–437; 10.3109/08916934.2014.921810 (2014).

51. Deane, J. A. & Fruman, D. A. Phosphoinositide 3-kinase: diverse roles in immune cell activation. *Annual review of immunology* **22,** 563–598; 10.1146/annurev.immunol.22.012703.104721 (2004).

52. Salim, K. Distinct specificity in the recognition of phosphoinositides by the pleckstrin homology domains of dynamin and Bruton's tyrosine kinase. *EMBO J.* **15,** 6241–6250 (1996).

53. M. Falasca. Activation of phospholipase Cγ by PI 3-kinase-induced PH domain-mediated membrane targeting. *The EMBO journal,* 414–422 (1998).

54. Hers, I. Akt signalling in health and disease. *Cellular signalling* (2011).

55. Manning, B. D. & Cantley, L. C. AKT/PKB signaling: navigating downstream. *Cell* **129,** 1261–1274; 10.1016/j.cell.2007.06.009 (2007).

56. Zhang, X., Tang, N., Hadden, T. J. & Rishi, A. K. Akt, FoxO and regulation of apoptosis. *Biochimica et biophysica acta* **1813,** 1978–1986; 10.1016/j.bbamcr.2011.03.010 (2011).

57. Srinivasan, L. *et al.* PI3 kinase signals BCR-dependent mature B cell survival. *Cell* **139,** 573–586; 10.1016/j.cell.2009.08.041 (2009).

58. Angelo Castello *et al.* Nck-mediated recruitment of BCAP to the BCR regulates the PI(3)K-Akt pathway in B cells. *Nature immunology,* 966–975 (2013).

59. Lam, K. P., Kühn, R. & Rajewsky, K. In vivo ablation of surface immunoglobulin on mature B cells by inducible gene targeting results in rapid cell death. *Cell* **90,** 1073–1083; 10.1016/s0092-8674(00)80373-6 (1997).

60. Wienands, J., Larbolette, O. & Reth, M. Evidence for a preformed transducer complex organized by the B cell antigen receptor. *Proceedings of the National Academy of Sciences of the United States of America* **93,** 7865–7870; 10.1073/pnas.93.15.7865 (1996).

61. Monroe, J. G. ITAM-mediated tonic signalling through pre-BCR and BCR complexes. *Nature reviews. Immunology* **6,** 283–294; 10.1038/nri1808 (2006).

62. Cheng, P. C., Dykstra, M. L., Mitchell, R. N. & Pierce, S. K. A role for lipid rafts in B cell antigen receptor signaling and antigen targeting. *The Journal of experimental medicine* **190,** 1549–1560; 10.1084/jem.190.11.1549 (1999).

63. Cherukuri, A., Dykstra, M. & Pierce, S. K. Floating the raft hypothesis: lipid rafts play a role in immune cell activation. *Immunity* **14,** 657–660; 10.1016/s1074-7613(01)00156-x (2001).

64. Thomas, M. L. & Brown, E. J. Positive and negative regulation of Src-family membrane kinases by CD45. *Immunology today* **20,** 406–411; 10.1016/s0167-5699(99)01506-6 (1999).

65. Akatsu, C. *et al.* The inhibitory coreceptor CD22 restores B cell signaling by developmentally regulating Cd45-/- immunodeficient B cells. *Science signaling* **15,** eabf9570; 10.1126/scisignal.abf9570 (2022).

66. Nitschke, L., Carsetti, R., Ocker, B., Köhler, G. & Lamers, M. C. CD22 is a negative regulator of B-cell receptor signalling. *Current biology : CB* **7,** 133–143; 10.1016/S0960-9822(06)00057-1 (1997).

67. Yasuda, S., Zhou, Y., Wang, Y., Yamamura, M. & Wang, J.-Y. A model integrating tonic and antigen-triggered BCR signals to predict the survival of primary B cells. *Scientific reports* **7,** 14888; 10.1038/s41598-017-13993-x (2017).

68. Corso, J., Słabicki, M., Hüllein, J. & Zenz, T. *Elucidation of tonic and activated B-cell receptor signaling in Burkitt's lymphoma provides insights into regulation of cell survival* (2016).

69. Küppers, R. Mechanisms of B-cell lymphoma pathogenesis. *Nature reviews. Cancer* **5,** 251–262; 10.1038/nrc1589 (2005).

70. Buchner, M. & Müschen, M. Targeting the B-cell receptor signaling pathway in B lymphoid malignancies. *Current opinion in hematology* **21,** 341–349; 10.1097/MOH.0000000000000048 (2014).

71. Burger, J. A. & Wiestner, A. Targeting B cell receptor signalling in cancer: preclinical and clinical advances. *Nature reviews. Cancer* **18,** 148–167; 10.1038/nrc.2017.121 (2018).

72. Young, R. M. & Staudt, L. M. Targeting pathological B cell receptor signalling in lymphoid malignancies. *Nature reviews. Drug discovery* **12,** 229–243; 10.1038/nrd3937 (2013).

73. Davis, R. E. *et al.* Chronic active B-cell-receptor signalling in diffuse large B-cell lymphoma. *Nature* **463,** 88–92; 10.1038/nature08638 (2010).

74. Keller, U., Nilsson, J. A., Maclean, K. H., Old, J. B. & Cleveland, J. L. Nfkb 1 is dispensable for Myc-induced lymphomagenesis. *Oncogene* **24,** 6231–6240; 10.1038/sj.onc.1208779 (2005).

75. Schmitz, R. *et al.* Burkitt lymphoma pathogenesis and therapeutic targets from structural and functional genomics. *Nature* **490,** 116–120; 10.1038/nature11378 (2012).

76. Chew, V. & Lam, K.-P. Leupaxin negatively regulates B cell receptor signaling. *The Journal of biological chemistry* **282,** 27181–27191; 10.1074/jbc.M704625200 (2007).

77. Yang, J. & Reth, M. Receptor Dissociation and B-Cell Activation. *Current topics in microbiology and immunology* **393,** 27–43; 10.1007/82_2015_482 (2016).

78. Tolar, P. Cytoskeletal control of B cell responses to antigens. *Nature reviews. Immunology* **17,** 621–634; 10.1038/nri.2017.67 (2017).

79. Kusumi, A. *et al.* Paradigm shift of the plasma membrane concept from the two-dimensional continuum fluid to the partitioned fluid: high-speed single-molecule tracking of membrane molecules. *Annual review of biophysics and biomolecular structure* **34,** 351–378; 10.1146/annurev.biophys.34.040204.144637 (2005).

80. Mattila, P. K., Batista, F. D. & Treanor, B. Dynamics of the actin cytoskeleton mediates receptor cross talk: An emerging concept in tuning receptor signaling. *The Journal of cell biology* **212,** 267–280; 10.1083/jcb.201504137 (2016).

81. Treanor, B. *et al.* The Membrane Skeleton Controls Diffusion Dynamics and Signaling through the B Cell Receptor. *Immunity* **32,** 187–199; 10.1016/j.immuni.2009.12.005 (2010).

82. Neisch, A. L. & Fehon, R. G. Ezrin, Radixin and Moesin: key regulators of membrane-cortex interactions and signaling. *Current opinion in cell biology* **23,** 377–382; 10.1016/j.ceb.2011.04.011 (2011).

83. Treanor, B., Depoil, D., Bruckbauer, A. & Batista, F. D. Dynamic cortical actin remodeling by ERM proteins controls BCR microcluster organization and integrity. *The Journal of experimental medicine* **208,** 1055–1068; 10.1084/jem.20101125 (2011).

84. Song, W., Liu, C. & Upadhyaya, A. The pivotal position of the actin cytoskeleton in the initiation and regulation of B cell receptor activation☆. *Biochimica et biophysica acta* **1838**; 10.1016/j.bbamem.2013.07.016 (2013).

85. Thrasher, A. J. & Burns, S. Wiskott-Aldrich syndrome: a disorder of haematopoietic cytoskeletal regulation. *Microscopy research and technique* **47,** 107–113; 10.1002/(SICI)1097-0029(19991015)47:2<107::AID-JEMT3>3.0.CO;2-H (1999).

86. Moulding, D. A., Record, J., Malinova, D. & Thrasher, A. J. Actin cytoskeletal defects in immunodeficiency. *Immunological reviews* **256,** 282–299; 10.1111/imr.12114 (2013).

87. Simon, H. U., Mills, G. B., Hashimoto, S. & Siminovitch, K. A. Evidence for defective transmembrane signaling in B cells from patients with Wiskott-Aldrich syndrome. *The Journal of clinical investigation* **90,** 1396–1405; 10.1172/JCI116006 (1992).

88. Liu, C. *et al.* N-wasp is essential for the negative regulation of B cell receptor signaling. *PLoS biology* **11,** e1001704; 10.1371/journal.pbio.1001704 (2013).

89. Amann, K. J. & Pollard, T. D. The Arp2/3 complex nucleates actin filament branches from the sides of pre-existing filaments. *Nature cell biology* **3,** 306–310; 10.1038/35060104 (2001).

90. Rotty, J. D., Wu, C. & Bear, J. E. New insights into the regulation and cellular functions of the ARP2/3 complex. *Nature reviews. Molecular cell biology* **14,** 7–12; 10.1038/nrm3492 (2013).

91. Bolger-Munro, M. *et al.* Arp2/3 complex-driven spatial patterning of the BCR enhances immune synapse formation, BCR signaling and B cell activation. *eLife* **8**; 10.7554/eLife.44574 (2019).

92. Rey-Suarez, I. *et al.* WASP family proteins regulate the mobility of the B cell receptor during signaling activation. *Nature communications* **11,** 439; 10.1038/s41467-020-14335-8 (2020).

93. Kao, H.-Y. The actinin family proteins: biological function and clinical implications. *Cell & bioscience* **5,** 48; 10.1186/s13578-015-0039-5 (2015).

94. Sjöblom, B., Salmazo, A. & Djinović-Carugo, K. Alpha-actinin structure and regulation. *Cellular and molecular life sciences : CMLS* **65,** 2688–2701; 10.1007/s00018-008-8080-8 (2008).

95. Quick, Q. & Skalli, O. Alpha-actinin 1 and alpha-actinin 4: contrasting roles in the survival, motility, and RhoA signaling of astrocytoma cells. *Experimental cell research* **316,** 1137–1147; 10.1016/j.yexcr.2010.02.011 (2010).

96. Honda, K. The biological role of actinin-4 (ACTN4) in malignant phenotypes of cancer. *Cell & bioscience* **5,** 41; 10.1186/s13578-015-0031-0 (2015).

97. Aksenova, V. *et al.* Actin-binding protein alpha-actinin 4 (ACTN4) is a transcriptional co-activator of RelA/p65 sub-unit of NF-kB. *Oncotarget* **4,** 362–372; 10.18632/oncotarget.901 (2013).

98. Xuan ZhaoKuo-Sheng Hsu, Jun Hee Lim & and Leslie A. Bruggeman. α-Actinin 4 Potentiates Nuclear Factor κ-Light-chain-enhancer of Activated B-cell (NF-κB) Activity in Podocytes Independent of Its Cytoplasmic Actin Binding Function. *J Biol Chem.,* 338–349 (2015).

99. Honda, K. *et al.* Actinin-4, a novel actin-bundling protein associated with cell motility and cancer invasion. *The Journal of cell biology* **140,** 1383–1393; 10.1083/jcb.140.6.1383 (1998).

100. Zhang, S. *et al.* α-Actinin1 promotes tumorigenesis and epithelial-mesenchymal transition of gastric cancer via the AKT/GSK3β/β-Catenin pathway. *Bioengineered* **12,** 5688–5704; 10.1080/21655979.2021.1967713 (2021).

101. Youssoufian, H., McAfee, M. & Kwiatkowski, D. J. Cloning and chromosomal localization of the human cytoskeletal alpha-actinin gene reveals linkage to the beta-spectrin gene. *American Journal of Human Genetics* **47,** 62–71 (1990).

102. Millake, D. B., Blanchard, A. D., Patel, B. & Critchley, D. R. The cDNA sequence of a human placental alpha-actinin. *Nucleic acids research* **17,** 6725; 10.1093/nar/17.16.6725 (1989).

103. Feng, Y. *et al.* α-actinin1 and 4 tyrosine phosphorylation is critical for stress fiber establishment, maintenance and focal adhesion maturation. *Experimental cell research* **319,** 1124–1135; 10.1016/j.yexcr.2013.02.009 (2013).

104. String Interaction Network. ACTN1 Protein (Human). Available at https://version-11-5.string-db.org/cgi/network?networkId=bW1I4BaDKa4x (2023).

105. String Interaction Network. ACTN4 Protein (Human). Available at string-db.org/cgi/network?networkId=b8QNoXj1EwdR (2023).

106. Izaguirre, G. *et al.* The cytoskeletal/non-muscle isoform of alpha-actinin is phosphorylated on its actin-binding domain by the focal adhesion kinase. *The Journal of biological chemistry* **276,** 28676–28685; 10.1074/jbc.M101678200 (2001).

107. Egerton, M., Moritz, R. L., Druker, B., Kelso, A. & Simpson, R. J. Identification of the 70kD heat shock cognate protein (Hsc70) and alpha-actinin-1 as novel phosphotyrosine-containing proteins in T lymphocytes. *Biochemical and biophysical research communications* **224,** 666–674; 10.1006/bbrc.1996.1082 (1996).

108. Shao, H. *et al.* Focal segmental glomerulosclerosis ACTN4 mutants binding to actin: regulation by phosphomimetic mutations. *Scientific reports* **9,** 15517; 10.1038/s41598-019-51825-2 (2019).

109. Shao, H., Travers, T., Camacho, C. J. & Wells, A. The carboxyl tail of alpha-actinin-4 regulates its susceptibility to m-calpain and thus functions in cell migration and spreading. *The international journal of biochemistry & cell biology* **45,** 1051–1063; 10.1016/j.biocel.2013.02.015 (2013).

110. Weins, A. *et al.* Disease-associated mutant alpha-actinin-4 reveals a mechanism for regulating its F-actin-binding affinity. *Proceedings of the National Academy of Sciences of the United States of America* **104,** 16080–16085; 10.1073/pnas.0702451104 (2007).

111. Thomas, D. G. & Robinson, D. N. The fifth sense: Mechanosensory regulation of alpha-actinin-4 and its relevance for cancer metastasis. *Seminars in cell & developmental biology* **71,** 68–74; 10.1016/j.semcdb.2017.05.024 (2017).

112. Murphy, A. C. H. & Young, P. W. The actinin family of actin cross-linking proteins - a genetic perspective. *Cell & bioscience* **5,** 49; 10.1186/s13578-015-0029-7 (2015).

113. Ben-Bassat, H. *et al.* Establishment in continuous culture of a new type of lymphocyte from a "Burkitt like" malignant lymphoma (line D.G.-75). *International journal of cancer* **19,** 27–33; 10.1002/ijc.2910190105 (1977).

114. Gabay, C., Ben-Bassat, H., Schlesinger, M. & Laskov, R. Somatic mutations and intraclonal variations in the rearranged Vkappa genes of B-non-Hodgkin's lymphoma cell lines. *European journal of haematology* **63,** 180–191; 10.1111/j.1600-0609.1999.tb01766.x (1999).

115. Hay, R. J., Caputo, J. L. & and Macy M. L. ATCC Quality Control Methods for Cell Lines. *ATCC* (1992).

116. Klein, G., Giovanella, B., Westman, A., Stehlin, J. S. & Mumford, D. An EBV-genome-negative cell line established from an American Burkitt lymphoma; receptor characteristics. EBV infectibility and permanent conversion into EBV-positive sublines by in vitro infection. *Intervirology* **5,** 319–334; 10.1159/000149930 (1975).

117. Benjamin, D. *et al.* Immunoglobulin secretion by cell lines derived from African and American undifferentiated lymphomas of Burkitt's and non-Burkitt's type. *Journal of immunology (Baltimore, Md. : 1950)* **129,** 1336–1342 (1982).

118. Farrell, P. J., Allan, G. J., Shanahan, F., Vousden, K. H. & Crook, T. p53 is frequently mutated in Burkitt's lymphoma cell lines. *The EMBO journal* **10,** 2879–2887; 10.1002/j.1460-2075.1991.tb07837.x (1991).

119. Klein, E. *et al.* Surface IgM-kappa specificity on a Burkitt lymphoma cell in vivo and in derived culture lines. *Cancer research* **28,** 1300–1310 (1968).

120. Kreck, B. *et al.* Base-pair resolution DNA methylome of the EBV-positive Endemic Burkitt lymphoma cell line DAUDI determined by SOLiD bisulfite-sequencing. *Leukemia* **27,** 1751–1753; 10.1038/leu.2013.4 (2013).

121. Richter, J. *et al.* Recurrent mutation of the ID3 gene in Burkitt lymphoma identified by integrated genome, exome and transcriptome sequencing. *Nature genetics* **44,** 1316–1320; 10.1038/ng.2469 (2012).

122. Pajic, A. *et al.* Cell cycle activation by c-myc in a burkitt lymphoma model cell line. *International journal of cancer* **87,** 787–793; 10.1002/1097-0215(20000915)87:6<787::aid-ijc4>3.0.co;2-6 (2000).

123. Polack, A. *et al.* c-myc activation renders proliferation of Epstein-Barr virus (EBV)-transformed cells independent of EBV nuclear antigen 2 and latent membrane protein 1. *Proceedings of the National Academy of Sciences of the United States of America* **93,** 10411–10416; 10.1073/pnas.93.19.10411 (1996).

124. Tindall, K. R. & Kunkel, T. A. Fidelity of DNA synthesis by the Thermus aquaticus DNA polymerase. *Biochemistry* **27,** 6008–6013; 10.1021/bi00416a027 (1988).

125. Weber, K. & Osborn, M. The reliability of molecular weight determinations by dodecyl sulfate-polyacrylamide gel electrophoresis. *The Journal of biological chemistry* **244,** 4406–4412 (1969).

126. Towbin, H., Staehelin, T. & Gordon, J. Electrophoretic transfer of proteins from polyacrylamide gels to nitrocellulose sheets: procedure and some applications. *Proceedings of the National Academy of Sciences of the United States of America* **76,** 4350–4354; 10.1073/pnas.76.9.4350 (1979).

127. Barman, A., Deb, B. & Chakraborty, S. A glance at genome editing with CRISPR-Cas9 technology. *Current genetics* **66,** 447–462; 10.1007/s00294-019-01040-3 (2020).

128. Pougach, K. *et al.* Transcription, processing and function of CRISPR cassettes in Escherichia coli. *Molecular microbiology* **77,** 1367–1379; 10.1111/j.1365-2958.2010.07265.x (2010).

129. Zhang, B. CRISPR/Cas gene therapy. *Journal of cellular physiology* **236,** 2459–2481; 10.1002/jcp.30064 (2021).

130. Ran, F. A. *et al.* Genome engineering using the CRISPR-Cas9 system. *Nature protocols* **8,** 2281–2308; 10.1038/nprot.2013.143 (2013).

131. Abraham, L. *et al.* Limitations of Qdot labelling compared to directly-conjugated probes for single particle tracking of B cell receptor mobility. *Scientific reports* **7,** 11379; 10.1038/s41598-017-11563-9 (2017).

132. Chaumont, F. de *et al.* Icy: an open bioimage informatics platform for extended reproducible research. *Nature methods* **9,** 690–696; 10.1038/nmeth.2075 (2012).

133. Berglund, A. J. Statistics of camera-based single-particle tracking. *Physical review. E, Statistical, nonlinear, and soft matter physics* **82,** 11917; 10.1103/PhysRevE.82.011917 (2010).

134. Sander, S. *et al.* Synergy between PI3K signaling and MYC in Burkitt lymphomagenesis. *Cancer cell* **22,** 167–179; 10.1016/j.ccr.2012.06.012 (2012).

135. Ryan, J., Montero, J., Rocco, J. & Letai, A. iBH3: simple, fixable BH3 profiling to determine apoptotic priming in primary tissue by flow cytometry. *Biological chemistry* **397,** 671–678; 10.1515/hsz-2016-0107 (2016).

136. Keppler, S. J. *et al.* Wiskott-Aldrich Syndrome Interacting Protein Deficiency Uncovers the Role of the Co-receptor CD19 as a Generic Hub for PI3 Kinase Signaling in B Cells. *Immunity* **43,** 660–673; 10.1016/j.immuni.2015.09.004 (2015).

137. Li, J. *et al.* The Coordination Between B Cell Receptor Signaling and the Actin Cytoskeleton During B Cell Activation. *Frontiers in immunology* **9,** 3096; 10.3389/fimmu.2018.03096 (2018).

138. Liu, C. *et al.* Actin reorganization is required for the formation of polarized B cell receptor signalosomes in response to both soluble and membrane-associated antigens. *Journal of immunology (Baltimore, Md. : 1950)* **188,** 3237–3246; 10.4049/jimmunol.1103065 (2012).

139. Riedl, J. *et al.* Lifeact: a versatile marker to visualize F-actin. *Nature methods* **5,** 605–607; 10.1038/nmeth.1220 (2008).

140. Shao, H., Wu, C. & Wells, A. Phosphorylation of alpha-actinin 4 upon epidermal growth factor exposure regulates its interaction with actin. *The Journal of biological chemistry* **285,** 2591–2600; 10.1074/jbc.M109.035790 (2010).

141. Havranek, O. *et al.* Molecular Aspects of Tonic B-Cell Receptor Signaling in Diffuse Large B-Cell Lymphoma Provide Biomarkers and Targets for Specific Inhibition. *Blood* **128,** 779; 10.1182/blood.V128.22.779.779 (2016).

142. Sarbassov, D. D., Guertin, D. A., Ali, S. M. & Sabatini, D. M. Phosphorylation and regulation of Akt/PKB by the rictor-mTOR complex. *Science (New York, N.Y.)* **307,** 1098–1101; 10.1126/science.1106148 (2005).

143. Saito, S. *et al.* RASAL3, a novel hematopoietic RasGAP protein, regulates the number and functions of NKT cells. *European journal of immunology* **45,** 1512–1523; 10.1002/eji.201444977 (2015).

144. Yoo, Y., Ho, H. J., Wang, C. & Guan, J.-L. Tyrosine phosphorylation of cofilin at Y68 by v-Src leads to its degradation through ubiquitin-proteasome pathway. *Oncogene* **29,** 263–272; 10.1038/onc.2009.319 (2010).

145. Liu, H., Lu, Z.-G., Miki, Y. & Yoshida, K. Protein kinase C delta induces transcription of the TP53 tumor suppressor gene by controlling death-promoting factor Btf in the apoptotic response to DNA damage. *Molecular and cellular biology* **27,** 8480–8491; 10.1128/mcb.01126-07 (2007).

146. Jaffe, E. S. & Pittaluga, S. Aggressive B-cell lymphomas: a review of new and old entities in the WHO classification. *Hematology. American Society of Hematology. Education Program* **2011,** 506–514; 10.1182/asheducation-2011.1.506 (2011).

147. Neiman, P. E., Thomas, S. J. & Loring, G. Induction of apoptosis during normal and neoplastic B-cell development in the bursa of Fabricius. *Proceedings of the National Academy of Sciences of the United States of America* **88,** 5857–5861; 10.1073/pnas.88.13.5857 (1991).

148. Victora, G. D. *et al.* Identification of human germinal center light and dark zone cells and their relationship to human B-cell lymphomas. *Blood* **120,** 2240–2248; 10.1182/blood-2012-03-415380 (2012).

149. D'Sa-Eipper, C. & Chinnadurai, G. Functional dissection of Bfl-1, a Bcl-2 homolog: anti-apoptosis, oncogene-cooperation and cell proliferation activities. *Oncogene* **16,** 3105–3114; 10.1038/sj.onc.1201851 (1998).

150. D'Sa-Eipper, C., Subramanian, T. & Chinnadurai, G. bfl-1, a bcl-2 homologue, suppresses p53-induced apoptosis and exhibits potent cooperative transforming activity. *Cancer research* **56,** 3879–3882 (1996).

151. Kos, C. H. *et al.* Mice deficient in alpha-actinin-4 have severe glomerular disease. *The Journal of clinical investigation* **111,** 1683–1690; 10.1172/JCI17988 (2003).

152. Ding, Z. *et al.* A retrovirus-based protein complementation assay screen reveals functional AKT1-binding partners. *Proceedings of the National Academy of Sciences of the United States of America* **103,** 15014–15019; 10.1073/pnas.0606917103 (2006).

153. Tentler, D., Lomert, E., Novitskaya, K. & Barlev, N. A. Role of ACTN4 in Tumorigenesis, Metastasis, and EMT. *Cells* **8**; 10.3390/cells8111427 (2019).

154. Wang, Q. *et al.* NHERF1 inhibits beta-catenin-mediated proliferation of cervical cancer cells through suppression of alpha-actinin-4 expression. *Cell death & disease* **9,** 668; 10.1038/s41419-018-0711-x (2018).

155. Desouza, M., Gunning, P. W. & Stehn, J. R. The actin cytoskeleton as a sensor and mediator of apoptosis. *Bioarchitecture* **2,** 75–87; 10.4161/bioa.20975 (2012).

156. Field, J. The Actin Cytoskeleton and Cell Survival. *Recent Advances in Clinical Medicine* (2010).

157. Cybulsky, A. V. & Kennedy, C. R. J. Podocyte Injury Associated with Mutant α-Actinin-4. *Journal of signal transduction* **2011,** 563128; 10.1155/2011/563128 (2011).

158. Parameswaran, N. & Gupta, N. Re-defining ERM function in lymphocyte activation and migration. *Immunological reviews* **256,** 63–79; 10.1111/imr.12104 (2013).

159. Avalos, A. *et al.* Hem-1 regulates protective humoral immunity and limits autoantibody production in a B cell-specific manner. *JCI insight* **7**; 10.1172/jci.insight.153597 (2022).

160. Natkanski, E. *et al.* B cells use mechanical energy to discriminate antigen affinities. *Science (New York, N.Y.)* **340,** 1587–1590; 10.1126/science.1237572 (2013).

161. Jaqaman, K. & Grinstein, S. Regulation from within: the cytoskeleton in transmembrane signaling. *Trends in cell biology* **22,** 515–526; 10.1016/j.tcb.2012.07.006 (2012).

162. Mattila, P. K. *et al.* The actin and tetraspanin networks organize receptor nanoclusters to regulate B cell receptor-mediated signaling. *Immunity* **38,** 461–474; 10.1016/j.immuni.2012.11.019 (2013).

163. Kohlhas, V., Hallek, M. & Nguyen, P.-H. Constitutive activation of Lyn kinase enhances BCR responsiveness, but not the development of CLL in Eμ-TCL1 mice. *Blood advances* **4,** 6106–6116; 10.1182/bloodadvances.2020002584 (2020).

164. Freeman, S. A. *et al.* Cofilin-mediated F-actin severing is regulated by the Rap GTPase and controls the cytoskeletal dynamics that drive lymphocyte spreading and BCR microcluster formation. *Journal of immunology (Baltimore, Md. : 1950)* **187,** 5887–5900; 10.4049/jimmunol.1102233 (2011).

165. Schweighoffer, E. *et al.* The BAFF receptor transduces survival signals by co-opting the B cell receptor signaling pathway. *Immunity* **38,** 475–488; 10.1016/j.immuni.2012.11.015 (2013).

166. Ackermann, J. A. *et al.* Syk tyrosine kinase is critical for B cell antibody responses and memory B cell survival. *Journal of immunology (Baltimore, Md. : 1950)* **194,** 4650–4656; 10.4049/jimmunol.1500461 (2015).

167. Walter, R. *et al.* HSP90 promotes Burkitt lymphoma cell survival by maintaining tonic B-cell receptor signaling. *Blood* **129,** 598–608; 10.1182/blood-2016-06-721423 (2017).

168. Hobeika, E. *et al.* CD19 and BAFF-R can signal to promote B-cell survival in the absence of Syk. *The EMBO journal* **34,** 925–939; 10.15252/embj.201489732 (2015).

169. Honigberg, L., Chen, J., Smith, A. & Buggy, J. Levels of tonic BCR signaling predict response to the Btk inhibitor PCI-32765. *Cancer research* **68,** 2396 (2008).

170. Honigberg, L. A. *et al.* The Bruton tyrosine kinase inhibitor PCI-32765 blocks B-cell activation and is efficacious in models of autoimmune disease and B-cell malignancy. *Proceedings of the National Academy of Sciences of the United States of America* **107,** 13075–13080; 10.1073/pnas.1004594107 (2010).

171. Engelke, M. *et al.* Macromolecular assembly of the adaptor SLP-65 at intracellular vesicles in resting B cells. *Science signaling* **7,** ra79; 10.1126/scitranslmed.2005104 (2014).

8 Curriculum vitae